3-26-2015

Fatigue Behavior of IM7/BMI 5250-4 Composite at Room and Elevated Temperatures

James T. Tipton

FATIGUE BEHAVIOR OF IM7/BMI 5250-4 COMPOSITE AT ROOM AND ELEVATED TEMPERATURES

THESIS

J. Tucker Tipton, 2nd Lieutenant, USAF

AFIT-ENY-MS-15-M-241

DEPARTMENT OF THE AIR FORCE
AIR UNIVERSITY

AIR FORCE INSTITUTE OF TECHNOLOGY

Wright-Patterson Air Force Base, Ohio

AFIT-ENY-MS-15-M-241

FATIGUE BEHAVIOR OF IM7/BMI 5250-4 COMPOSITE AT ROOM AND ELEVATED TEMPERATURES

THESIS

Presented to the Faculty

Department of Aeronautics and Astronautics

Graduate School of Engineering and Management

Air Force Institute of Technology

Air University

Air Education and Training Command

In Partial Fulfillment of the Requirements for the

Degree of Master of Science in Aeronautical Engineering

J. Tucker Tipton, BS

2nd Lieutenant, USAF

March 2015

AFIT-ENY-MS-15-M-241

FATIGUE BEHAVIOR OF IM7/BMI 5250-4 COMPOSITE AT ROOM AND ELEVATED TEMPERATURES

J. Tucker Tipton, BS

2nd Lieutenant, USAF

Committee Membership:

Dr. Marina Ruggles-Wrenn
Chair

Dr. Thomas Eason
Member

Dr. Richard Hall
Member

AFIT-ENY-MS-15-M-241

Abstract

The tension-tension fatigue and tension-compression fatigue behaviors of the IM7/BMI 5250-4 composite were investigated. The tension-tension fatigue of the composite with 0/90 and ±45 fiber orientations was studied at 23, 170, and 190°C. The tension-compression fatigue of the composite with 0/90 fiber orientation was examined at 23°C. The tensile and compressive properties of the composite were also evaluated at room and elevated temperatures for both 0/90 and ±45 fiber orientations. Elevated temperature had little effect on the tensile properties of the 0/90 fiber orientation, but strongly influenced the ±45 tensile properties as well as the compressive properties of both fiber orientations. The 0/90 cross-ply exhibited a much stronger tension-tension fatigue performance than the ±45 cross-ply. Elevated temperature had little influence on the tension-tension fatigue response of both fiber orientations. The 0/90 composite exhibited reduced fatigue lives under tension-compression fatigue compared to the tension-tension cycling. The increased influence of the matrix on tension-compression fatigue response is evident.

Acknowledgments

First and foremost, I have to say thank you to my lord and savior Jesus Christ who has sustained me through many trials. I would like to express my sincere appreciation to my faculty advisor, Dr. Marina Ruggles-Wrenn, for all of her guidance, direction, and advice. I would like to thank Mr. Barry Page for his continual assistance in maintaining lab equipment. His support was irreplaceable. Thank you to Mr. Wilbur Lacy for his assistance with equipment malfunctions and to Mr. John Hixenbaugh for his assistance with keeping chemicals and materials stocked and available. To my family, thank you for all the support and encouragement over the past 18 months. Finally, to my wife, thank you for your endless support and understanding. You have made this process much more feasible.

J. Tucker Tipton

Table of Contents

Page

List of Figures

List of Tables

Nomenclature

Symbol	Definition
E	Young's Modulus (GPa)
N	Cycles
R	Stress Ratio
S or σ_{max}	Maximum Stress (MPa)
T	Temperature (°C)
T_g	Glass Transition Temperature (°C)

List of Acronyms

Acronym	Definition
AFIT	Air Force Institute of Technology
AFRL	Air Force Research Laboratory
ATF	Advanced Tactical Fighter
HTPMC	High Temperature Polymer Matrix Composite
MPT	Multi-Purpose Testware
MTS	Material Test Systems
PMC	Polymer Matrix Composite
UCS	Ultimate Compressive Strength
UTS	Ultimate Tensile Strength

FATIGUE BEHAVIOR OF IM7/BMI 5250-4 COMPOSITE AT ROOM AND ELEVATED TEMPERATURES

I. Introduction

1.1 Motivation

As the world leader in air, space, and cyberspace, the United States Air Force is constantly seeking to maintain its global dominance through both tactical and technological advancements. Currently, composite materials are one of the driving factors in the development of new and improved aircraft. The capabilities of engineering alloys, such as aluminum and steel, have been maximized, but the demand for improved material performance is continually increasing. Without composites, these design demands could not be met. Figure 1 shows the growth of composite usage in aircraft over the past 40 years and a predicted continuation of that trend into the foreseeable future. These high strength-to-weight ratio materials have provided capabilities that were never before possible. In consideration of the advanced tactical fighter (ATF), "advanced composites enable the ATF to meet improved performance requirements such as reduced drag, low radar observability and increased resistance to temperatures generated at high speeds" [1, pp. 58-59]. Composites also made stealth capabilities possible. For example, "the B-2 derives much of its stealth qualities from the material properties of composites and their ability to be molded into complex shapes" [1, p. 59]. Composites have exhibited excellent performance in helicopter rotors and other intense vibratory regimes. Composites have also improved the producibility and maintainability of many aircraft. "In an experimental program that Boeing undertook, 11,000 metal parts were replaced by 1,500 composite

ones, thus eliminating 90% of the vehicle's fasteners" [1, p. 60]. Also, these materials often exhibit corrosion resistance which makes them desirable for use in the aerospace environment.

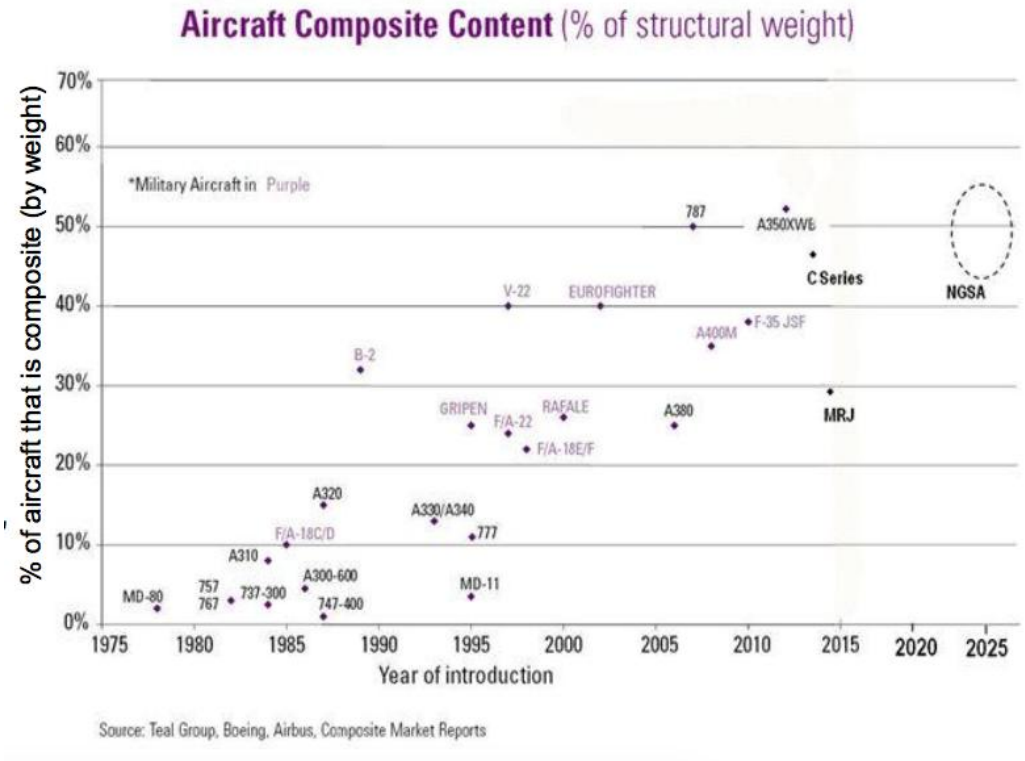

Figure 1: Composite Usage in Aircraft by Year [2, p. 11]

Due to their increased complexity in production, parts made from composite materials are often more expensive than parts made from standard engineering alloys. A cost-benefit analysis must be conducted before the implementation of composites. Despite the larger initial cost, composite materials tend to exhibit improved fatigue performance over engineering alloys [3], which can decrease total cost over the life of the aircraft. The use of composites can decrease maintenance and required replacement parts.

This research focused on composite materials that are known as Polymer Matrix Composites (PMCs). One of the greatest benefits to some PMCs is their thermal

capabilities. These composites are typically referred to as High Temperature Polymer Matrix Composites (HTPMCs) because they are designed to operate at elevated temperatures that may be experienced on the skin of an aircraft at high speeds or even in engine components. HTPMCs typically utilize a polyimide or bismaleimide resin. "Polyimide resins excel in high-temperature environments where their thermal resistance, oxidative stability, low coefficient of thermal expansion and solvent resistance benefit the design" [4, p. 7]. These resins tend to be the limiting factor for the operating temperature of these materials. Therefore, as their research and development improve, many more possible applications will become available for replacement by HTPMCs.

1.2 Objective

The objective of this research effort was to determine the mechanical properties of the IM7/BMI 5250-4 composite under fatigue loading at a range of test temperatures. Both 0/90 and ±45 fiber orientations were tested under monotonic tension at 23, 170, and 190°C to determine the ultimate tensile strength (UTS) of the material at each temperature. Similarly, both fiber orientations were tested under monotonic compression at 23 and 170°C to determine the ultimate compressive strength (UCS). Tension-tension fatigue tests were performed at 23, 170, and 190°C on both fiber orientations, and fully-reversed tension-compression fatigue tests were performed at 23°C on the 0/90 fiber orientation to determine the tension-compression fatigue performance. Both fiber orientations were included to determine fiber-dominated and matrix-dominated performances and behaviors of the material.

1.3 Methodology

The following process was used as the methodology for testing of the material:

1. Conduct room temperature modulus tests to determine specimen-to-specimen variability and panel variability
2. Conduct room temperature monotonic tension and compression tests to failure to determine UTS and UCS
3. Compare results between fiber orientations
4. Conduct elevated temperature monotonic tension and compression tests to failure to determine UTS and UCS at 170 and 190°C
5. Compare results and determine effects of fiber orientation and temperature
6. Conduct room temperature tension-tension fatigue tests
7. Conduct elevated temperature tension-tension fatigue tests
8. Conduct room temperature tension-compression fatigue tests
9. Compare results between loading condition, temperature, and fiber orientation
10. Perform optical microscopy on failed specimens to determine failure mechanisms

II. Background

2.1 Composite Materials

A composite material is defined as "a material system consisting of two or more phases on a macroscopic scale, whose mechanical performance and properties are designed to be superior to those of the constituent materials acting independently" [5, p. 1]. This concept has been used dating back to the ancient Egyptians and their use of clay bricks reinforced with straw, but it is most commonly used in steel-reinforce concrete today [5, p. 2]. Composites also exist in nature. For example, "wood is a composite- it is made from long cellulose fibers (a polymer) held together by a much weaker substance called lignin… The two weak substances- lignin and cellulose- together form a much stronger one," [6, p. 1]. Composites allow for two or more materials that cannot meet a design requirement to be combined so that they can meet a project's needs. Modern day composites have been adapted into automobiles, aircraft, marine vessels, and sporting goods. These modern composites are classified into polymer matrix composites, metal matrix composites, ceramic matrix composites, carbon/carbon composites, and hybrid composites [7, p. 6]. A polymer matrix composite was used in this study; therefore, PMCs will be the foundation of this discussion.

Typically, a PMC is composed of a continuous phase, or matrix, and a dispersed phase, or reinforcement [5]. The reinforcement is comprised of many individual fibers that can be laid in sheets, woven, or braided together. They provide the stiffness and strength of the composite material. The matrix material fills the space between the reinforcement fibers and distributes the shear among the fibers. In PMCs, either a

thermoset or thermoplastic polymeric resin is utilized as the matrix material [7]. A thermoset resin can be formed into its shape as a liquid and then cured using heat or a catalyst to become a solid [4]. They maintain their material properties once the curing process is complete. Contrary to thermosets, a thermoplastic resin "can be softened repeatedly by an increase in temperature and hardened by a decrease in temperature," and their material properties can fluctuate accordingly [4, p. 8]. In most composites, the region of interaction between the fibers and the matrix plays a vital role in the behavior of the material. This region is referred to as the interface region. A strong bond in the interface region is required for PMCs so that the shear loads are transferred appropriately between the fibers.

Composite materials are composed of layers of these fiber and matrix materials where the fibers can either be unidirectional or woven together in different weave patterns. Individually, these layers are referred to as a lamina or a ply, and, together, they create a laminate. The number of plies can be altered in order to change the thickness of the material. The nomenclature used to label these composites is formatted inside brackets as a list of the fiber orientation of each ply separated by commas. If the plies are oriented in such a way as to be symmetric about the centerline of the layup, then the laminate is considered symmetric and can be represented by only the first half of the fiber orientations with an "s" following the brackets [8]. For example, Figure 2 shows two laminates that can be labeled as [0,0,0,0,0,0,0,0] and [0,90,+45,-45,-45,+45,90,0] from left to right. These labels can be abbreviated as $[0]_8$ to note that there are 8 plies all oriented at 0° and $[0,90,+45,-45]_s$ to show that the layup is symmetric.

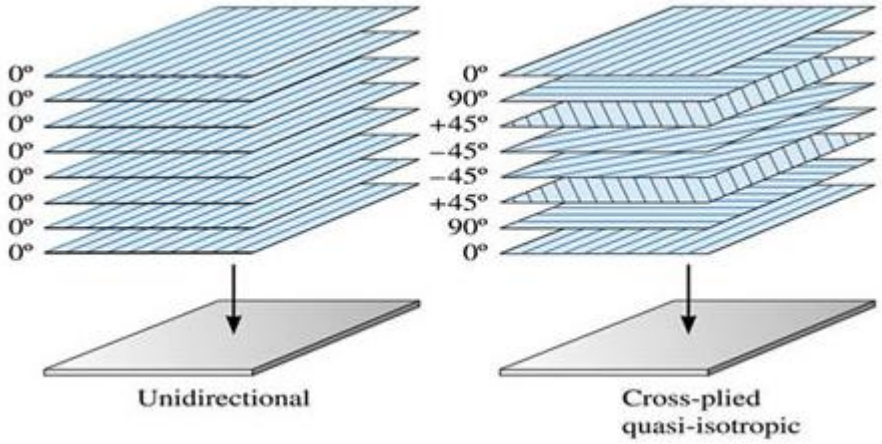

Figure 2: Layers of a Laminated Composite [9]

The laminate method for manufacturing composite materials is incredibly useful, but it has one major drawback. "The major cause of degradation in stiffness and strength of laminated composite materials is the growth of delamination between individual composite layers. Excess delamination may result in ultimate fatigue failure" [10, p. 1].

2.2 Related Research

Research projects on several related topics have been conducted in the past at the Air Force Institute of Technology (AFIT). In order to provide a baseline for this research effort, it is important to understand what data has previously been collected about the same material. A study of the BMI 5250-4 neat resin was conducted followed by research on the effects of prior aging on the fatigue response and creep response of the IM7/BMI 5250-4 composite. All of these research efforts provide a solid background for the material of interest.

In 2006, Baliconis tested the BMI 5250-4 neat resin to determine its material properties, because it is important to understand the properties of the individual materials

before the materials are combined to form a composite. The BMI 5250-4 neat resin is designed to operate between 82°C and 204°C; therefore, his testing was conducted at 191°C [11]. Baliconis determined that loading rate had no change on the modulus of the BMI 5250-4 resin as shown in Figure 3. He noticed that the increase in temperature from 23 to 191°C caused a significant decrease in both modulus and UTS of the resin. He also observed that the modulus decreased about 35% and the UTS decreased roughly 37% due to this increase in temperature [11].

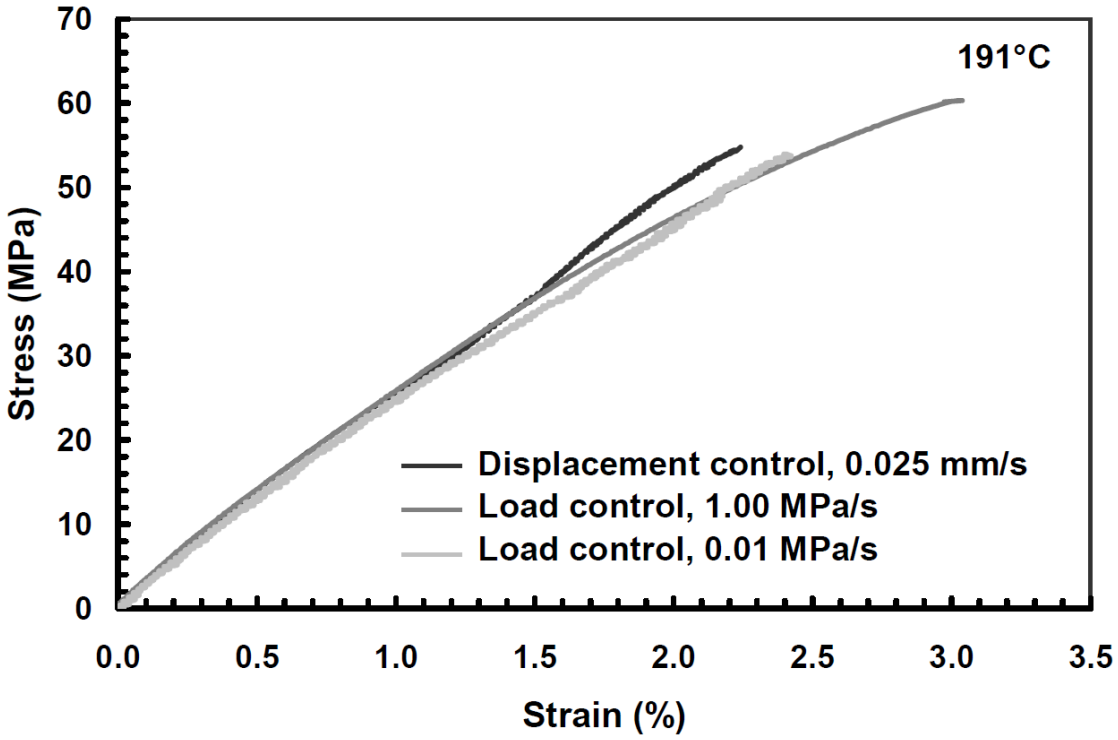

Figure 3: Stress-Strain Curves for BMI 5250-4 Neat Resin at 191°C [11]

In 2007, Ladrido investigated the effects of prior aging on the IM7/BMI 5250-4 composite material when exposed to fatigue cycling. She conducted both monotonic tension-to-failure tests and tension-tension fatigue tests on the IM7/BMI 5250-4 composite. She tested unaged specimens as well as specimens that had been aged for 10,

50, 100, 250, 500, and 1,000 hours at 191°C. She determined that an increased period of prior aging extended the elastic region of the stress-strain curve for the ±45 specimens, while the 0/90 specimens were unaffected [12]. Table 1 displays her data for tension-tension fatigue tests conducted on the ±45 specimens at 191°C. From this data, she concluded that fatigue life decreases as prior aging time increases [12]. This data is summarized in Table 1 and Figure 4.

Table 1: Prior Aging Effects on Fatigue of ±45 Specimens (Reproduced from [12])

Aging Time (h)	σ_{max} (MPa)	σ_{max} (% UTS)	Cycles to Failure
0	132	80	120
0	99	60	100000
0	66	40	100000
0	115.5	70	100000
10	115.5	70	100000
50	115.5	70	67738
100	115.5	70	49130
250	115.5	70	51927
500	115.5	70	51762
1000	115.5	70	19277

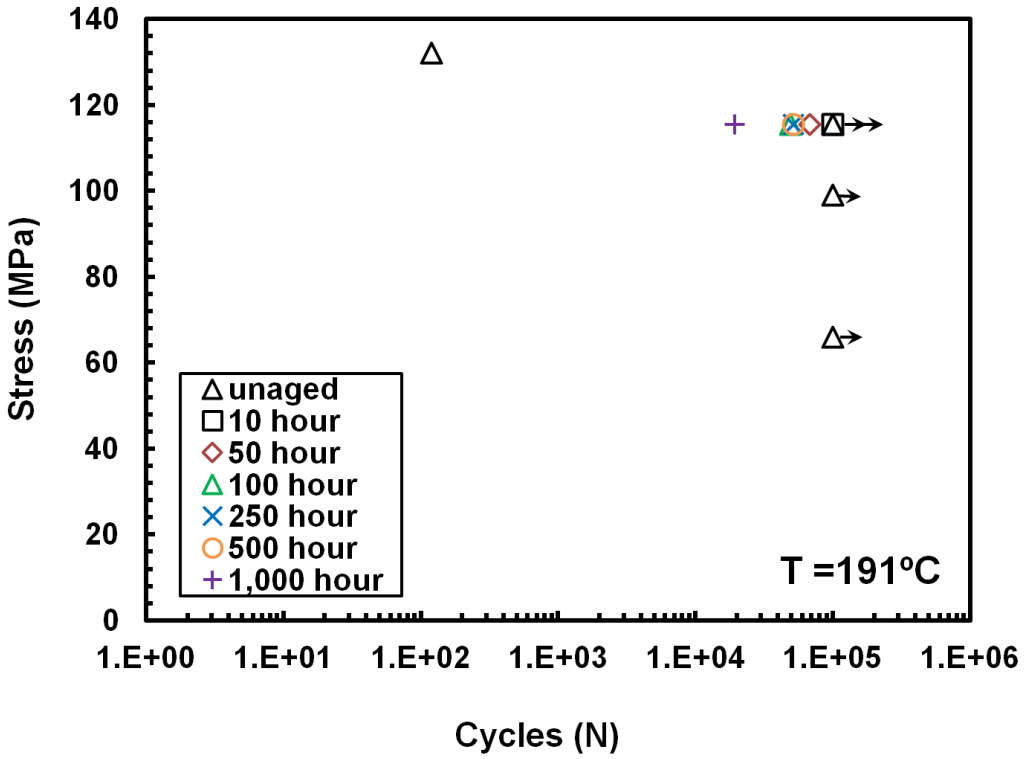

Figure 4: Effects of Prior Aging on Fatigue Response of ±45 Specimens at 191°C (Constructed from [12] data). Arrow Indicates Specimen Achieved Fatigue Run-Out.

Also in 2007, Salvia researched the effects of prior aging on the creep response of the IM7/BMI 5250-4 composite. During his monotonic tension-to-failure tests, he found that the unaged ±45 specimens had an average UTS of 165 MPa and an average modulus of 14.8 GPa at 191°C [13]. He also determined the average UTS and modulus of the 0/90 specimens to be 849 MPa and 60.9 GPa, respectively [13]. During his investigation into the effects of prior aging, he discovered that increased aging time was detrimental to the UTS of both fiber orientations due to the degradation of the matrix that occurred. Finally, Salvia determined that increased prior aging time also increased strain accumulated during creep and recovery strain [13].

Many studies have been conducted on different materials under fatigue loading. Fatigue testing studies the response of a material as it is exposed to repeated cycling from a minimum load to a maximum load. Different materials respond to fatigue testing in a variety of ways, but the objective of the testing is to determine the endurance limit (if one exists for that material). The endurance limit is considered "the stress level below which a material has an 'infinite' life," which is typically defined as a life greater than one million cycles [14, p. 1]. Theoretically, a material cycled in fatigue at a stress level below this limit would never fail. Due to time constraints, it is unrealistic to prove that theory. Therefore, for the purpose of this research, the endurance limit will be considered the stress at which the test specimen reaches 100,000 cycles. An example of 1045 steel reaching the endurance limit on a maximum stress vs. cycles to failure (S-N) curve is shown in Figure 5.

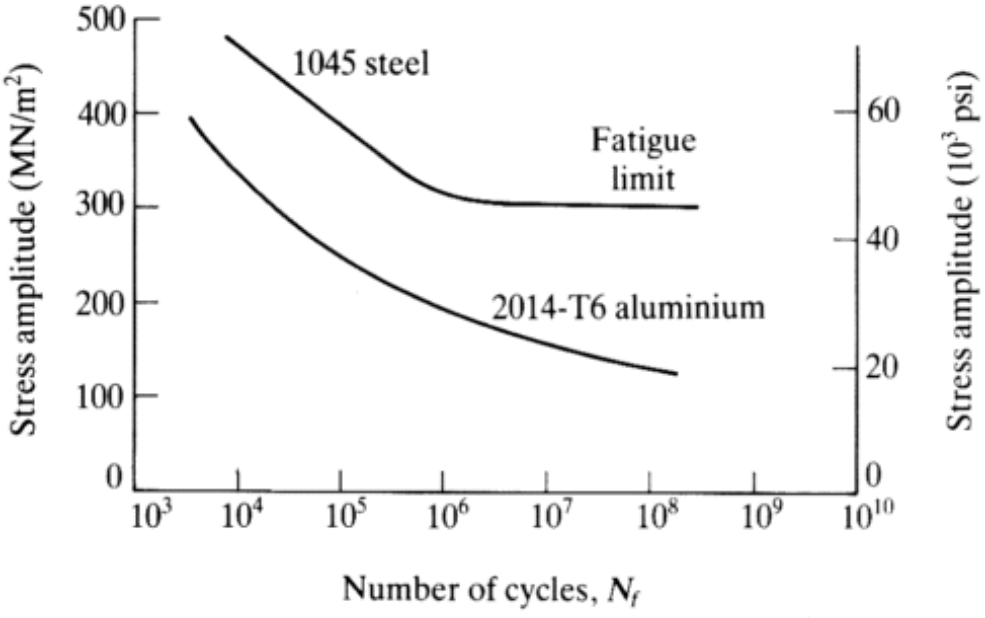

Figure 5: Example of Steel Reaching the Endurance Limit on S-N Curve [15]

III. Material and Test Specimen

3.1 Material

3.1.1 Reinforcement Material

The IM7 carbon fibers were used as the reinforcement material in the IM7/BMI 5250-4 composite. These fibers give the material its strength and stiffness. They are the backbone of the composite that allow it to bear the high loads that occur during aerospace applications. The IM7 carbon fibers exhibit a superb combination of high elastic modulus and high tensile strength with a low or slightly negative coefficient of thermal expansion [16]. Thousands of individual fibers that are bunched together are known as fiber tows [17]. The tows are woven into a weave pattern to form a fabric of carbon fibers before the matrix material is added [17].

3.1.2 Matrix Material

The matrix material used in this composite is the BMI 5250-4 bismaleimide resin. Bismaleimides are thermosetting resins that offer a higher temperature capability and toughness than epoxy resins and exhibit excellent performance at ambient and elevated temperatures [4, p. 8]. These materials were designed specifically to withstand elevated temperatures in aircraft engines and other high temperature applications [4, p. 8]. From a chemical standpoint, BMI resin derives its advantageous properties from the "polymer chains that become highly cross-linked during cure" [7, p. 7]. Due to the "three-dimensionally crosslinked, thermoset structures" that are formed from polyaddition reactions that occur with itself [18, p. 1], these bismaleimide resins remain rigid once they have been cured and cannot be altered by reheating [7]. The bismaleimide matrix

holds the IM7 fibers together and distributes the stress applied to the material between the fibers. It is often selected because of its “epoxy-like processing” which makes part manufacturing more feasible [19, p. 100].

Due to its superior performance capabilities, the BMI 5250-4 resin has been used in a number of aeronautical applications. This list includes parts of the wings of the C-17 cargo aircraft, structures utilized in thrust reversers, and the tail boom of the Model 412/212 helicopter made by Bell Helicopter Textron [19]. Most notably, the BMI 5250-4 resin was used in conjunction with the IM7 carbon fibers to form the composite material that makes up 12% of the airframe of the Air Force’s F-22 Raptor [19].

3.1.3 Composite Material

The IM7/5250-4 graphite/bismaleimide material system was supplied to the Air Force Research Laboratory (AFRL) in prepreg form. Four different types of cross-ply laminate panels, $[0/90]_{6s}$, $[0/90]_{10s}$, $[\pm45]_{6s}$, and $[\pm45]_{10s}$, were fabricated and cured in an autoclave. The cure cycle consisted of 6 h at 191°C followed by a 6-h post-cure at 227°C. As the temperature increases during the first part of the cure cycle, the viscosity of the resin decreases until the resin becomes a fluid. At about 165°C, the viscosity reaches a minimum value then begins to rise. During the hold at 191°C, a continuous cross-linked network is formed. Crosslinking, degree of cure, and the elastic modulus of the matrix continue to increase during the hold period. The postcure relieves some of the inelastic curing stresses and may also increase the glass transition temperature (T_g) of the matrix resin.

3.2 Test Specimen

Composite panels were provided by AFRL. The test specimens were machined to specifications at the AFIT model and fabrication shop using diamond grinding to prevent damage to the material. The tension-tension fatigue specimens were cut from 3-mm thick panels according to the drawing in Figure 6. The tension-tension fatigue specimens with 0/90 fiber orientation were cut from panels with $[0/90]_{6s}$ layup, and the tension-tension specimens with ±45 fiber orientation were cut from panels with $[+45/-45]_{6s}$ layup.

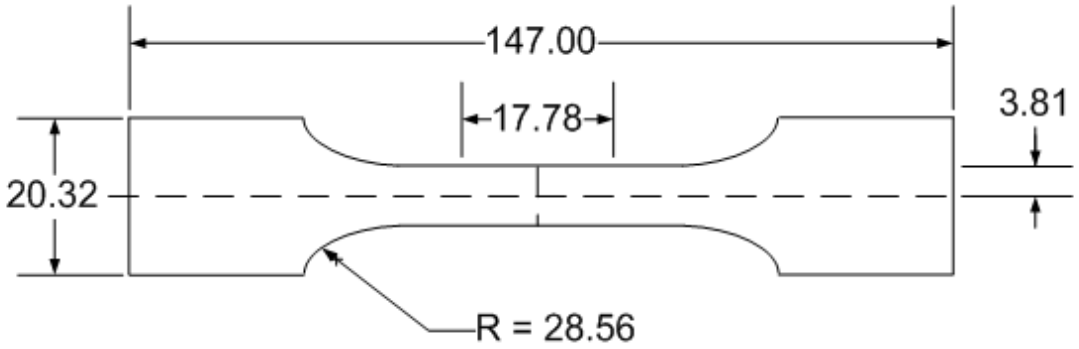

Figure 6: Tension-Tension Fatigue Test Specimen. All Dimensions are in mm. All Tolerances are ±0.025 mm.

Because tension-compression fatigue involves compressive loading, buckling failure modes are possible. Specimens with hourglass-shaped gage sections were designed to minimize the potential for buckling. The hourglass specimens have been used successfully in tension-compression fatigue testing of polymer matrix composites [20]. Corum et al [21] evaluated the stress concentration inherent in an hourglass specimen to demonstrate its adequacy for tension-compression testing. The hourglass-shaped tension-compression fatigue specimens were cut from 5-mm thick panels according to the drawing in Figure 7. The tension-compression specimens with 0/90 fiber orientation were

cut from panels with $[0/90]_{10s}$ layup, and the tension-compression specimens with ±45 fiber orientation were cut from panels with $[+45/-45]_{10s}$ layup.

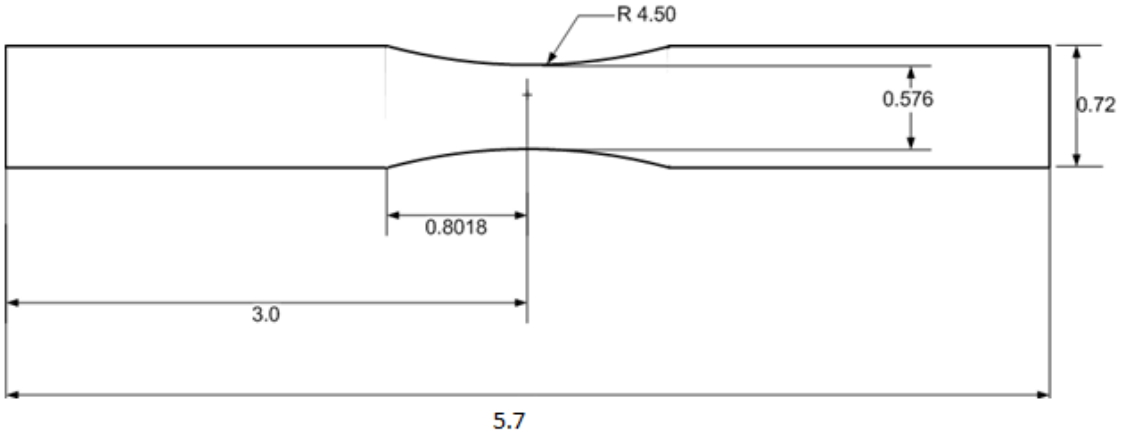

Figure 7: Tension-Compression Fatigue Test Specimen. All Dimension are in Inches. All Tolerances are ±0.001 in.

All the specimens were individually labeled. The labeling scheme used a "T" to denote tension-tension fatigue specimens or a "C" to denote tension-compression fatigue specimens, followed by the panel number and specimen number. For example, the specimen labeled T41-5 was the tension-tension fatigue specimen 5 cut from panel 14041. Likewise, the specimen labeled C70-20 was the tension-compression fatigue specimen 20 cut from panel 14070. Once all specimens were labeled, they were washed in a bath of household dish soap and warm water, scrubbed with a coarse bristled brush, and rinsed with warm water to remove any remaining particulates from the machining process. Nitrile gloves were worn when handling the washed specimens to prevent contamination from skin oils. The specimens were dried with a paper towel and placed in an aluminum pan for moisture content removal in a vacuum oven. Due to space limitations in the vacuum oven, specimens were dried in two batches. Six to eight specimens were randomly selected for periodic weight measurements in order to monitor

the moisture content throughout the drying process. Those specimens were weighed using a Mettler Toledo Lab balance with a ±0.9 mg accuracy. All specimens were dried in an Isotemp model 282A vacuum oven at 105°C and a pressure of about 2 in. Hg. Periodically, the selected specimens were removed from the oven and weighed, and their weights were recorded. After about 9 days, it was determined that the weight loss of the specimens had stabilized, indicating that moisture was removed. Changes in specimen weight with drying time are depicted in Figure 8.

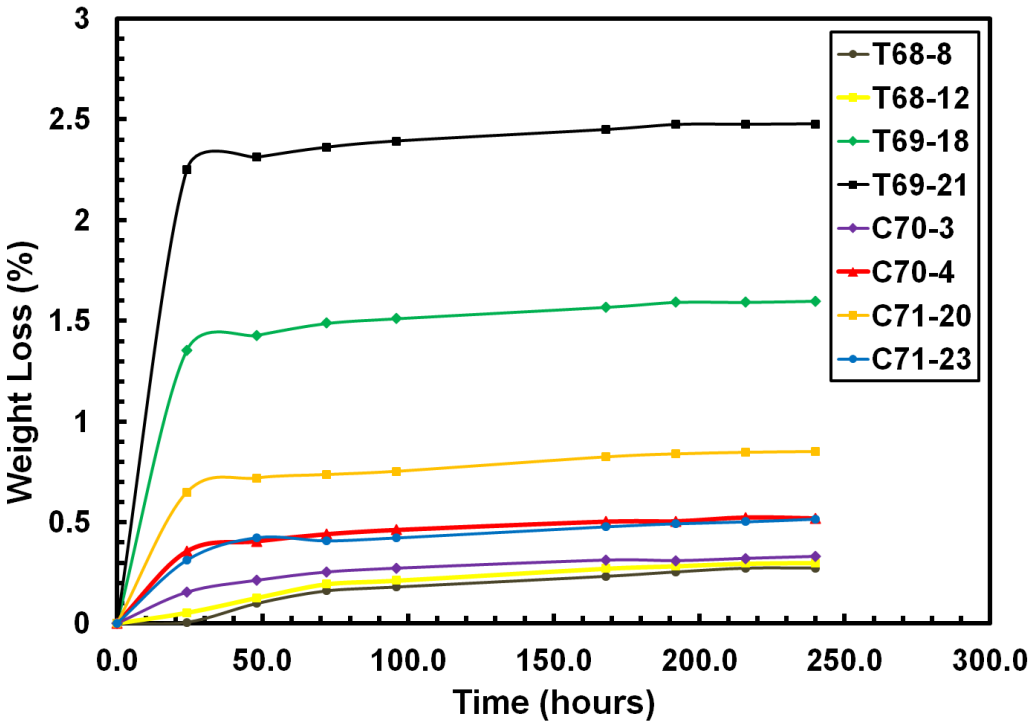

Figure 8: Change in Specimen Weight with Drying Time

After drying, the test specimens were promptly moved from the vacuum oven to a desiccator in order to prevent re-absorption of moisture from the ambient air. Each test specimen remained in the desiccator at ~15% RH until the actual test.

Prior to testing, tabs were bonded to the gripping sections of each specimen using the M-bond 200 adhesive. The tabs evenly distribute the gripping pressure applied to the test specimen while preventing damage from the grips. The thin fiberglass tabs (Figure 9 (a)) were used for all tension-tension fatigue specimens. A greater gripping pressure was required to prevent the specimen from slipping in the grips during tension-compression fatigue tests. Therefore, the thicker fiberglass tabs shown in Figure 9 (b) were utilized for the tension-compression fatigue specimens. Finally, in order to determine the retained tensile properties of the tension-compression specimens that achieved fatigue run-out of 10^5 cycles, the grip pressure had to be increased again. This increased pressure caused crushing of the thick fiberglass tabs. Hence the aluminum tabs depicted in Figure 9 (c) were used instead. With the aluminum tabs attached, the two tension-compression specimens that achieved run-out were successfully tested in tension to failure.

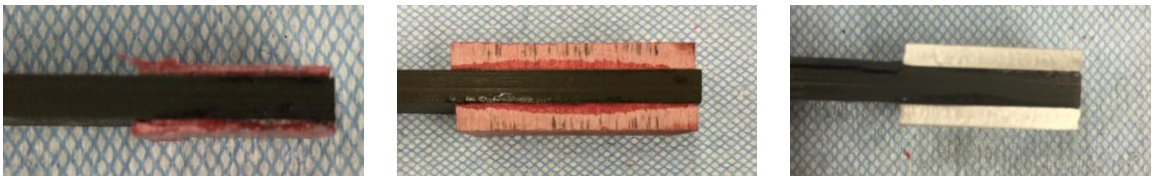

(a) (b) (c)

Figure 9: Test Specimen Outfitted with (a) Thin Fiberglass Tabs, (b) Thick Fiberglass Tabs, and (c) Aluminum Tabs

Two small indentations were made in the side of the specimen gage section to ensure contact with the extensometer rods. The indentations were 12.7 mm (0.5 in.) apart and centered in the gage section. The indentations were made using a small hammer and a punch tool provided by Material Test Systems (MTS). These indentations were small enough as to not cause a significant stress concentration or crack initiation.

IV. Experimental Setup and Test Procedures

This section provides a detailed description of the test equipment and setup, test procedures, temperature calibrations, and optical microscopy used to accomplish this research.

4.1 Testing Equipment

All tests conducted in this research utilized a vertically configured 810 MTS machine with a 22 kip load cell and hydraulic wedge grips shown in Figure 10.

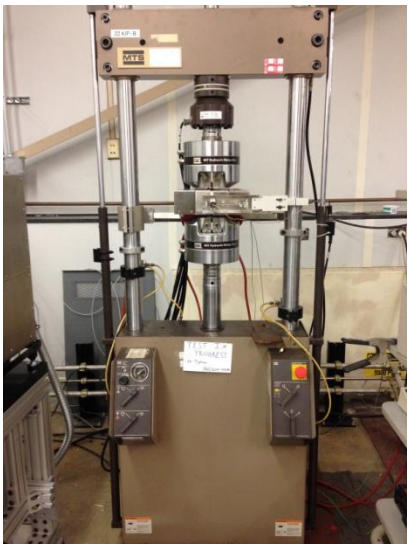

Figure 10: 810 MTS Machine Setup

The grip pressure was set at 15 MPa for all tests using specimens outfitted with the thin fiberglass tabs in order to prevent slippage. When the specimens outfitted with the thick fiberglass tabs were used, the grip pressure was decreased to 6 MPa. This level of grip pressure was sufficient to prevent slippage but not so high as to crush the tabs. For the specimens outfitted with the aluminum tabs, the grip pressure was set to 17 MPa. This level of grip pressure was required to prevent the test specimen from slipping out of the

grips during loading. Note that the specimens were placed in the grips in a manner to maximize the contact area between the specimen and the grip wedges.

An MTS extensometer model 632, shown in Figure 11, with a 12.7-mm (0.5 in.) gage length was used to measure strain. For the tests conducted at elevated temperature, an MTS 653 furnace, depicted in Figure 11, was used along with an MTS temperature controller to provide a high-temperature environment inside the test chamber.

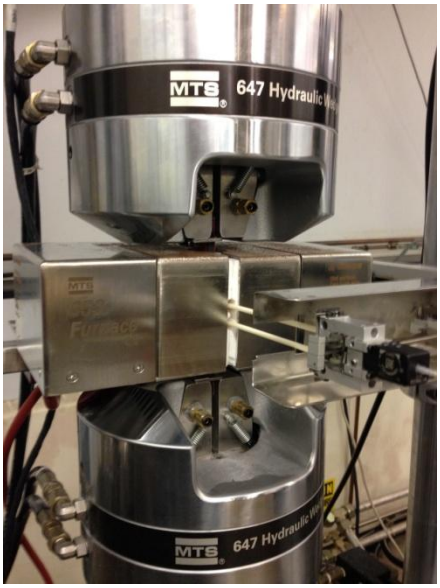

Figure 11: Test assembly showing the MTS 653 furnace and the Extensometer

An MTS FlexTest® 40 digital controller was used to generate input signals and to collect the data. A configuration file was built using the station builder, and all test procedures were generated using the Multi-Purpose Testware (MPT) package in the station manager. In the MPT, the test procedures were created to perform the desired operations for each specific test type and to collect the desired data. The following data were collected in all tests: force, strain, displacement, force command, upper temperature (where applicable), lower temperature (where applicable), and time.

4.2 Test Procedures

The following types of tests were performed in this research: tension-to-failure tests, compression-to-failure tests, tension-tension fatigue tests, and fully reversed tension-compression fatigue tests. In addition, elastic modulus measurements were performed for several specimens randomly selected from each composite panel.

4.2.1 Elastic Modulus Measurements

The elastic modulus of several specimens from each composite panel was measured at room temperature. The purpose of these tests was to determine the specimen-to-specimen variability within each composite panel as well as the property variability between panels. Three different 0/90 specimens were chosen at random from each panel using the RANDBETWEEN function in excel. The 0/90 specimens were loaded in force control to 20 MPa in 30 s and unloaded to near zero stress in 30 s. This process was repeated three times in order to determine an average elastic modulus. During unloading, the load was reduced to 50 N for the tension-tension fatigue specimens and to 100 N for the tension-compression fatigue specimens to avoid putting the specimens into compression. The same procedure was utilized for the ± 45 specimens. In this case, the specimens were loaded only to 10 MPa in order to remain in the linear elastic region of the stress-strain behavior. The elastic modulus of each specimen was determined by taking the slope of the best fit line though all of the acquired data displayed on a stress-strain graph.

4.2.2 Monotonic Tension to Failure Tests

The tension-to-failure tests were conducted in order to determine the elastic modulus, UTS, and failure strain. The tension tests were performed at room temperature

(23°C), 170°C, and 190°C in displacement control with a constant displacement rate of 0.025 mm/s. Two specimens from two 0/90 panels and two specimens from two ±45 panels were tested. Failure was determined to have occurred when a dramatic decrease in tensile load was observed.

4.2.3 Monotonic Compression to Failure Tests

Compression-to-failure tests were conducted on the hourglass-shaped specimens in order to determine the compressive modulus, UCS, and strain at failure. The compression tests were performed at 23 and 170°C in displacement control with a constant displacement rate of 0.025 mm/s. Two specimens from two 0/90 panels and two specimens from two ±45 panels were tested. Failure was defined by a significant drop in compressive load.

4.2.4 Tension-Tension Fatigue Tests

Tension-tension fatigue testing was conducted at 23, 170, and 190°C in force control with a sinusoidal waveform at a frequency of 1 Hz and a minimum to maximum stress ratio of R=0.1. Specimens with both the 0/90 and the ±45 fiber orientations were tested. Different maximum stress levels were considered for each material orientation. Tension-tension fatigue run-out was set to 10^5 cycles. This cycle count represents the number of loading cycles expected in aerospace applications at temperatures considered in this research. All specimens that achieved run-out were subjected to tensile tests to failure at the corresponding test temperature in laboratory air to determine the retained strength and stiffness.

4.2.5 Fully Reversed Fatigue Tests

Tension-compression fatigue tests were conducted at room temperature in force control with a sinusoidal waveform at a frequency of 1 Hz and a minimum to maximum stress ratio of R= -1. Only the 0/90 specimens were tested in tension-compression fatigue. Tension-compression fatigue run-out was set to 10^5 cycles. This cycle count represents the number of loading cycles expected in aerospace applications at the temperature of interest. All specimens that achieved run-out were subjected to tensile test to failure at 23°C in laboratory air to determine the retained strength and stiffness.

4.3 Testing at Elevated Temperature

In order to ensure that the test specimens were tested at the desired temperature in the furnace, a temperature calibration was conducted. Two K-type thermocouples were attached to a tension-tension test specimen, one on each side of the test section, using Kapton® tape and aluminum wire to ensure the thermocouples remained flush with the surface of the test specimen (Figure 12).

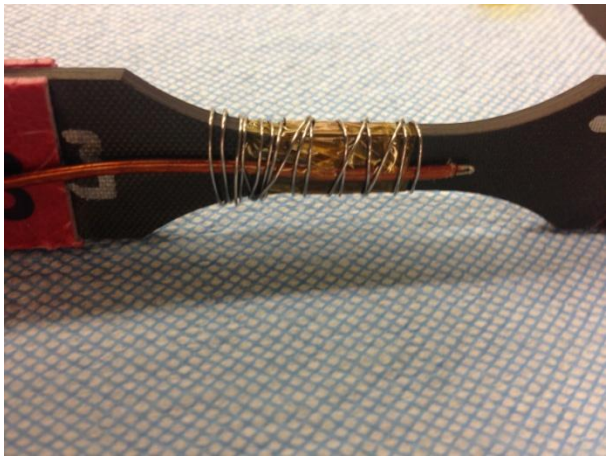

Figure 12: K-Type Thermocouples Attached to Tension-Tension Specimen for Temperature Calibration

The thermocouples were connected to an Omega HH501DK thermometer, shown in Figure 13, in order to accurately read the temperature of the specimen.

Figure 13: Omega HH501DK Type-K Thermometer

The test specimen was mounted in the MTS testing machine under force control and held at zero force to allow for thermal expansion of the material while the temperature was increased. The dual-zone furnace and the two temperature controllers utilize non-contacting control thermocouples exposed to the ambient environment near the test specimen. The temperature settings were increased slowly until the specimen temperature reached 170°C (the desired test temperature). The 170°C specimen temperature corresponded to a command of 140°C on both temperature controllers. In order to validate the temperature calibration, a procedure was created to autonomously raise the specimen temperature. The test specimen was again mounted in the MTS machine under force control. Zero force was commanded for the duration of the temperature calibration. The settings of the temperature controllers were increased at a rate of 5°C per minute until they reached 75°C. Then a rate of 2°C per minute was utilized until the temperature controllers reached the setting of 135°C. Finally, the settings on the temperature

controllers were raised to the desired 140°C at a rate of 1°C per minute. This process ensured that the specimen temperature did not overshoot the desired test temperature. The meter read the specimen temperature of 170°C at the end of this process, thus validating the temperature calibration. This process was repeated on a tension-compression specimen in order to ensure that a consistent result was produced for the different specimen geometry. Finally, the thermal expansion coefficients were obtained and found to be in agreement with published data, thus confirming the temperature calibration procedure.

An additional temperature calibration was performed in order to conduct testing at 190°C. The same process as before was utilized. It was determined that a command temperature of 156°C on both controllers produced a specimen temperature of 190°C. The automated heat-up process again began with a rate of 5°C per minute until both controllers reached the 75°C setting. From there, a rate of 2°C per minute was used to reach a controller setting of 150°C. Finally, a rate of 1°C per minute was utilized to bring the specimen to the final test temperature which corresponded to a temperature controller command of 156°C on both controllers.

4.4 Controller Tuning

Due to the use of different fiber orientations and different specimen geometries, it was important to have the FlexTest® 40 controller tuned properly in force control before starting a procedure. To do so, a test specimen was placed in the grips in force control with the load set to 0 N. The auto-tuning feature in the MTS software was used to tune the MTS machine in force control with load limits set so as to not damage the test

specimen. The auto-tuning process produced a P gain value of about 2 and an I gain value of about 0.4 for the 0/90 specimens. The tuning with the ±45 specimens resulted in a P gain of 8 and an I gain of 1.5 due to the drastic difference in their compliance. This process was repeated for each specimen type and fiber orientation.

4.5 Optical Microscopy

Specimens subjected to each type of test were examined under a Zeiss Discovery.V12 stereoscopic optical microscope equipped with a Zeiss AxioCam HRc digital camera (Figure 14).

Figure 14: Zeiss Optical Microscope

V. Results and Discussion

5.1 Assessment of Specimen-to-Specimen Variability

Due to minor imperfections or defects introduced during fabrication, mechanical properties may vary between the composite panels as well as within a single panel. Test specimens used in this research were cut from 16 different panels. In order to assess the specimen-to-specimen variability and variability between the panels, the room-temperature elastic modulus was measured for three specimens from each panel using the test procedure described in Section 4.2.1. The results of the elastic modulus measurements are summarized in Table 2.

Table 2: Elastic Modulus Results

Composite Panel	Specimen Type and Fiber Orientation	Average Modulus (GPa)	Standard Deviation (GPa)	Coefficient of Variation
T41	0/90° T	73.15	1.89	0.026
T42	0/90° T	84.12	3.11	0.037
T43	0/90° T	80.52	2.73	0.034
C53	0/90° C	69.75	6.01	0.086
C54	0/90° C	61.21	4.91	0.080
C55	0/90° C	70.62	10.01	0.142
T58	±45° T	21.82	4.34	0.199
T59	±45° T	23.48	3.60	0.153
T60	±45° T	21.97	0.72	0.033
T68	±45° T	18.11	2.75	0.152
T69	±45° T	21.58	1.04	0.048
C63	±45° C	21.66	1.32	0.061
C64	±45° C	24.42	1.58	0.065
C65	±45° C	22.26	1.03	0.046
C70	±45° C	22.32	1.66	0.074
C71	±45° C	19.74	1.49	0.075

The 0/90 specimens exhibited an average standard deviation among all panels of 4.78 GPa, and the ±45 specimens exhibited an average standard deviation of all panels of 1.89 GPa. Thus, the 0/90 panels showed greater variability in elastic modulus than the ±45 panels. This can be attributed to a number of factors. The mechanical behavior of the 0/90 composite is dominated by the fibers; therefore, slight misalignment of the fibers could cause significant differences in strength and stiffness. In contrast, fibers play a lesser role in the mechanical behavior of the ±45 panels. Hence the ±45 mechanical properties and behavior should be less susceptible to the fiber misalignment. Another contributing factor is fiber bunching that may occur during the layup process. In this case, the elastic modulus of the composite is lower initially and transitions to a higher value as the fibers straighten under load. An example of this phenomenon is depicted in Figure 15.

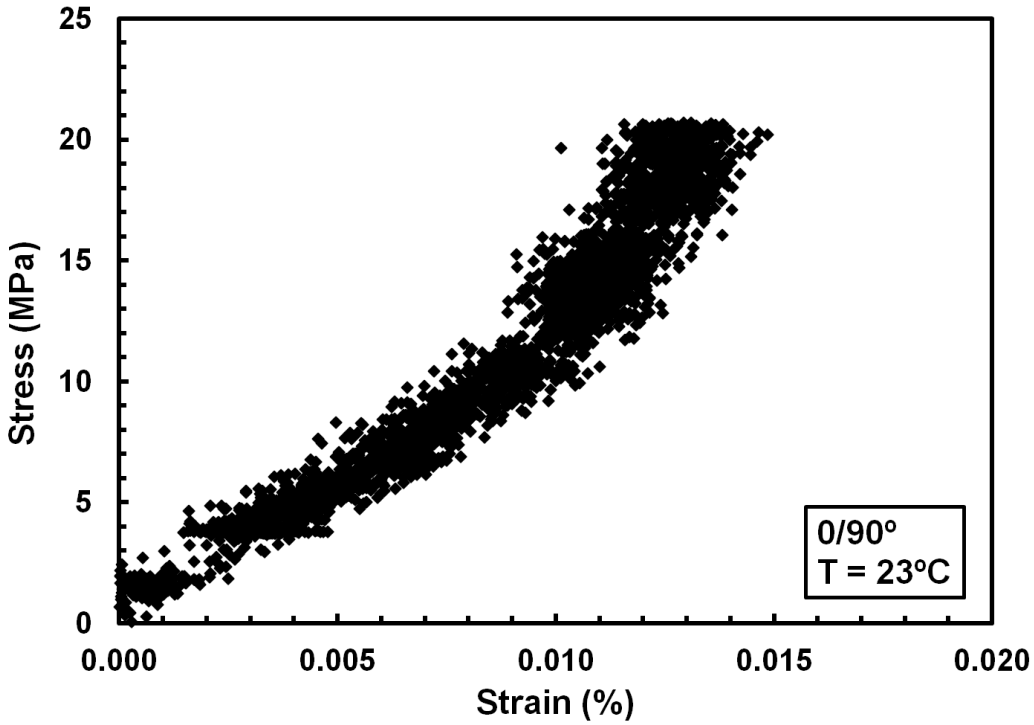

Figure 15: Effect of Fiber Bunching on Elastic Modulus of the Composite with 0/90 Fiber Orientation. Note the Increase in Elastic Modulus.

5.2 Thermal Expansion

The elevated temperature tests in this research were performed at 170°C and at 190°C. The temperature was increased to the desired test temperature through the following rates and controller temperatures: 5°C/min to 75°C, 2°C/min to 135°C, and 1°C/min to 140°C for 170°C tests and 5°C/min to 75°C, 2°C/min to 150°C, and 1°C/min to 156°C for 190°C tests. Thermal strain was measured and recorded during the temperature ramp up. Thermal strains produced in all tests performed at 170 and 190°C are shown in Table 3 and in Table 4, respectively.

Table 3: Thermal Strain Values Obtained for Specimens Tested at 170°C

Fiber Orientation	Specimen #	T_{upper} (°C)	T_{lower} (°C)	Thermal Strain (%)
0/90°	T41-8	155	148	0.016
	T42-1	168	143	0.00821
	T42-6	144	145	0.0536
	T42-9	156	140	0.00563
	T42-16	148	148	0.0337
	T42-18	148	148	0.0134
	T43-3	148	148	0.0318
	T43-8	148	148	0.0379
	T43-11	149	139	0.0138
	Average:	**151.56**	**145.22**	**0.024**
±45°	T58-1	148	140	0.0272
	T58-6	158	149	-0.044
	T58-20	159	150	0.0331
	T59-1	153	148	-0.025
	T59-20	157	149	-0.044
	T59-24	158	148	-0.025
	T60-3	158	146	-0.00675
	T60-13	152	149	-0.014
	T68-1	153	149	0.0099
	T68-9	145	140	0.0871
	T68-19	154	148	-0.019
	T69-5	152	149	-0.062
	T69-9	158	150	-0.025
	T69-23	153	148	-0.021
	Average:	**154.14**	**147.36**	**-0.0092**

Table 4: Thermal Strain Values Obtained for Specimens Tested at 190°C

Fiber Orientation	Specimen #	T_{upper} (°C)	T_{lower} (°C)	Thermal Strain (%)
0/90°	T41-12	169	159	0.0271
	T41-20	176	162	0.00265
	T42-2	170	156	0.00629
	T42-14	166	155	0.0548
	T42-24	169	160	0.0866
	T43-13	163	158	0.0572
	Average:	**168.83**	**158.33**	**0.039**
±45°	T58-3	173	157	0.0401
	T58-16	167	159	0.0136
	T58-24	167	156	0.0327
	T59-14	164	155	0.0333
	T68-7	168	155	0.0197
	T68-16	166	154	0.0228
	T69-6	164	156	0.0521
	T69-8	166	156	0.0326
	T69-18	163	157	0.0226
	T69-20	175	161	0.0687
	Average:	**166.67**	**156.56**	**0.034**

5.3 Monotonic Tension and Monotonic Compression

5.3.1 Monotonic Tension

The results of the monotonic tension tests performed at 23, 170, and 190°C are given in Table 5-Table 7. The elastic modulus was calculated by taking a best fit line of the initial linear portion of the stress-strain curve. Failure was determined to have occurred when a drastic decrease in load was observed accompanied by a large sound event.

Table 5: Summary of Tensile Properties Obtained at 23°C

Fiber Orientation	Specimen #	Elastic Modulus (GPa)	UTS (MPa)	Failure Strain (%)
0/90°	T42-7	86.16	1185	1.36
	T42-10	86.61	1191	1.39
	T42-11	85.64	1174	0.995
	T42-22	83.03	1197	1.2
	T43-7	78.79	1182	1.566
	T43-17	83.67	1186	1.252
±45°	T58-2	15.84	243	12.82
	T68-14	19.62	250	13.66
	T68-17	19.27	244	11.33

Table 6: Summary of Tensile Properties Obtained at 170°C

Fiber Orientation	Specimen #	Elastic Modulus (GPa)	UTS (MPa)	Failure Strain (%)
0/90°	T42-16	78.67	1064	1.36
	T42-18	116.4	1110	0.9
	T43-3	88.63	1113	1.29
	T43-8	84.59	1112	1.32
±45°	T68-23	29.55	225	16.02
	T68-24	15.94	223	17.88
	T69-1	35.5	227	16.23
	T69-3	16.51	225	19.66

Table 7: Summary of Tensile Properties Obtained at 190°C

Fiber Orientation	Specimen #	Elastic Modulus (GPa)	UTS (MPa)	Failure Strain (%)
0/90°	T41-12	76.04	965	1.1
	T41-20	141	1019	0.6
	T42-2	141.4	1003	0.62
	T42-24	73.96	994	1.4
±45°	T58-16	30.84	186	16.96
	T60-23	14.67	146	14.66
	T68-7	15.29	186	17.13
	T69-20	13.28	161	21.68

At room temperature (23°C), the average UTS of the 0/90 specimens was 1185 MPa with an average failure strain of 1.29% and an average elastic modulus of 83.98 GPa. At 23°C, the stress-strain behavior, typified in Figure 16, is linear elastic to failure.

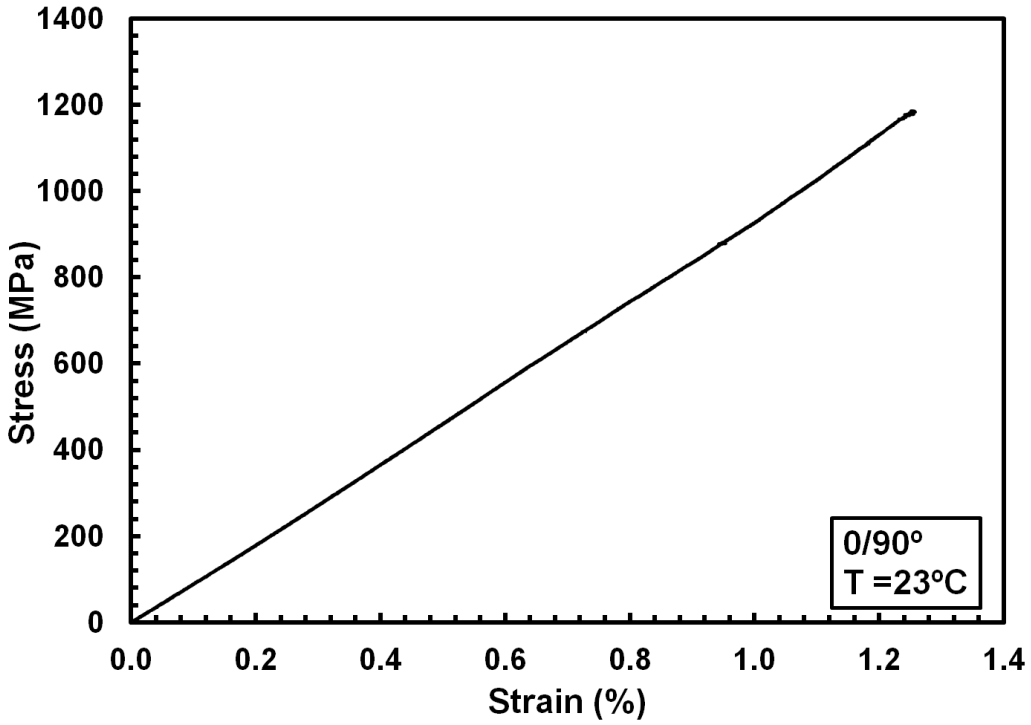

Figure 16: Representative Tensile Stress-Strain Curve Obtained for 0/90 Specimens at Room Temperature

At 23°C, the ±45 specimens produced an average UTS, failure strain, and modulus of 246 MPa, 12.60 %, and 18.24 GPa, respectively. The stress-strain behavior typical for specimens with ±45 fiber orientation is shown in Figure 17. The stress-strain curve shows an initial linear elastic region, but it becomes markedly nonlinear as the strain and stress approach 1.0% and 150 MPa, respectively. A slight drop in stress was observed following the transition from elastic to inelastic deformation. This is likely due to the failure of some plies in the specimen.

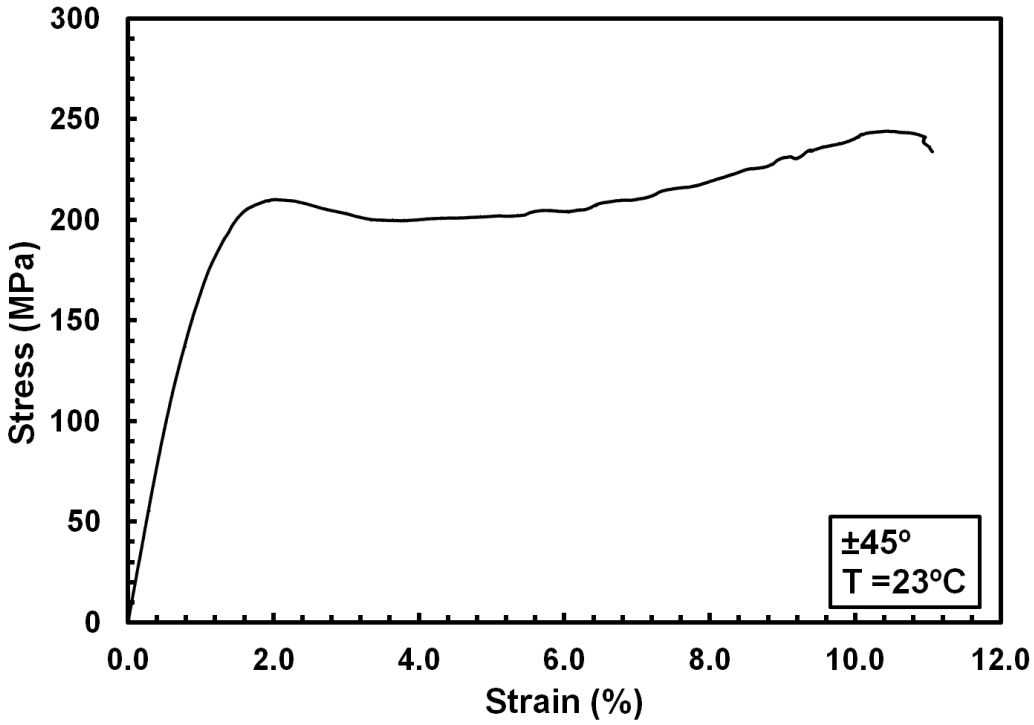

Figure 17: Representative Tensile Stress-Strain Curve Obtained for ±45 Specimens at Room Temperature

Figure 18 highlights the significant difference in strength and ductility between the two fiber orientations. The 0/90 specimens exhibit high strength and stiffness, but low failure strain. Conversely, the ±45 specimens produce much lower values of strength and stiffness, but larger values of failure strain. The 0/90 specimens exhibit linear elastic behavior until failure, while the stress-strain behavior of the ±45 specimens becomes strongly nonlinear as the stress exceeds 150 MPa.

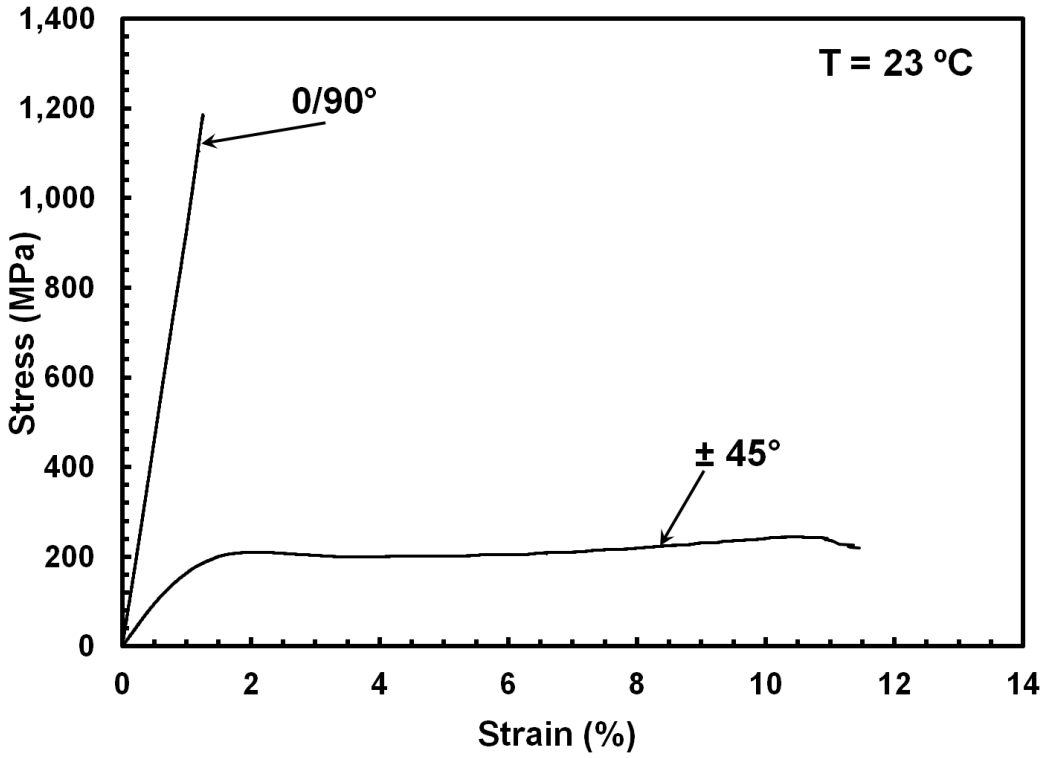

Figure 18: Representative Tensile Stress-Strain curves Obtained for 0/90 and ±45 Specimens at Room Temperature

At 170°C, the average UTS of the 0/90 specimens was 1100 MPa (7.17% decrease from the room temperature value), with an average Young's modulus of 92.07 GPa and an average failure strain of 1.22%. The ±45 specimens had an average UTS of 225 MPa (8.54% drop in UTS from the room temperature value), an average modulus of 24.38 GPa, and an average failure strain of 17.45%. The typical stress-strain curves obtained at 170°C for the 0/90 and ±45 fiber orientations are compared in Figure 19. A trend in stress-strain behavior similar to that noted at room temperature was observed again at 170°C.

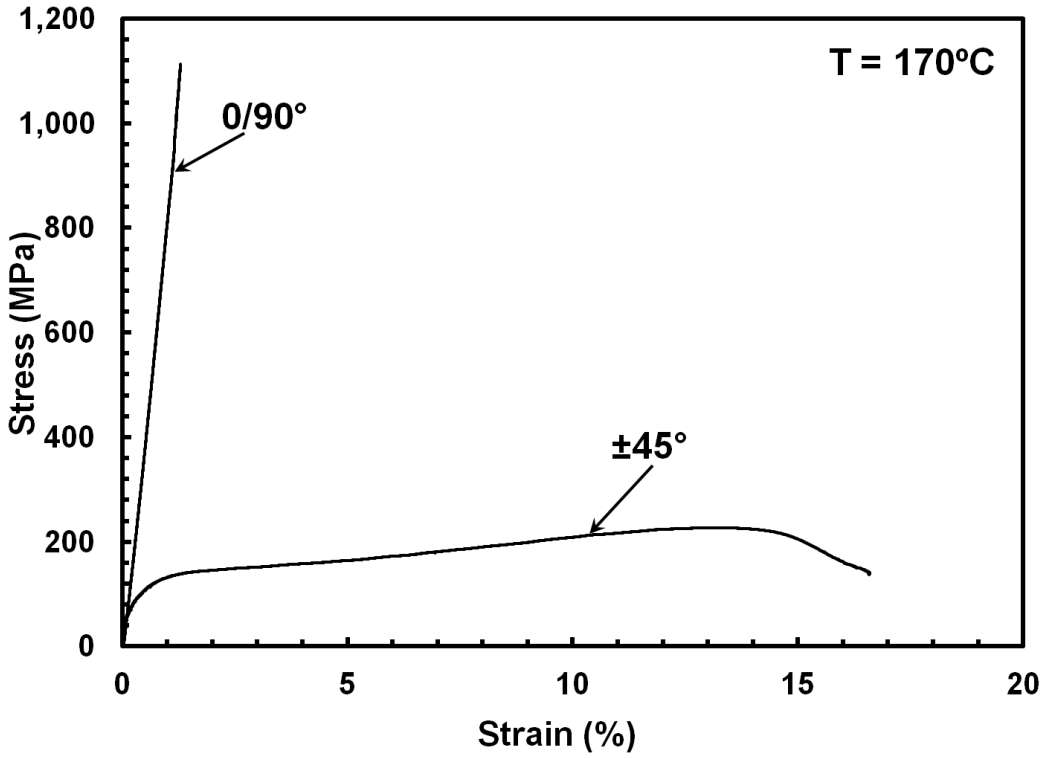

Figure 19: Representative Tensile Stress-Strain Curves Obtained for 0/90 and ±45 Specimens at 170°C

The strength and stiffness obtained for 0/90 fiber orientation at 170°C were only slightly lower than those obtained at 23°C (Figure 20). Apparently, elevated temperature has a minimal effect on the 0/90 tensile properties.

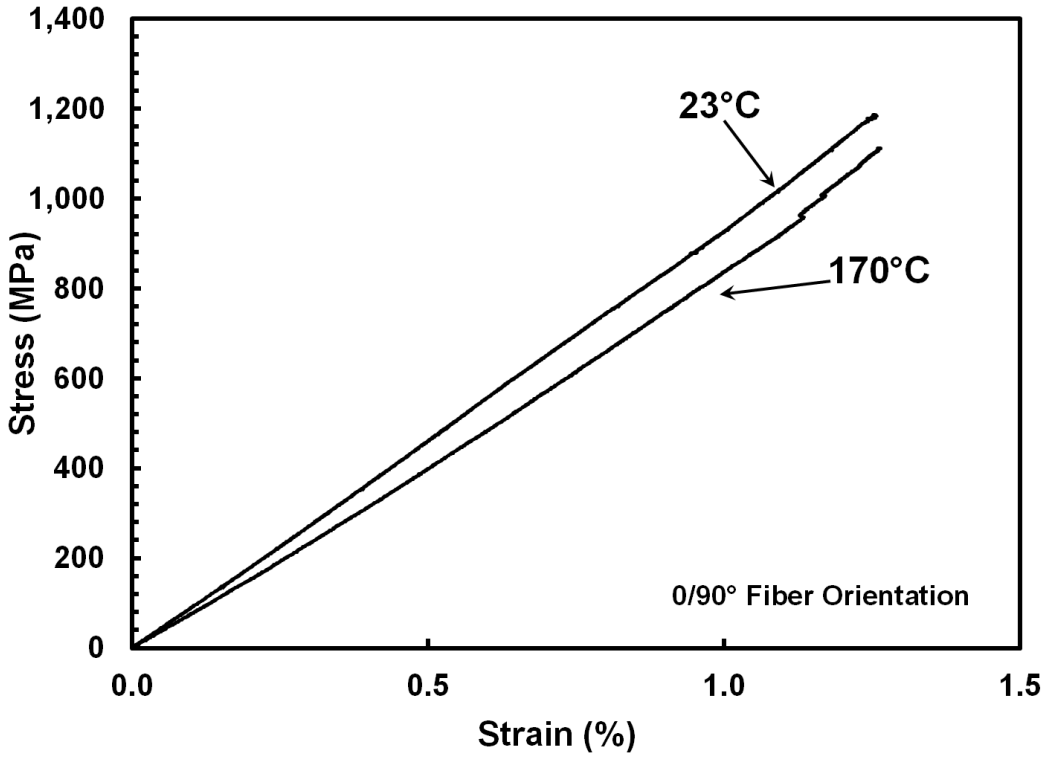

Figure 20: Representative Tensile Stress-Strain Curves Obtained for 0/90 Specimens at 23°C and 170°C

Conversely, increase in temperature from 23 to 170°C had a significant impact on the tensile properties of the ±45 specimens (Figure 21). Matrix plays a larger role in determining the properties and performance of a ±45 cross-ply, and matrix properties are typically more sensitive to temperature changes. At 170°C, the ±45 specimens produce a lower UTS along with a significantly larger failure strain. Furthermore, the ±45 composite exhibits a much smoother transition from linear to nonlinear deformation behavior at 170°C than at room temperature. Moreover, at 170°C, the transition from linear to nonlinear stress-strain behavior occurs at a much lower stress value.

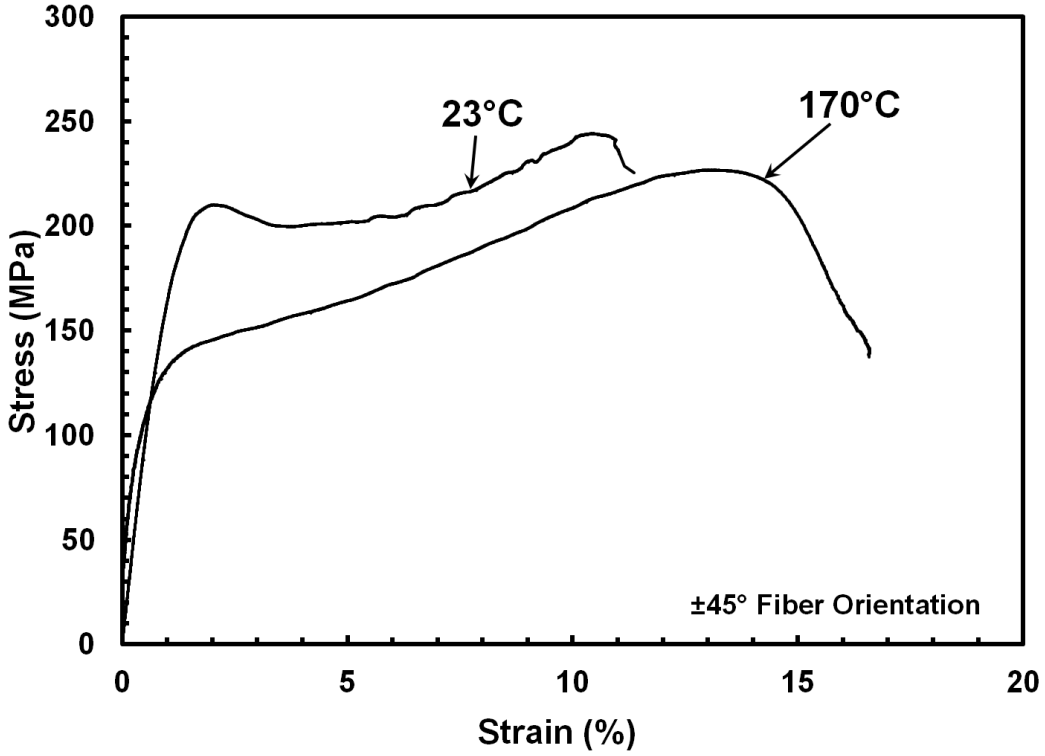

Figure 21: Representative Tensile Stress-Strain Curves Obtained for ±45 Specimens at 23°C and 170°C

Similar trends were observed in tests performed at 190°C. The 0/90 specimens had an average UTS of 995 MPa (16.03% decrease from room temperature value), an average modulus of 108.4 GPa and an average failure strain of 0.93%. The ±45 specimens produced an average UTS of 170 MPa (30.89% decrease from the room temperature value), an average modulus of 18.52 GPa, and an average failure strain of 17.61%. Figure 22 shows a comparison of the typical stress-strain curves obtained for the 0/90 specimens at all three test temperatures. Increasing temperature causes a decrease in UTS, but affects little else in the stress-strain curves.

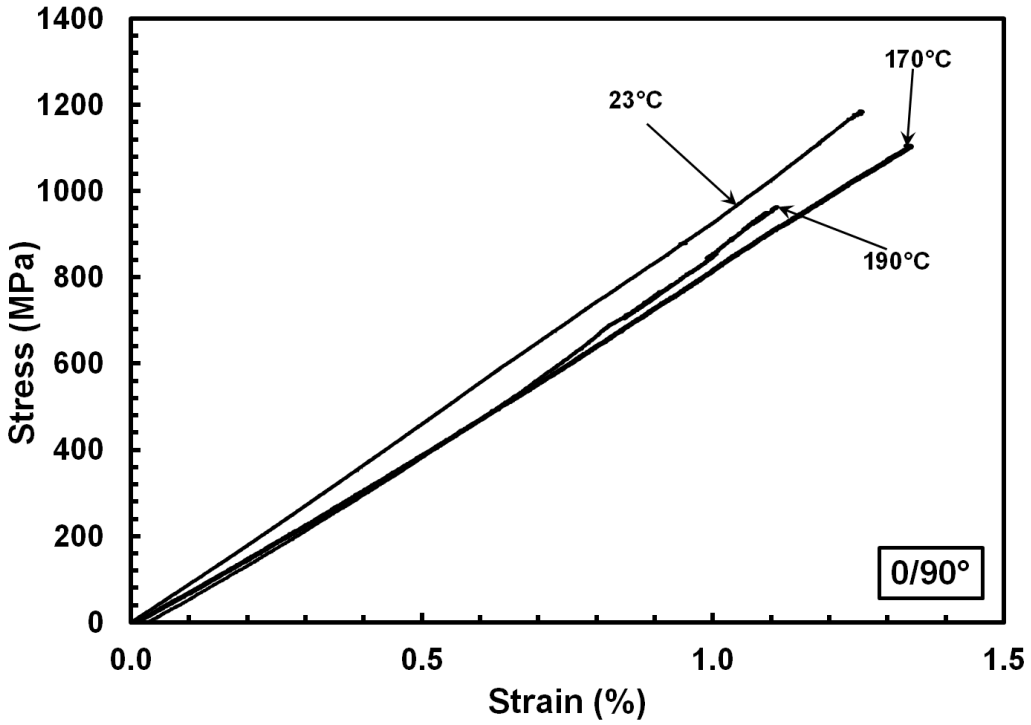

Figure 22: Representative Tensile Stress-Strain curves Obtained for 0/90 Specimens at 23°C, 170°C, and 190°C

The tensile stress-strain behaviors of the ±45 specimens at 23, 170, and 190°C are compared in Figure 23. The stress-strain curve obtained at 190°C is qualitatively similar to that produced at 170°C. However, a significant decrease in strength and stress at which the stress-strain behavior departs from linearity is seen in 190°C.

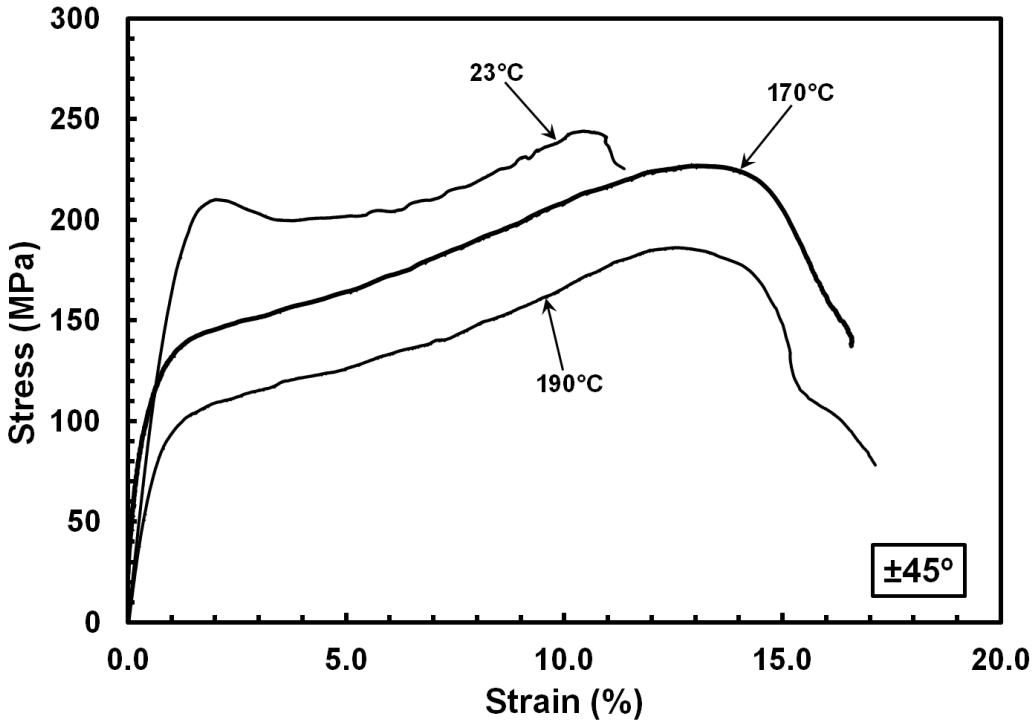

Figure 23: Representative Tensile Stress-Strain Curves Obtained for ±45 Specimens at 23°C, 170°C, and 190°C

The tensile stress-strain curves obtained for the IM7/BMI 5250-4 composite with 0/90 and ±45 fiber orientations at 23, 170, and 190°C are compared in Figure 24. At all temperatures of interest, the 0/90 specimens exhibit high strength. The temperature has little effect on the 0/90 strength, a fiber dominated mechanical property. Contrastingly, the tensile properties and stress-strain behavior of the ±45 specimens are less dependent on the fiber and, consequently, are more influenced by temperature.

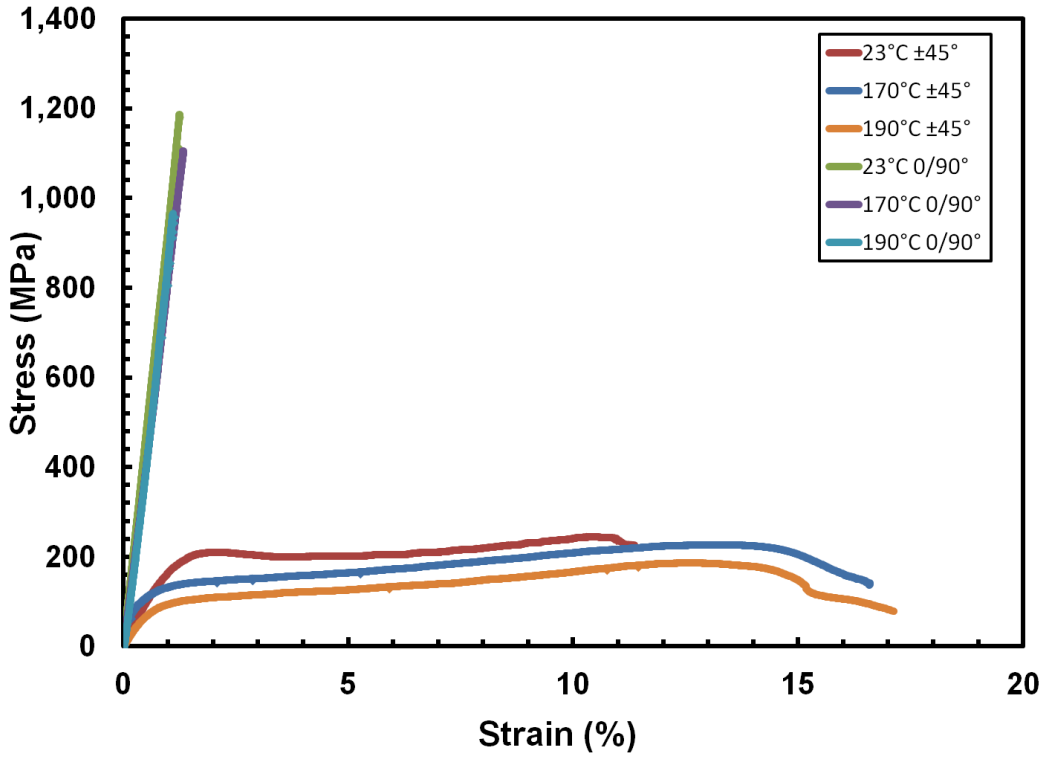

Figure 24: Representative Tensile Stress-Strain Curves Obtained for the IM7/BMI 5250-4 Composite at 23°C, 170°C, and 190°C

5.3.2 Monotonic Compression

The results for the monotonic compression tests performed in this study are displayed in Table 8 and Table 9.

Table 8: Summary of Compressive Properties Obtained at 23°C

Fiber Orientation	Specimen #	Elastic Modulus (GPa)	UCS (MPa)	Failure Strain (%)
0/90°	C54-4	55.82	-759	-3.94
	C54-21	65.44	-784	-2.47
	C55-13	66.33	-822	-1.54
	C55-24	75.7	-764	-1.06
±45°	C64-11	23.24	-209	-5.48
	C64-26	23.81	-208	-4.51
	C71-13	20.61	-211	-6.08
	C71-16	21.14	-212	-4.65

Table 9: Summary of Compressive Properties Obtained at 170°C

Fiber Orientation	Specimen #	Elastic Modulus (GPa)	UCS (MPa)	Failure Strain (%)
0/90°	C54-11	57.43	-397	-0.64
	C54-15	68.62	-340	-0.79
	C55-4	62.35	-408	-0.67
	C55-9	127.27	-372	-0.25
±45°	C64-5	17.62	-80	-7.53
	C64-9	30.89	-75	-8.13
	C70-4	33.56	-76	unavailable
	C70-11	16.18	-84	unavailable

The 0/90 specimens had an average UCS of -782 MPa, an average modulus of 65.85 GPa, and an average failure strain of -2.25%. As in the case of the tension tests, the ±45 specimens produced much lower values of strength and stiffness. The ±45 specimens had an average UCS of -211 MPa, an average modulus of 22.2 GPa, and an average failure strain of -5.18%. Stress-strain behavior in compression is typified in Figure 25 for the 0/90 fiber orientation and in Figure 26 for the ±45 fiber orientation.

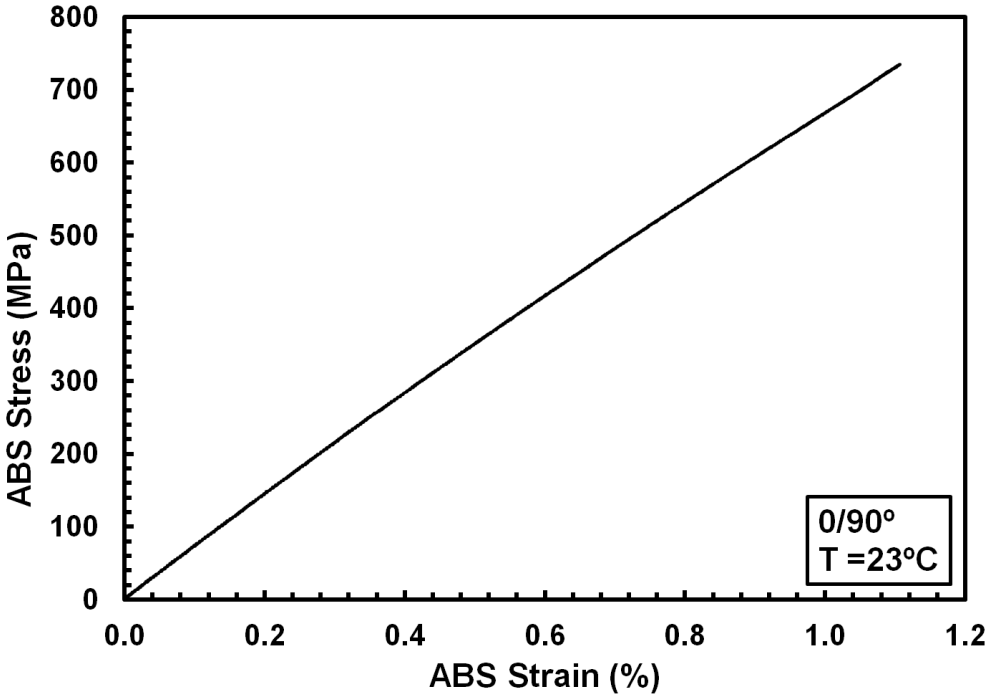

Figure 25: Representative Compression Stress-Strain Curve Obtained for 0/90 Fiber Orientation at 23°C

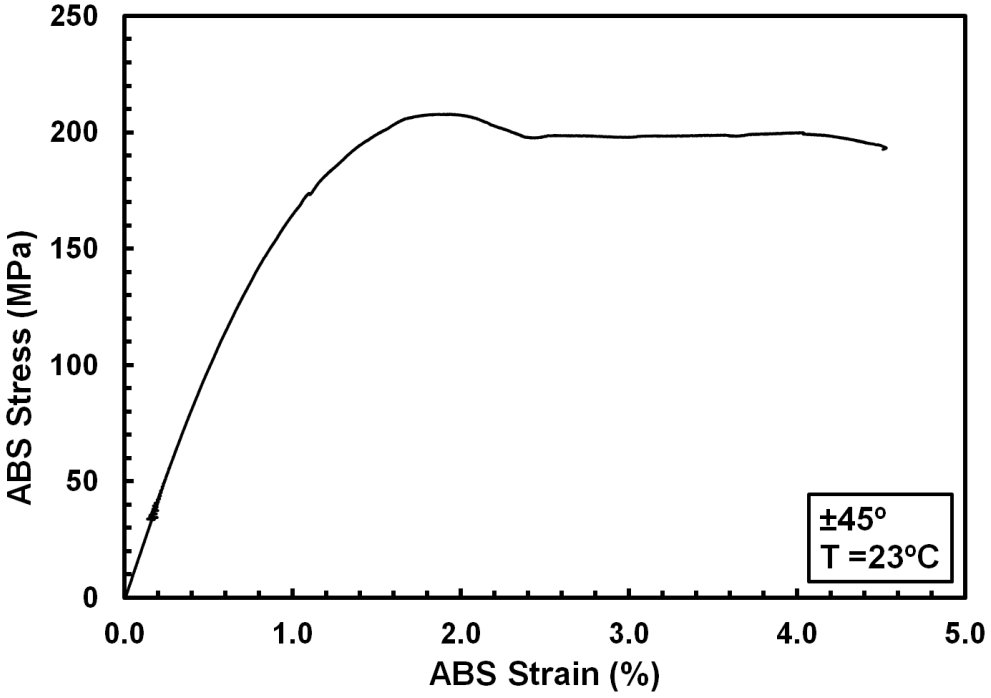

Figure 26: Representative Compression Stress-Strain curve Obtained for ±45 Fiber Orientation at 23°C

For both 0/90 and ±45 fiber orientations, stress-strain curves obtained in compression were similar to those produced in tension. As seen in Figure 27, the 0/90 stress-strain behavior is linear elastic to failure, while the ±45 stress-strain behavior shows an initial linear elastic portion then quickly departs from linearity. Moreover, the strength and stiffness of the 0/90 fiber orientation are much higher than those of the ±45 fiber orientation.

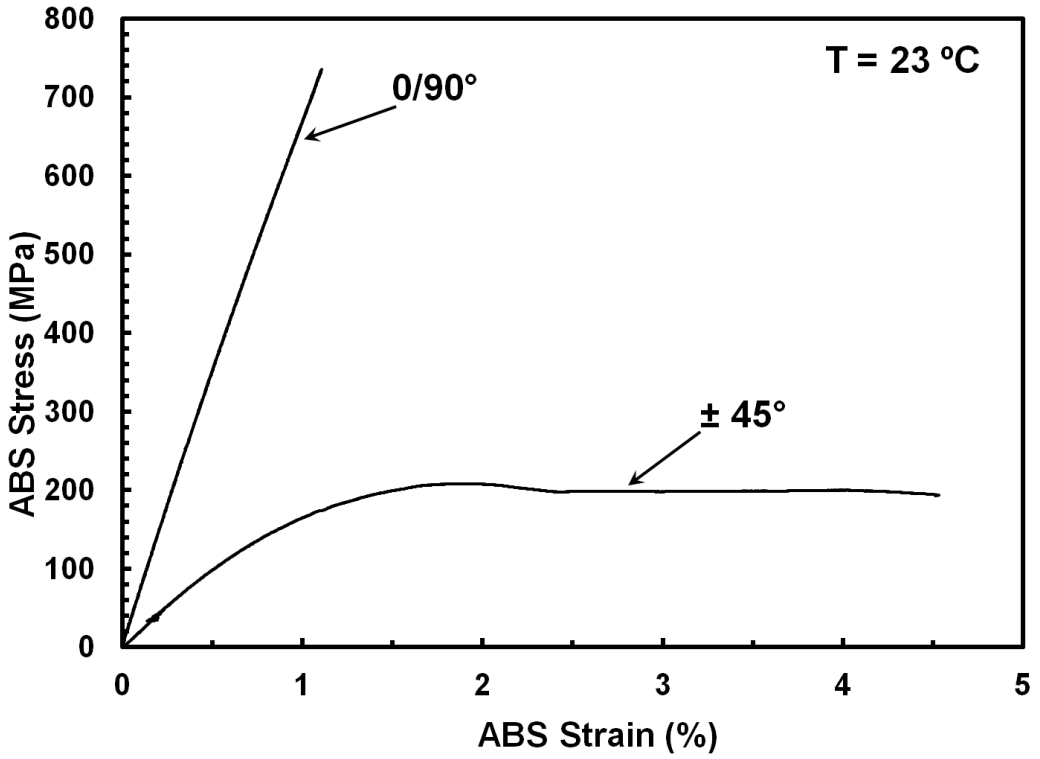

Figure 27: Representative Compression Stress-Strain Curves Obtained for 0/90 and ±45 Fiber Orientations at 23°C

When the temperature was raised to 170°C, the 0/90 specimens achieved an average UCS of -379 MPa, an average modulus of 78.92 GPa, and an average failure strain of -0.59%. Note a significant 51.53% decrease in UCS compared to the room-temperature value. At 170°C, the ±45 specimens had an average UCS of -78.75 MPa, an average modulus of

24.56 GPa, and an average failure strain of -7.98%. Again, note a drastic 62.68% drop in UCS compared to the room-temperature value. The changes in strength and stiffness with temperature for both fiber orientations are illustrated in Figure 28.

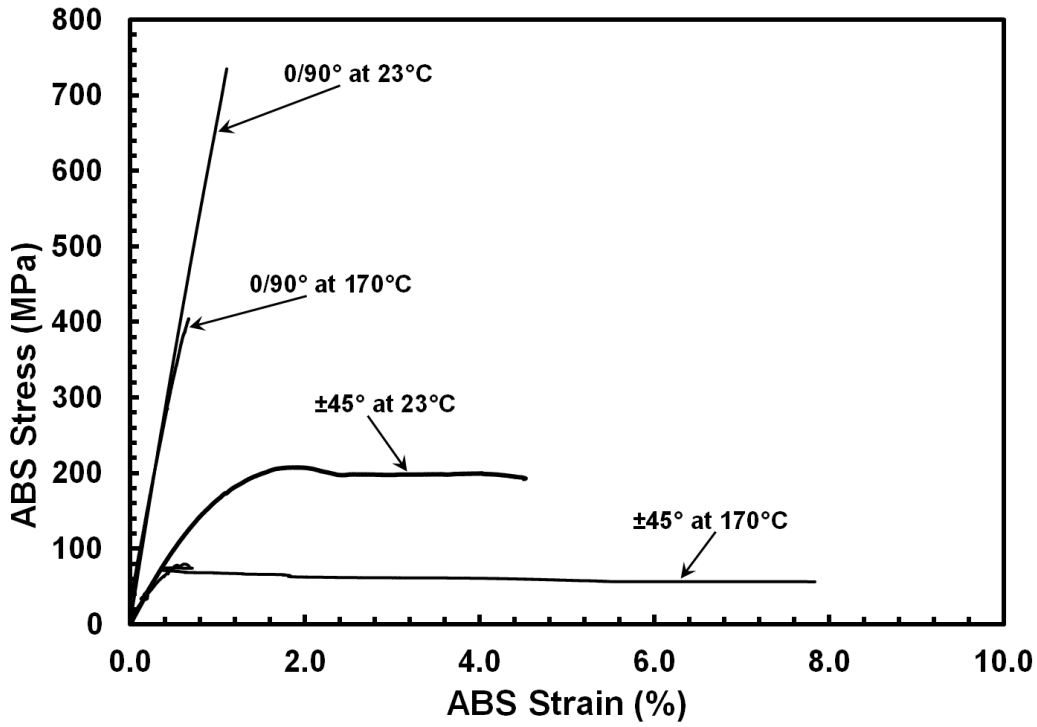

Figure 28: Representative Compression Stress-Strain Curves Obtained for 0/90 and ±45 Fiber Orientations at 23°C and 170°C

5.3.3 Tension vs. Compression

Like many other materials, the IM7/BMI 5250-4 composite behaved differently in tension and compression. Figure 29 emphasizes a dramatic difference in tensile and compressive properties obtained at 23°C for the 0/90 and ±45 fiber orientations. Recall that tensile behavior and properties of a 0/90 cross-ply are dominated by the strong and stiff fibers. Hence, we have high values of tensile strength and stiffness. In contrast, behavior of a 0/90 cross-ply in compression is strongly influenced by the weak matrix.

As a result, much lower values of strength and stiffness are produced in compression. The stress-strain behavior of the ±45 cross-ply is influenced equally by the fibers and the matrix. Hence the tensile and compressive stress-strain curves obtained for the ±45 specimens are qualitatively similar (Figure 30).

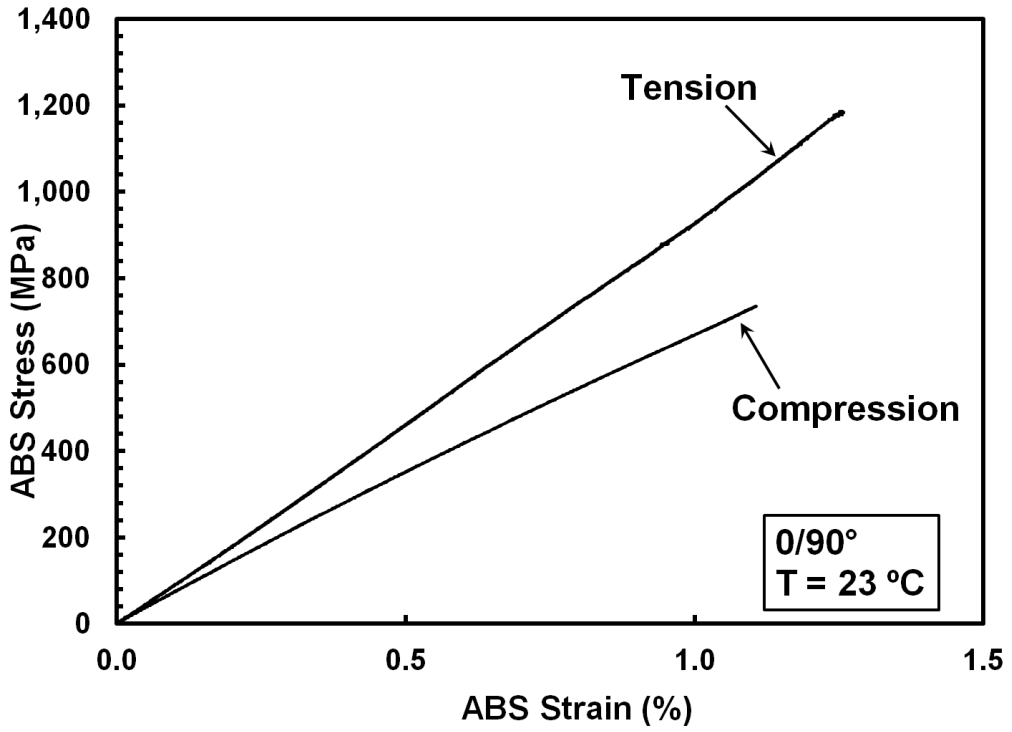

Figure 29: Representative Tension and Compression Stress-Strain Curves Obtained for 0/90 Fiber Orientation at 23°C

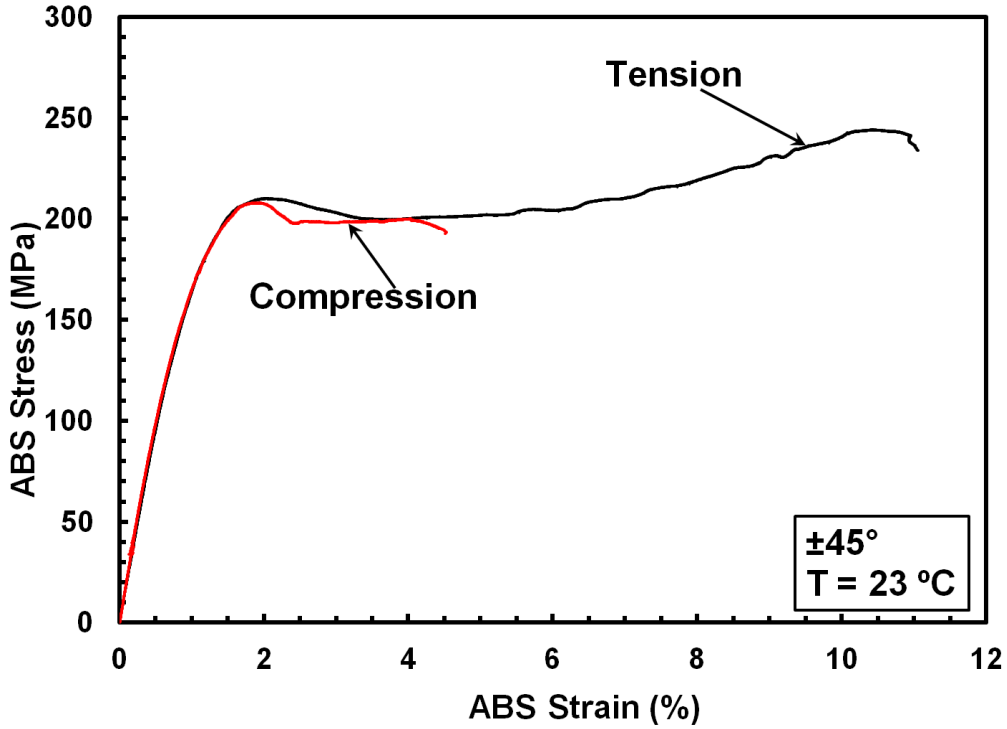

Figure 30: Representative Tension and Compression Stress-Strain Curves Obtained for ±45 Fiber Orientation at 23°C

Figure 31 further illustrates the significant differences in stress-strain behaviors of the 0/90 and ±45 specimens in tension and compression.

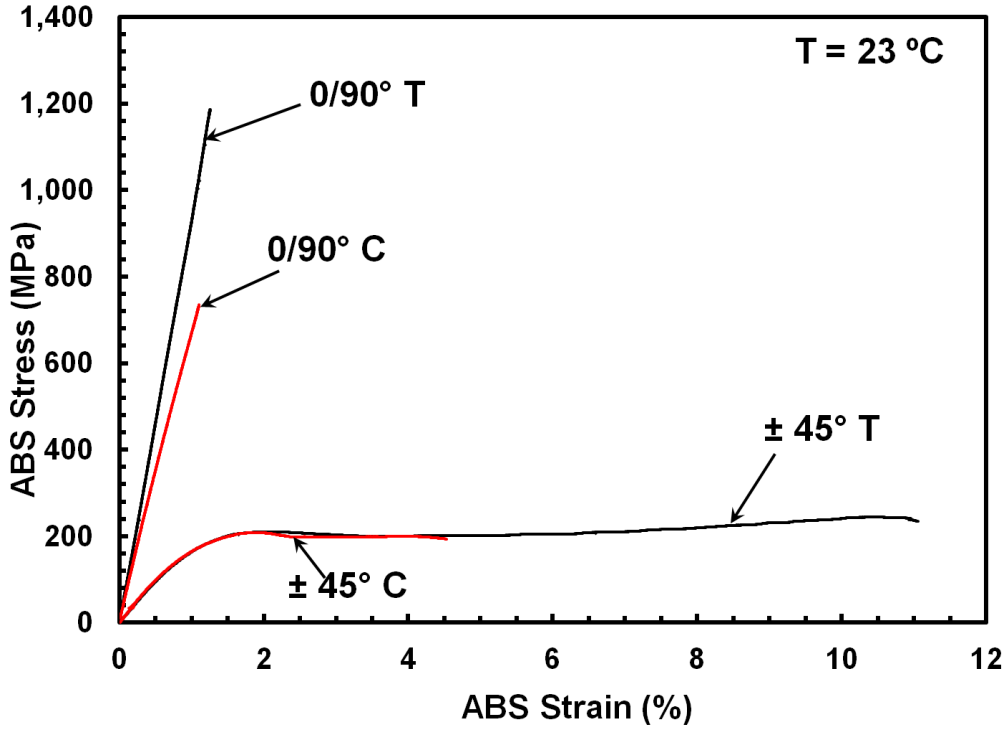

Figure 31: Representative Tension and Compression Stress-Strain Curves Obtained for 0/90 and ±45 Fiber Orientations at 23°C

5.4 Tension-Tension Fatigue

All tension-tension fatigue tests were performed in force control with a sinusoidal waveform at a frequency of 1 Hz with a minimum to maximum stress ratio of R=0.1. Fatigue run-out was defined as 10^5 cycles.

5.4.1 Tension-Tension Fatigue at 23°C

The results of the tension-tension fatigue tests at 23°C are summarized in Table 10 and Table 11.

Table 10: Tension-Tension Fatigue Results for 0/90 Specimens at 23°C

Specimen #	σ_{max} (MPa)	σ_{max} (% UTS)	Cycles to Failure
T41-18	950	80	100000
T43-12	1065	90	100000

Table 11: Tension-Tension Fatigue Results for ±45 Specimens at 23°C

Specimen #	σ_{max} (MPa)	σ_{max} (% UTS)	Cycles to Failure
T59-9	220	89.55	9
T58-12	220	89.55	9
T69-15	200	81.41	110
T60-18	200	81.41	250
T68-12	185	75.31	542
T69-2	185	75.31	458
T59-8	170	69.20	2930
T68-10	170	69.20	3106
T68-8	150	61.06	15582
T59-18	150	61.06	24466
T58-14	127	51.70	53329
T68-20	127	51.70	34444
T58-11	100	40.71	100000
T60-2	85	34.60	100000
T60-4	85	34.60	100000

The tension-tension fatigue results obtained for the 0/90 specimens at 23°C are also presented as the maximum stress vs. cycles to failure (S-N) curve in Figure 32.

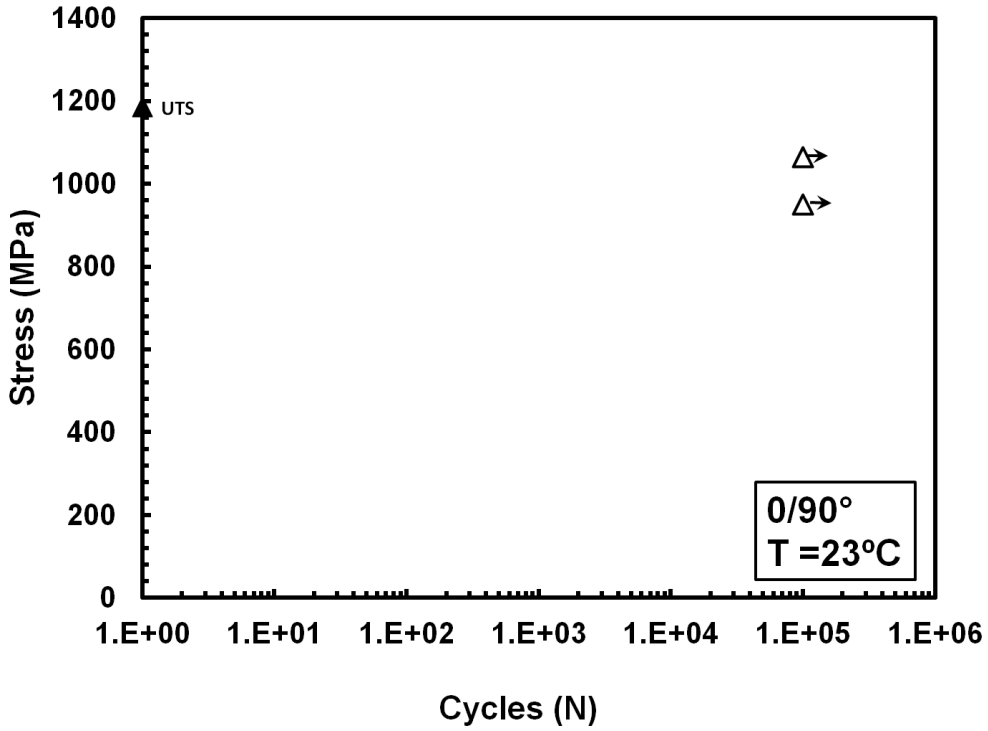

Figure 32: Maximum Stress vs. Cycles to Failure for the 0/90 Specimens at 23°C. Arrow Indicates Specimen Achieved Fatigue Run-Out.

As seen in Figure 32, the 0/90 specimens performed exceptionally well under tension-tension fatigue. Fatigue run-out of 10^5 cycles was reached for the maximum stress as high as 90% UTS. Figure 33 shows the evolution of the stress-strain hysteresis behavior with fatigue cycles for the maximum stress of 950 MPa (80% UTS). The stress-strain curves in Figure 33 are representative of the results obtained for the 0/90 fiber orientation in all tension-tension fatigue tests at 23°C. Results in Figure 33 reveal only minimal strain ratcheting (strain accumulation with cycles) and little stiffness loss. These observations are further confirmed in Figure 34 and Figure 35. Figure 34 shows only a slight increase in strain over the lifetime of the fatigue tests. Figure 35 shows virtually no change in normalized modulus (i.e. modulus normalized by the modulus obtained on the first cycle) with fatigue cycles.

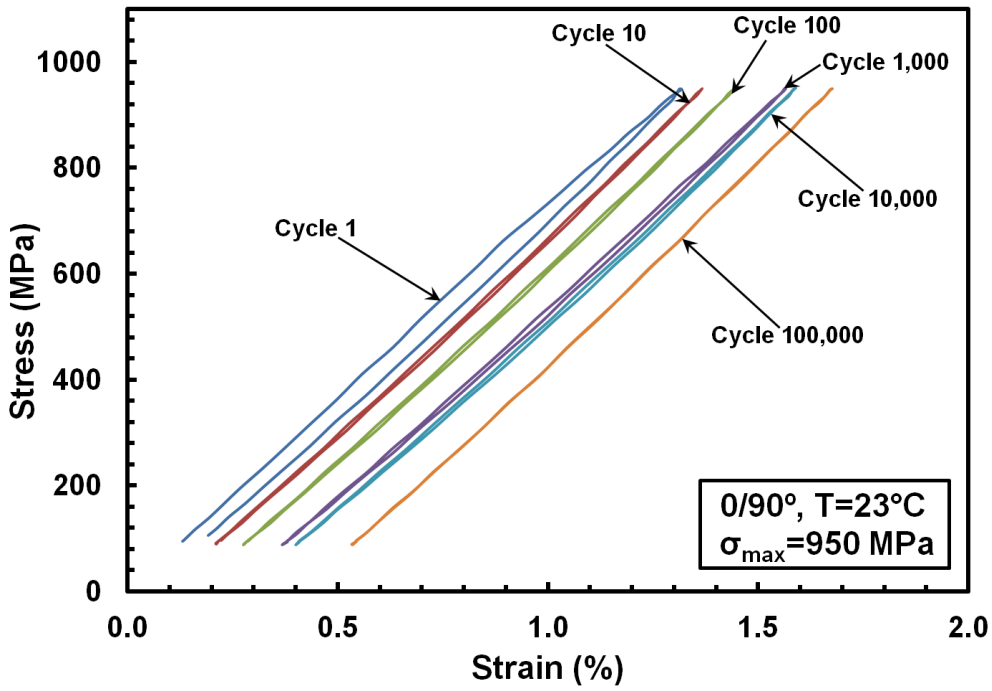

Figure 33: Evolution of Stress-Strain Hysteresis Response with Fatigue Cycles for Specimen T41-18 with 0/90 Fiber Orientation at 23°C

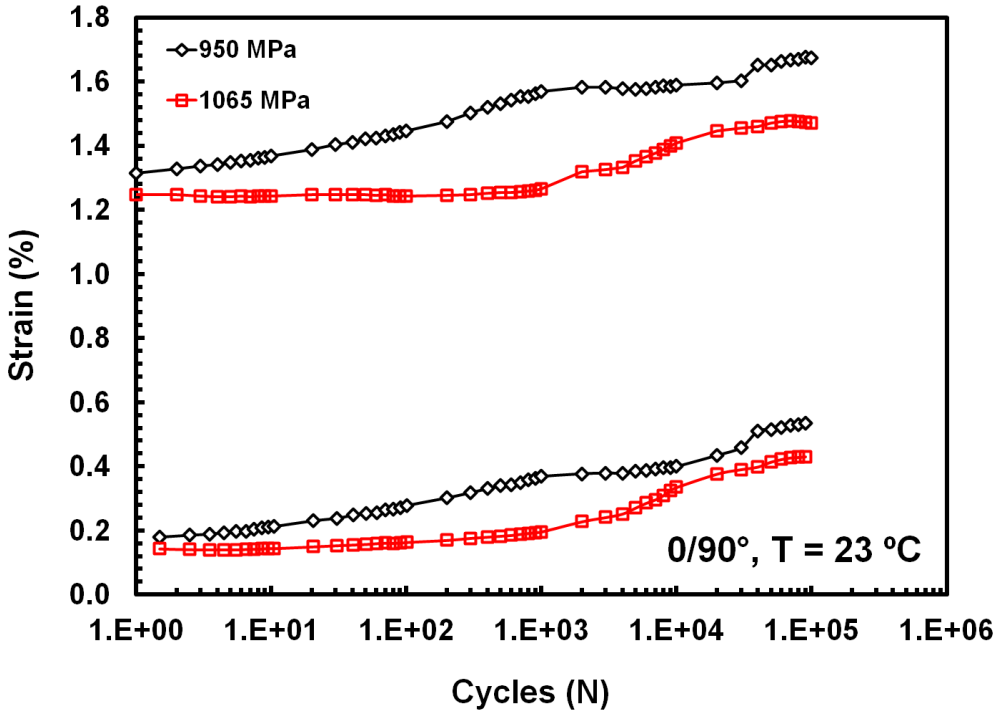

Figure 34: Minimum and Maximum Strains vs. Fatigue Cycles for 0/90 Specimens at 23°C

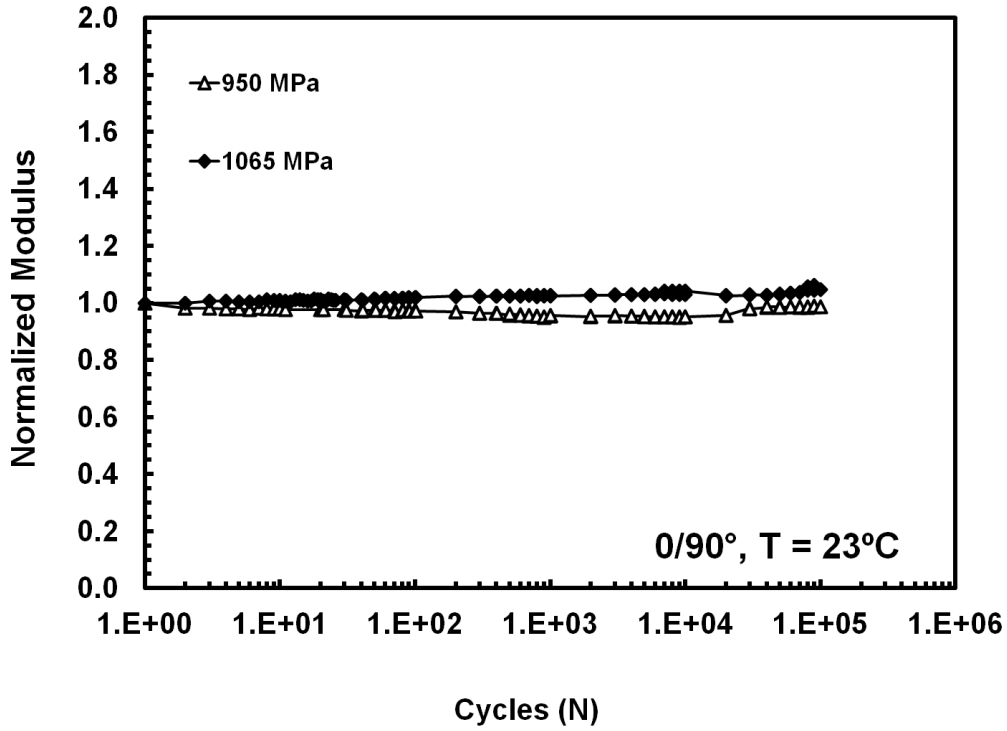

Figure 35: Normalized Modulus vs. Fatigue Cycles for 0/90 Specimens at 23°C

The tension-tension fatigue loading was much more demanding for the ±45 specimens as evidenced by the maximum stress vs. cycles to failure (S-N curve) in Figure 36. It is important to note that two tests were performed at most stress levels, and 220 MPa, 170 MPa, and 85 MPa show 2 data points each.

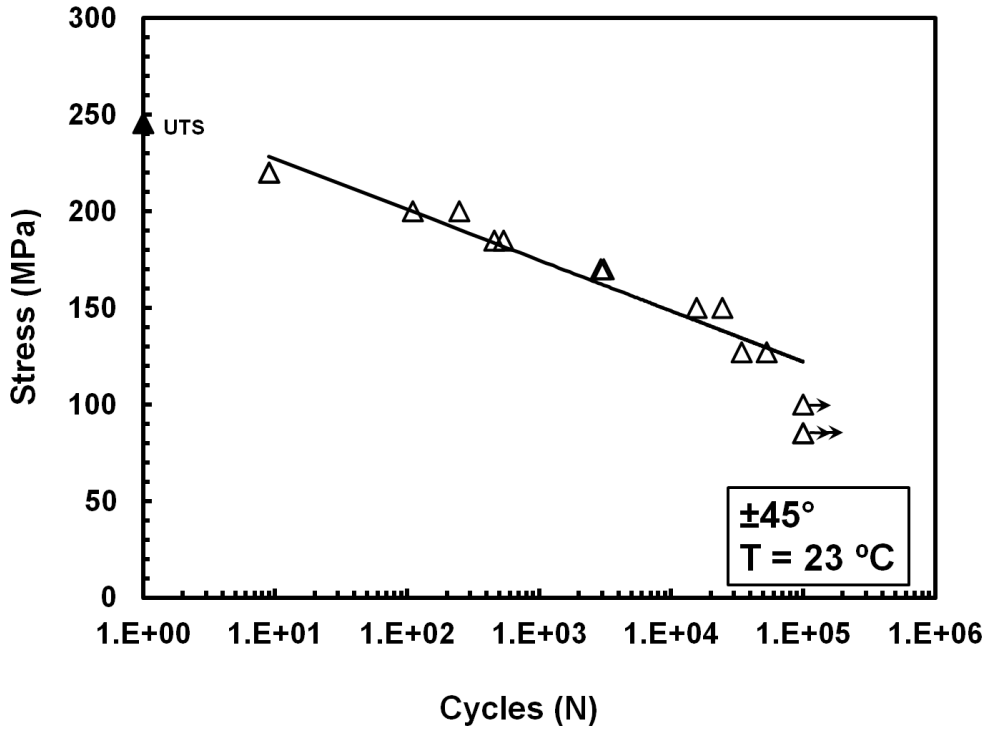

Figure 36: S-N Curve Obtained for the ±45 Specimens at 23°C. Arrow Indicates Specimen Achieved Fatigue Run-Out.

A weaker fatigue performance of the ±45 fiber orientation is a direct result of an increased influence of the matrix material on the composite performance. For the ±45 fiber orientation, fatigue run-out was achieved only at a maximum stress of 40% UTS. In Figure 37, the maximum and minimum strains stay almost constant until just before failure, where a rapid increase in strain was observed. Figure 38 shows minimal change in normalized modulus occurs until just prior to failure.

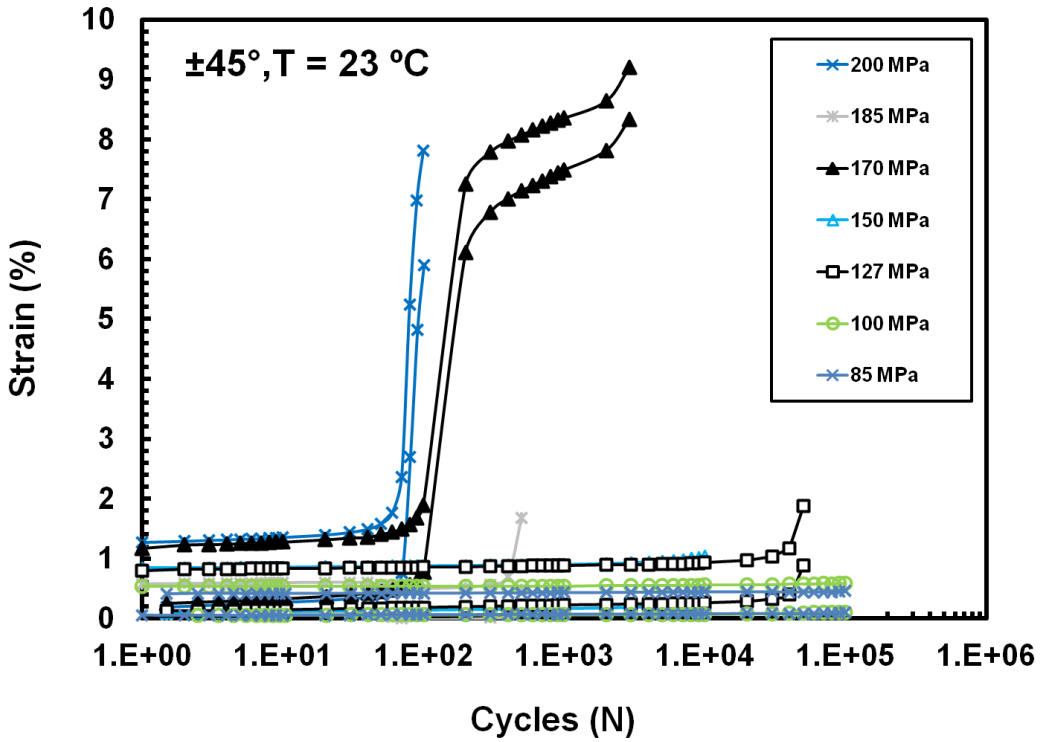

Figure 37: Minimum and Maximum Strains vs. Fatigue Cycles for ±45 Specimens at 23°C

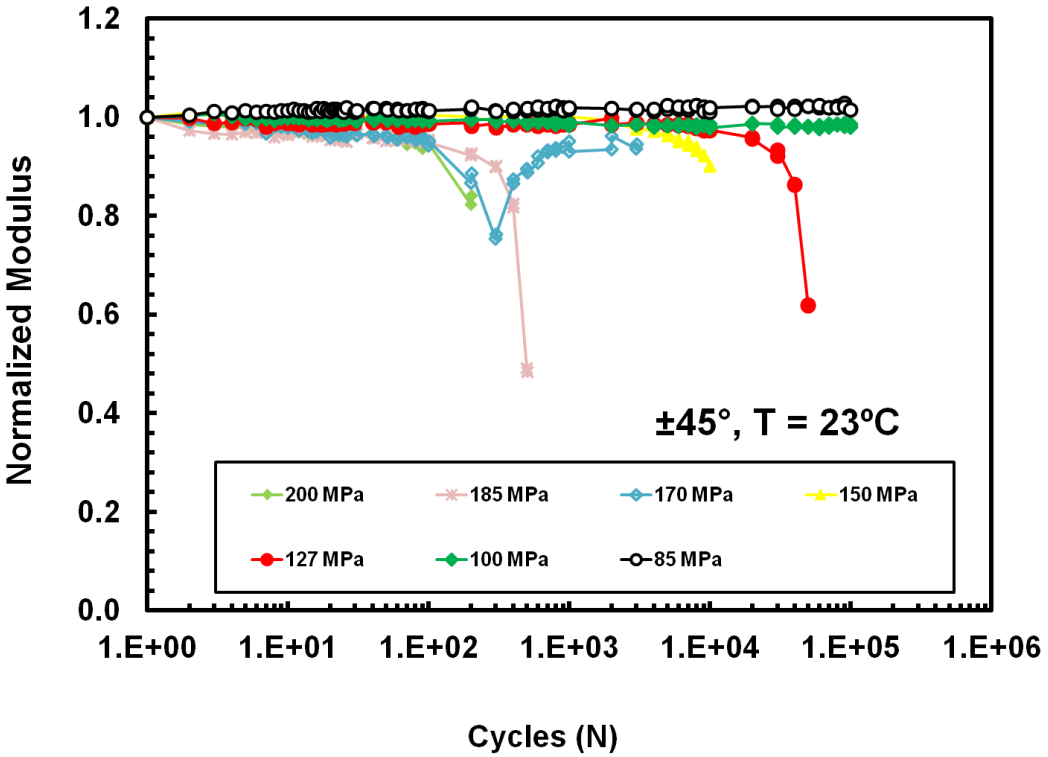

Figure 38: Normalized Modulus vs. Fatigue Cycles for ±45 Specimens at 23°C

However, for the ±45 fiber orientation, the evolution of the stress-strain hysteresis behavior with fatigue cycles changes drastically with the maximum stress. Results presented in Figure 39 for the maximum stress of 200 MPa are in stark contrast to the results obtained with the maximum stress of 100 MPa (Figure 40). The 200 MPa test accumulates a large amount of strain in very few cycles, while the 100 MPa test sees only a slight increase in strain over a much longer cycle life. Recall that fatigue run-out was achieved in the 100 MPa test.

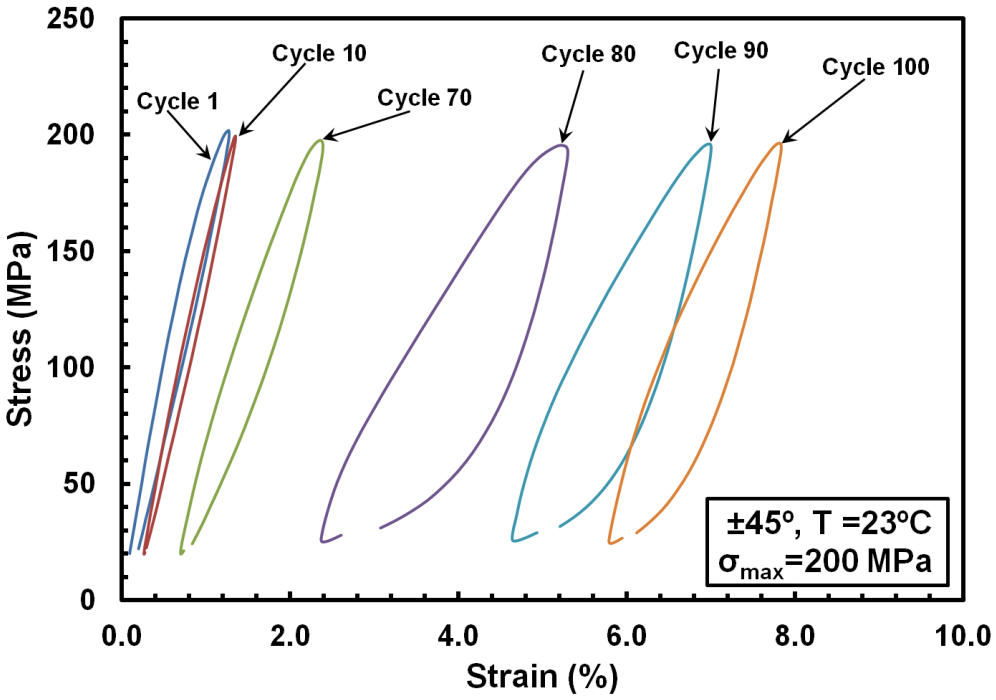

Figure 39: Evolution of Stress-Strain Hysteresis Response with Fatigue Cycles for Specimen T69-15 with ±45 Fiber Orientation at 23°C. σ_{max}=200 MPa.

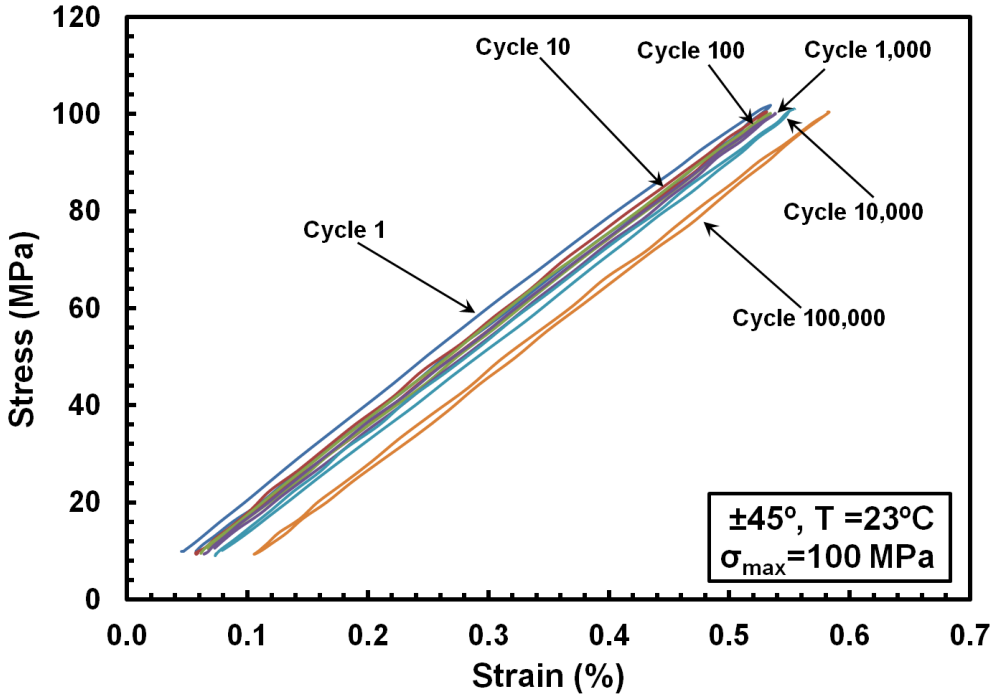

Figure 40: Evolution of Stress-Strain Hysteresis Response with Fatigue Cycles for Specimen T58-11 with ±45 Fiber Orientation at 23°C. σ_{max}=100 MPa.

Figure 41 compares the S-N curves obtained for the two fiber orientations under tension-tension fatigue. The ±45 specimens show a drastic reduction in fatigue life and overall fatigue performance.

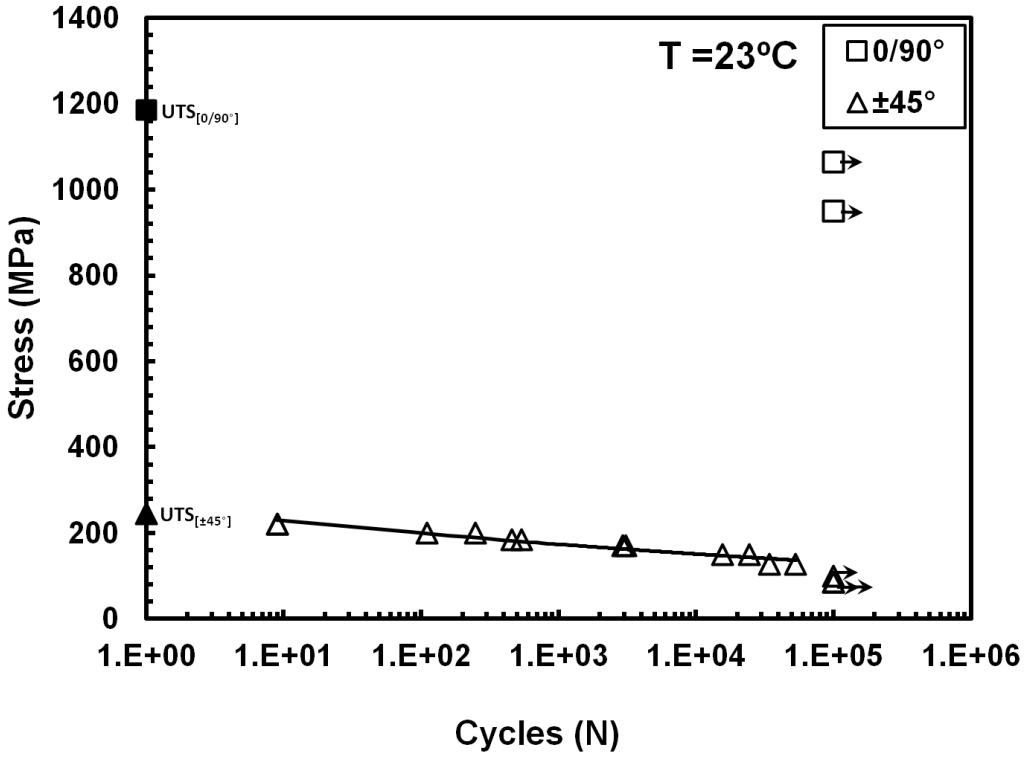

Figure 41: S-N Curves for ±45 and 0/90 Specimens at 23°C. Arrow Indicates Specimen Achieved Fatigue Run-Out.

5.4.2 Tension-Tension Fatigue at 170°C

The results of the tension-tension fatigue tests at 170°C are summarized in Table 12 and Table 13.

Table 12: Tension-Tension Fatigue Results for 0/90 Specimens at 170°C

Specimen #	σ_{max} (MPa)	σ_{max} (% UTS)	Cycles to Failure
T41-8	880	80.02	100000
T43-11	990	90.02	99424

Table 13: Tension-Tension Fatigue Results for ±45 Specimens at 170°C

Specimen #	σ_{max} (MPa)	σ_{max} (% UTS)	Cycles to Failure
T60-13	200	88.89	6
T69-23	200	88.89	51
T68-1	185	82.22	91
T59-1	185	82.22	232
T58-1	170	75.56	1140
T58-20	170	75.56	714
T68-19	150	66.67	9102
T69-9	150	66.67	1788
T69-5	127	56.44	10306
T68-3	127	56.44	9746
T58-6	110	48.89	27504
T60-3	110	48.89	82772
T59-20	100	44.44	100000
T68-9	100	44.44	100000

The tension-tension fatigue results obtained for the 0/90 specimens at 170°C are also presented as the maximum stress vs. cycles to failure (S-N) curve in Figure 42. Notably, the results obtained at 170°C are similar to those obtained at 23°C. Fatigue run-out was achieved at 880 MPa (80% UTS). The specimen tested at 990 MPa (90% UTS) failed after 99,424 cycles nearly achieving fatigue run-out of 10^5 cycles.

As expected, Figure 43 shows only a small increase in strain with cycles in the 880 MPa test. Likewise, Figure 44 shows virtually no change in normalized modulus over the duration of the 880 MPa test.

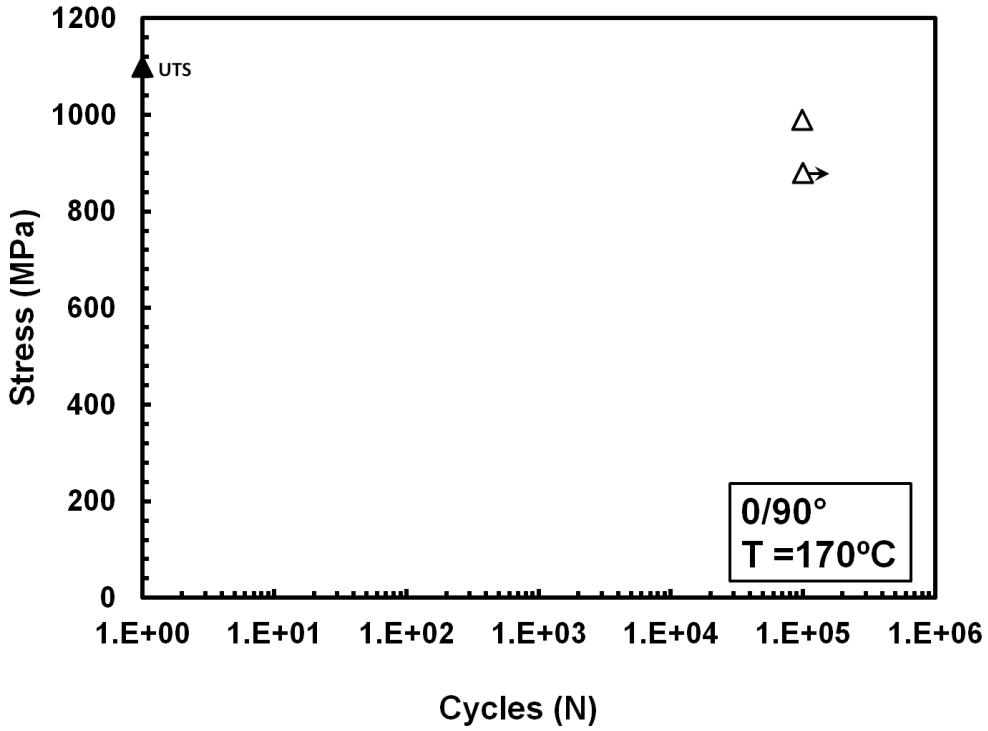

Figure 42: Maximum Stress vs. Cycles to Failure for the 0/90 Specimens at 170°C. Arrow Indicates Specimen Achieved Fatigue Run-Out.

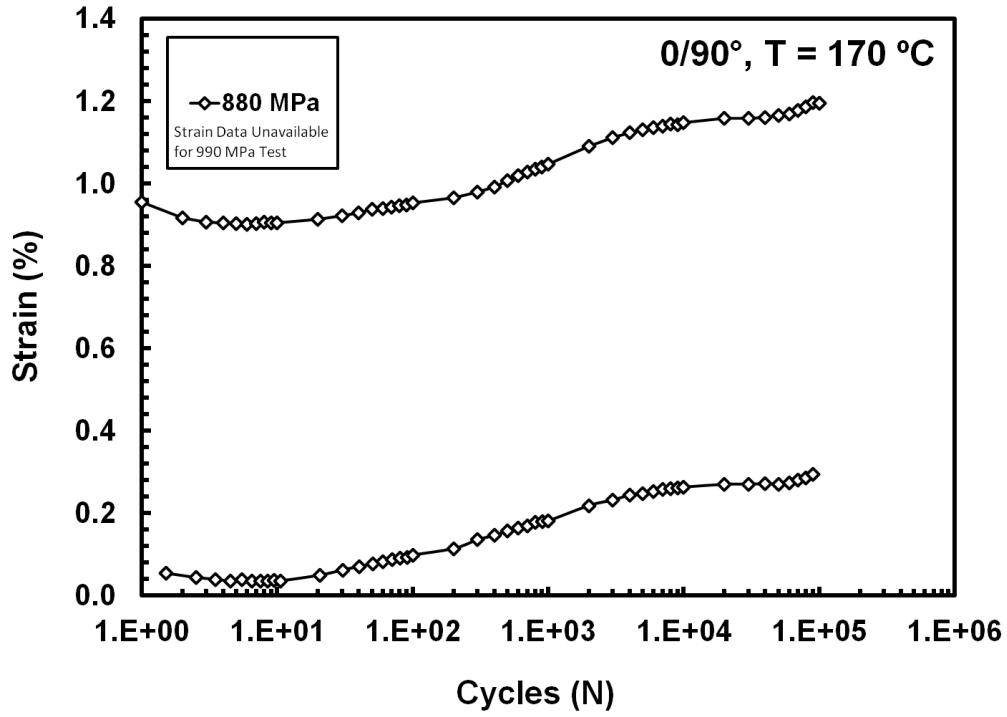

Figure 43: Minimum and Maximum Strains vs. Fatigue Cycles for 0/90 Specimens at 170°C

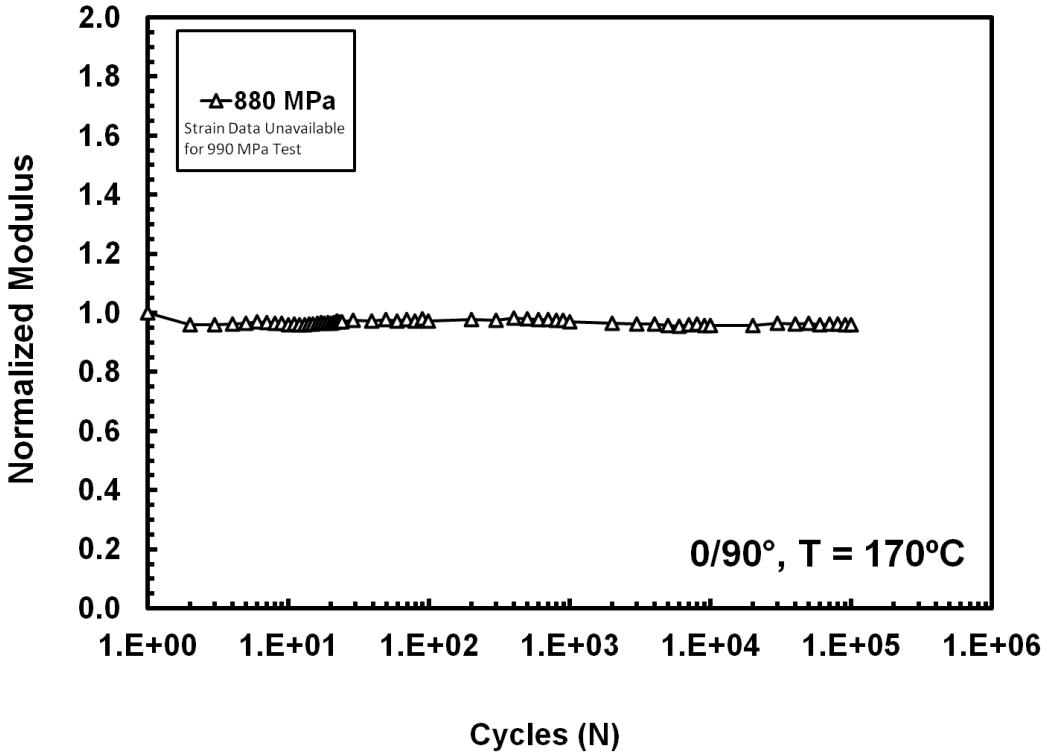

Figure 44: Normalized Modulus vs. Fatigue Cycles for 0/90 Specimens at 170°C

Figure 45 further confirms that little strain was accumulated over the 100,000 cycles at a maximum stress of 880 MPa. Furthermore, Figure 45 shows virtually no change in modulus with fatigue cycles.

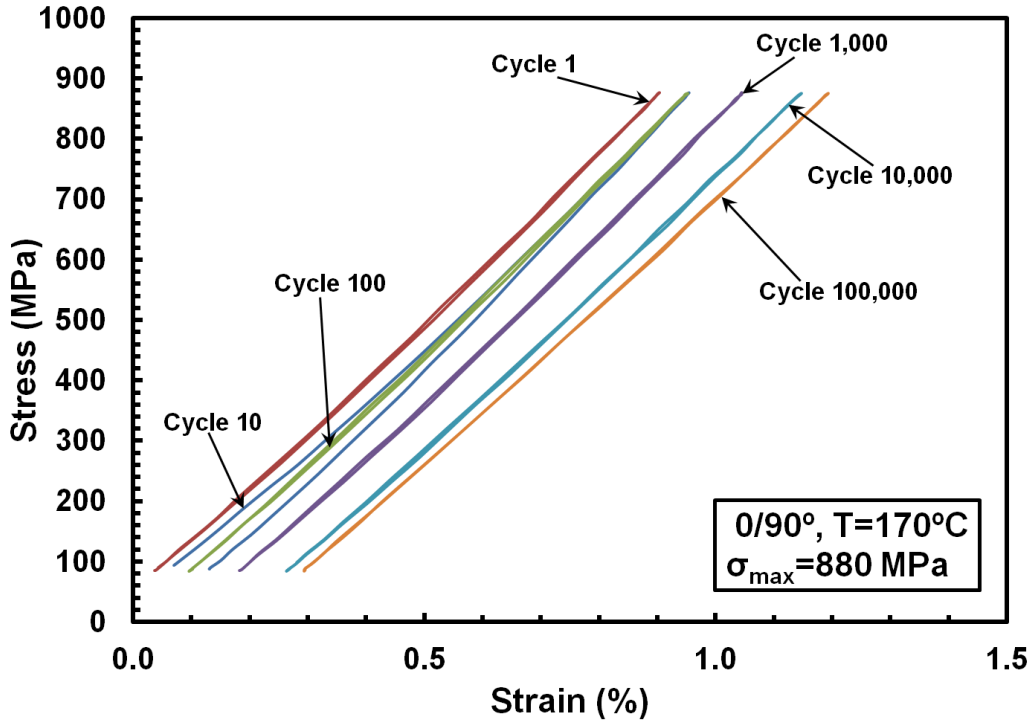

Figure 45: Evolution of Stress-Strain Hysteresis Response with Fatigue Cycles for Specimen T41-8 with 0/90 Fiber Orientation at 170°C

Tension-tension fatigue behavior of the ±45 specimens at 170°C was qualitatively similar to that at 23°C. The S-N curve obtained for the ±45 fiber specimens at 170°C is presented in Figure 46. At 170°C, fatigue run-out was achieved at a maximum stress level of 100 MPa (the same as at room temperature).

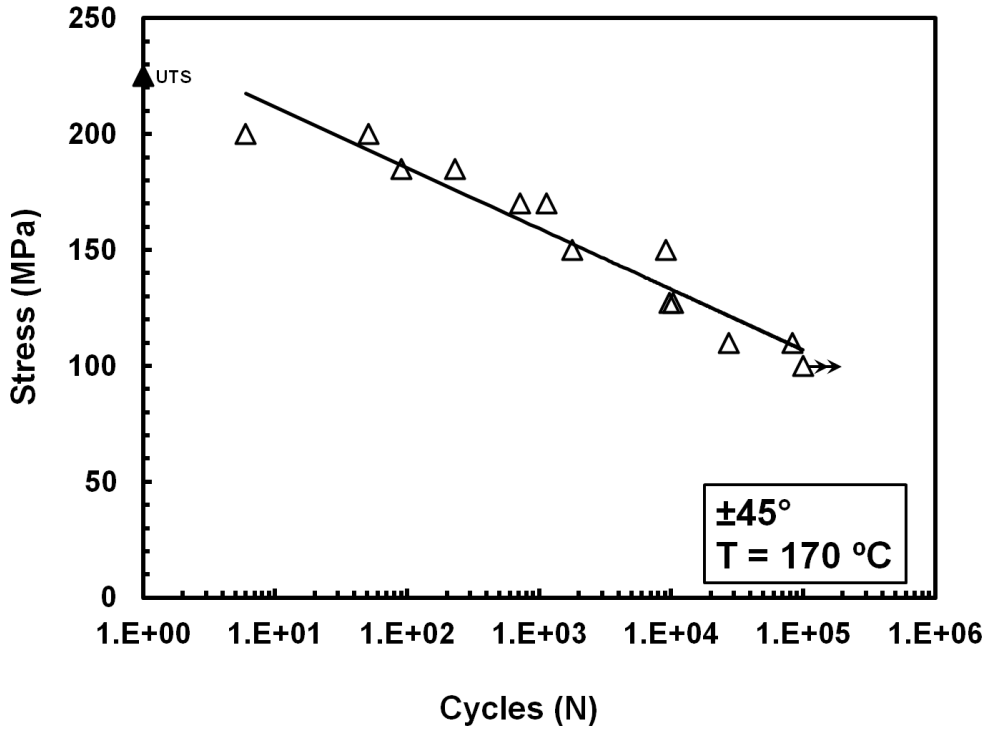

Figure 46: S-N Curve Obtained for the ±45 Specimens at 170°C. Arrow Indicates Specimen Achieved Fatigue Run-Out.

As in the case of room temperature tests, at 170°C, relatively little strain is accumulated with cycling until just prior to failure, where a rapid increase in strain is observed (Figure 47). Figure 48 shows that the normalized modulus remains nearly constant until just before failure. As the specimen approaches failure, a significant loss of normalized modulus and a noticeable increase in strain are observed. Two specimens exhibited an early decrease in normalized modulus followed by an extended period of constant normalized modulus. These changes were likely due to an early failure of a few plies which did not lead to the ultimate failure of the composite.

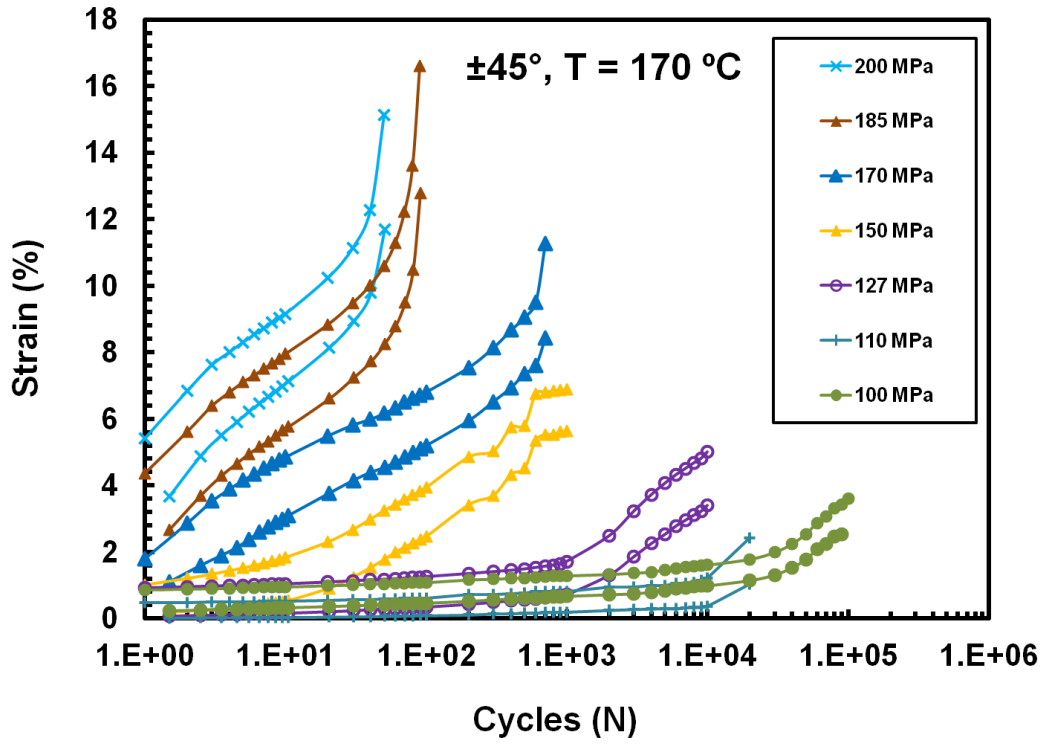

Figure 47: Maximum and Minimum Strains vs. Fatigue Cycles for ±45 Specimens at 170°C

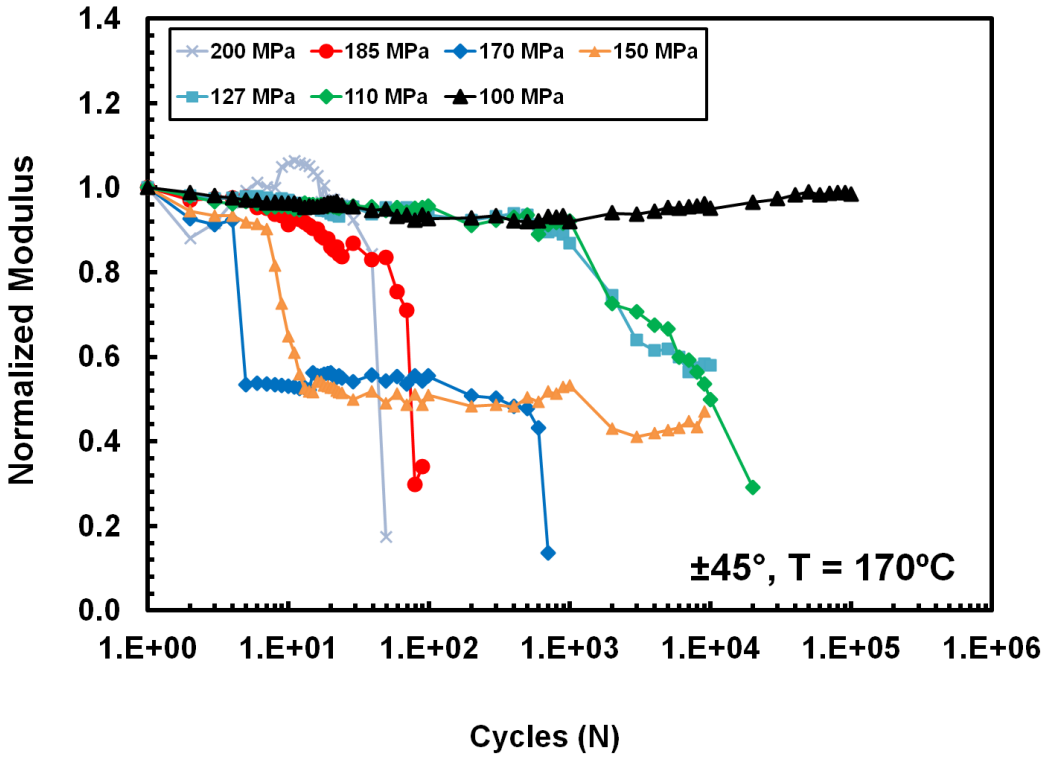

Figure 48: Normalized Modulus vs. Fatigue Cycles for ±45 Specimens at 170°C

The evolution of the stress-strain hysteresis behavior with fatigue cycles in the 200 MPa (89% UTS) test at 170°C in Figure 49 reveals dramatic strain accumulation early in fatigue life. On the contrary, in the 100 MPa (44% UTS) test very little strain is accumulated during the first 10^4 cycles, but a significant strain accumulation occurs by cycle 100,000 (Figure 50). The results in Figure 50 suggest that although this specimen reached the run-out condition of 10^5 cycles, it may have failed in fatigue shortly thereafter.

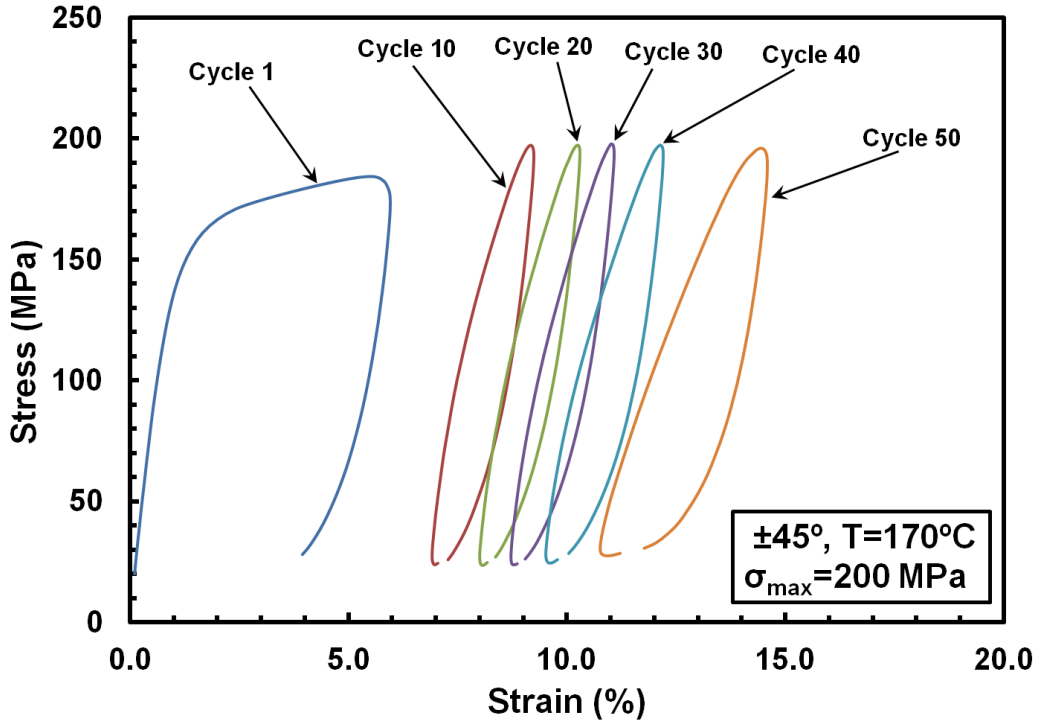

Figure 49: Evolution of Stress-Strain Hysteresis Response with Fatigue Cycles for Specimen T69-23 with ±45 Fiber Orientation at 170°C. σ_{max}=200 MPa.

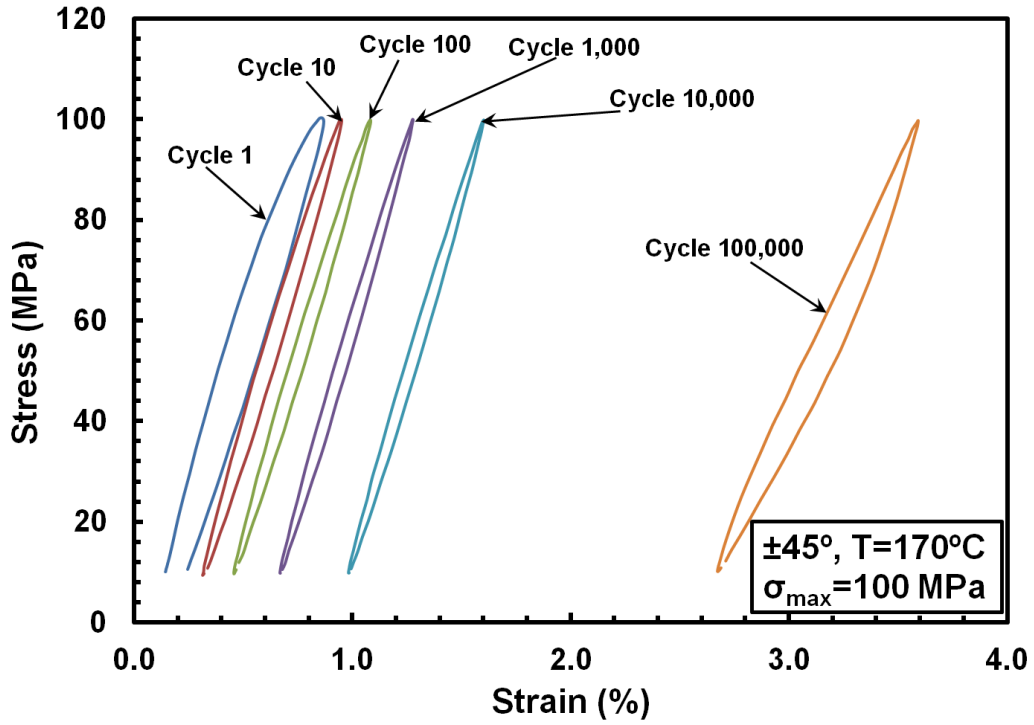

Figure 50: Evolution of Stress-Strain Hysteresis Response with Fatigue Cycles for Specimen T68-9 with ±45 Fiber Orientation at 170°C. σ_{max}=100 MPa.

The S-N curves obtained for the two fiber orientations under tension-tension fatigue at 170°C are compared in Figure 51. As at room temperature, at 170°C, the fatigue performance of the ±45 fiber orientation is much reduced compared to that of the 0/90 fiber orientation. As expected, superior fatigue performance is obtained along the fiber direction.

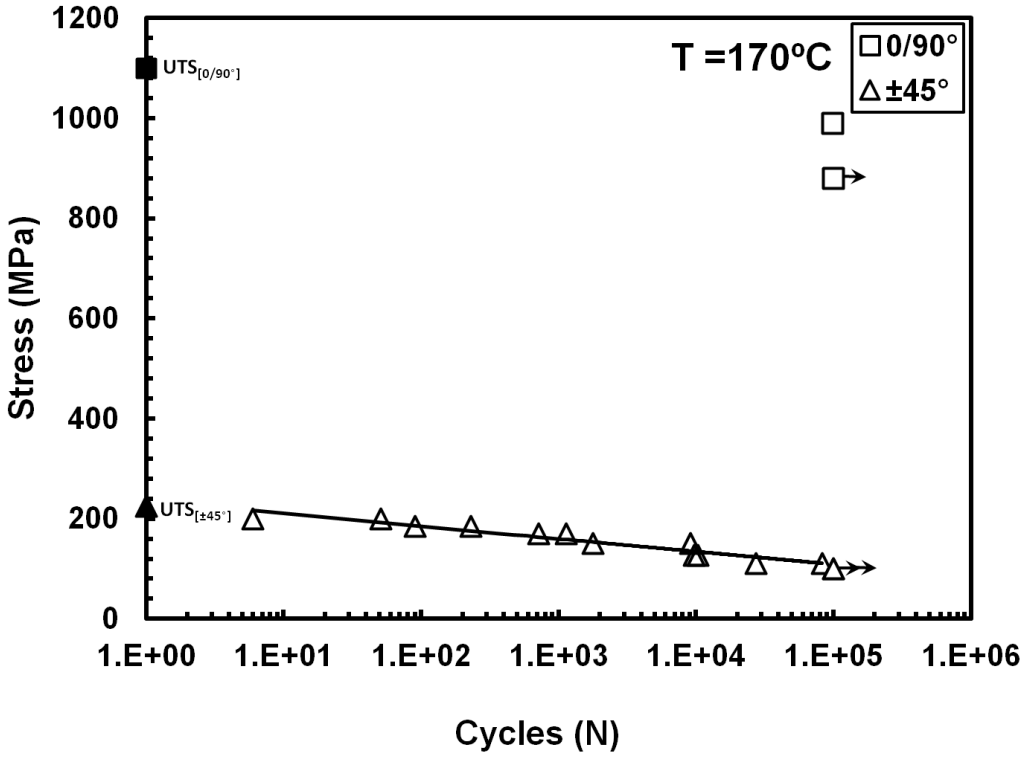

Figure 51: S-N Curves for ±45 and 0/90 Specimens at 170°C. Arrow Indicates Specimen Achieved Fatigue Run-Out.

5.4.3 Tension-Tension Fatigue at 190°C

Because the typical use temperature for the BMI 5250-4 resin is 170°C, testing at 190°C was expected to push the limits of the composite material. Therefore, only 0/90 specimens were successfully tested in tension-tension fatigue at 190°C. The results of the tension-tension fatigue tests conducted on the 0/90 specimens at 190°C are summarized in Table 14, and the results of the ±45 specimens tested in tension-tension fatigue at 190°C are summarized in Appendix A.

Table 14: Tension-Tension Fatigue Results for 0/90 Specimens at 190°C

Specimen #	σ_{max} (MPa)	σ_{max} (% UTS)	Cycles to Failure
T42-14	796	79.98	100000
T43-13	896	90.03	100000

Again, the 0/90 specimens performed as expected. Fatigue run-out was achieved at the maximum stress of 896 MPa (90% UTS) as in Figure 52.

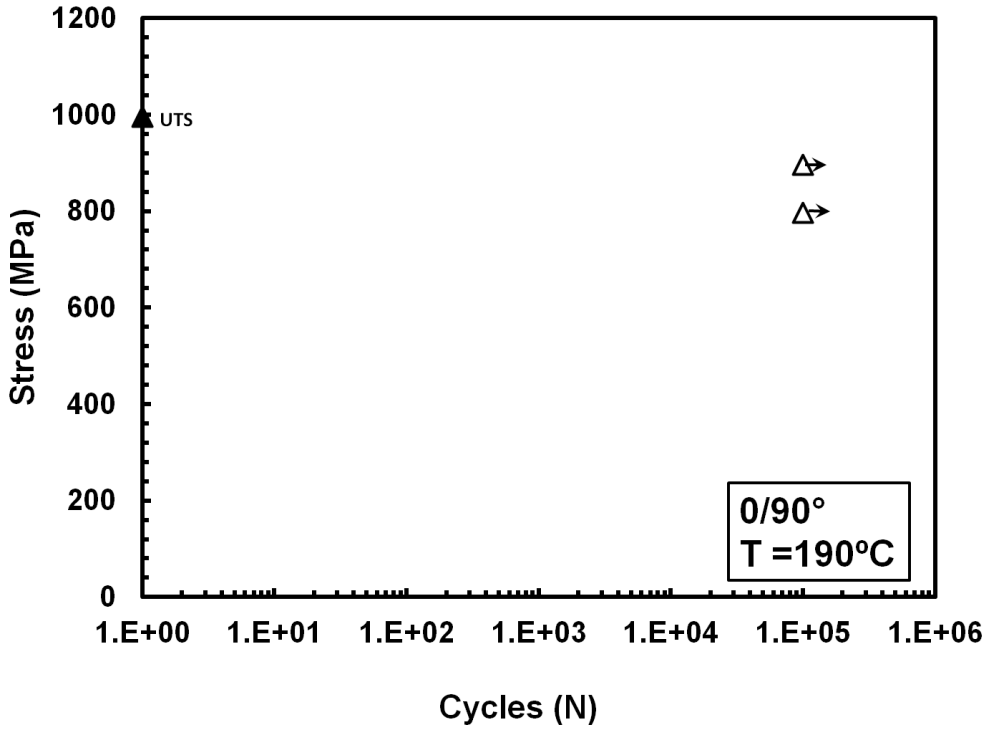

Figure 52: Maximum Stress vs. Cycles to Failure for the 0/90 Specimens at 190°C. Arrow Indicates Specimen Achieved Fatigue Run-Out.

Results in Figure 53 and Figure 54 show very little strain accumulation and change in normalized modulus over the duration of the test, respectively. Interestingly, towards the end of the test, a slight decrease in strain was observed (Figure 53) accompanied by a slight stiffening of the material (Figure 54). This change can be seen more clearly in the evolution of the stress-strain hysteresis loops shown in Figure 55. The hysteresis responses of additional specimens are included in Appendix B.

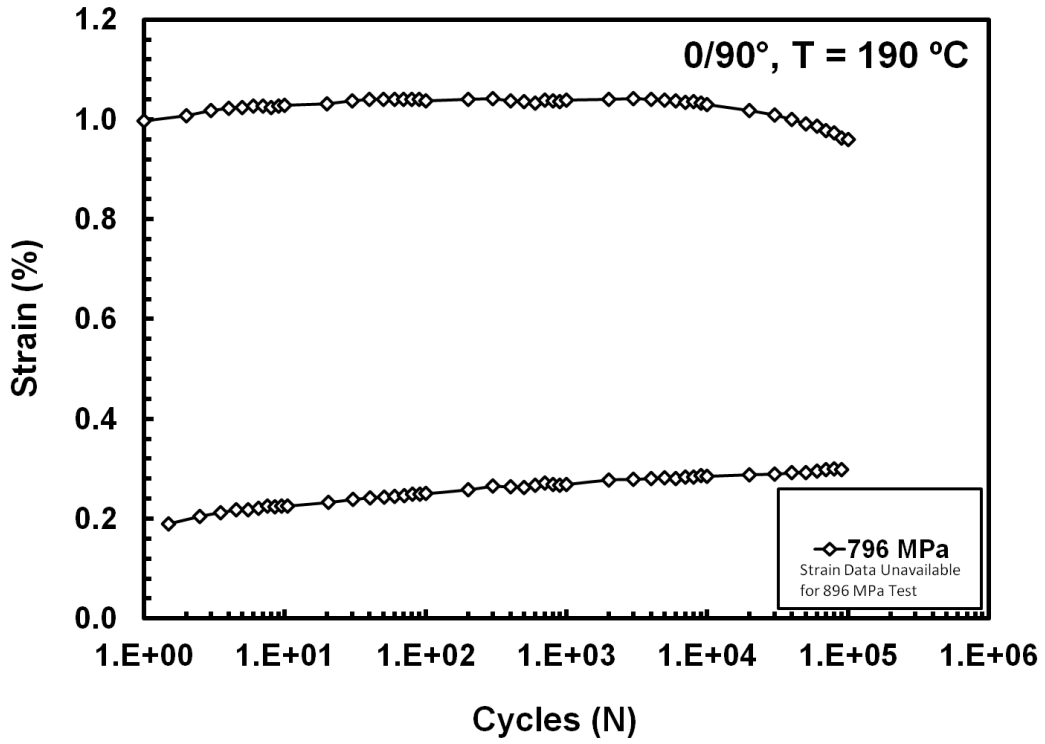

Figure 53: Minimum and Maximum Strains vs. Fatigue Cycles for 0/90 Specimens at 190°C

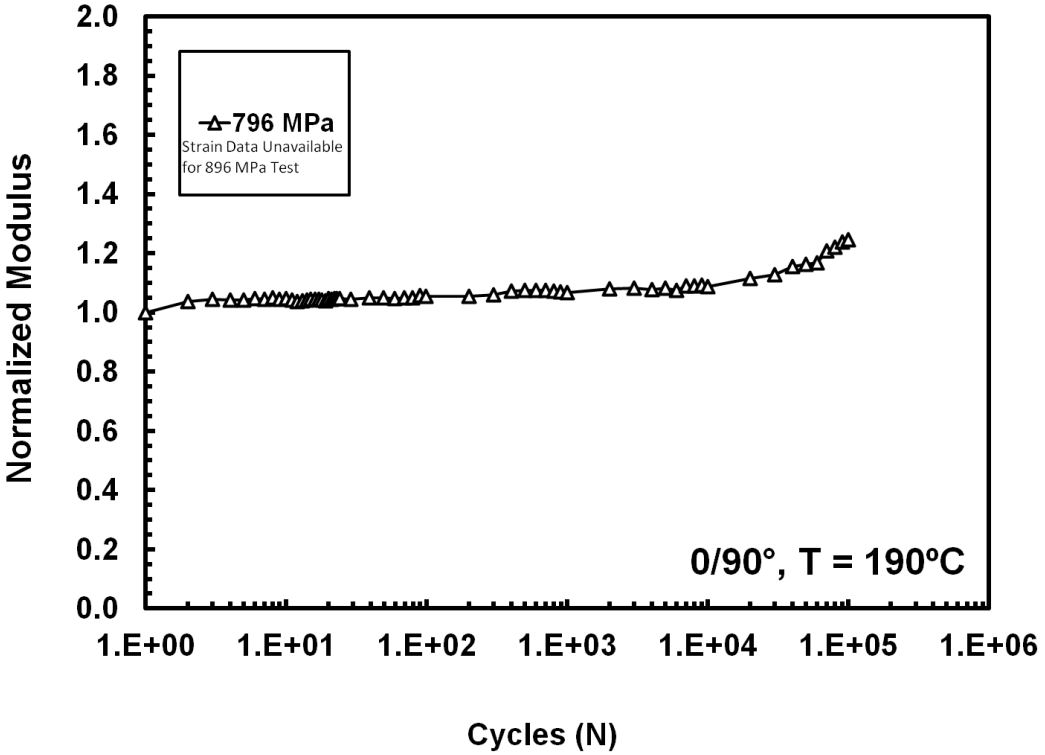

Figure 54: Normalized Modulus vs. Fatigue Cycles for 0/90 Specimens at 190°C

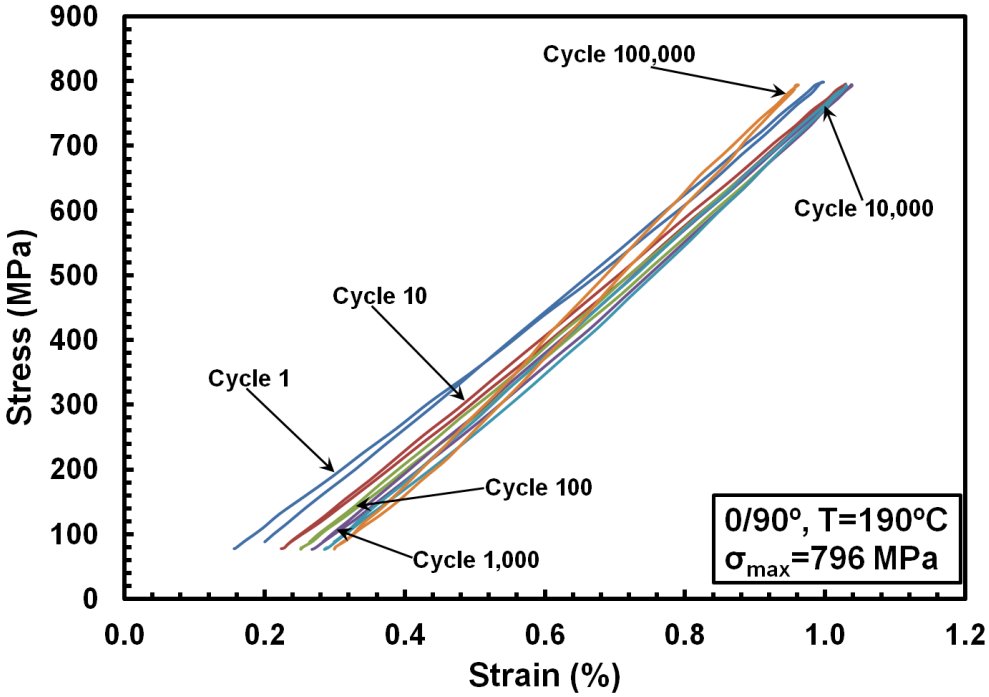

Figure 55: Evolution of Stress-Strain Hysteresis Response with Fatigue Cycles for Specimen T42-14 with 0/90 Fiber Orientation at 190°C

5.4.4 Effect of Temperature on Tension-Tension Fatigue

As shown in Figure 56 and Figure 57, increased temperature had virtually no effect on the fatigue performance of the 0/90 specimens. At all temperatures investigated in this work, fatigue run-out was reached at 80% and 90% of the UTS values associated with the test temperature.

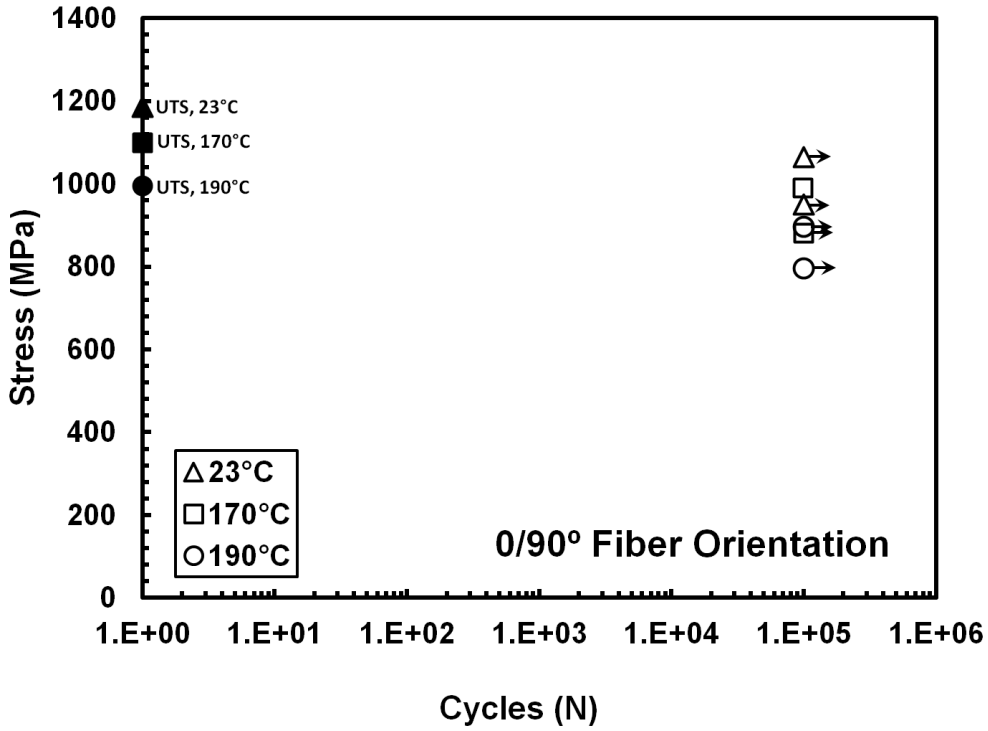

Figure 56: Maximum Stress vs. Cycles to Failure for the 0/90 Specimens at 23, 170, and 190°C. Arrow Indicated Specimen Achieved Fatigue Run-Out.

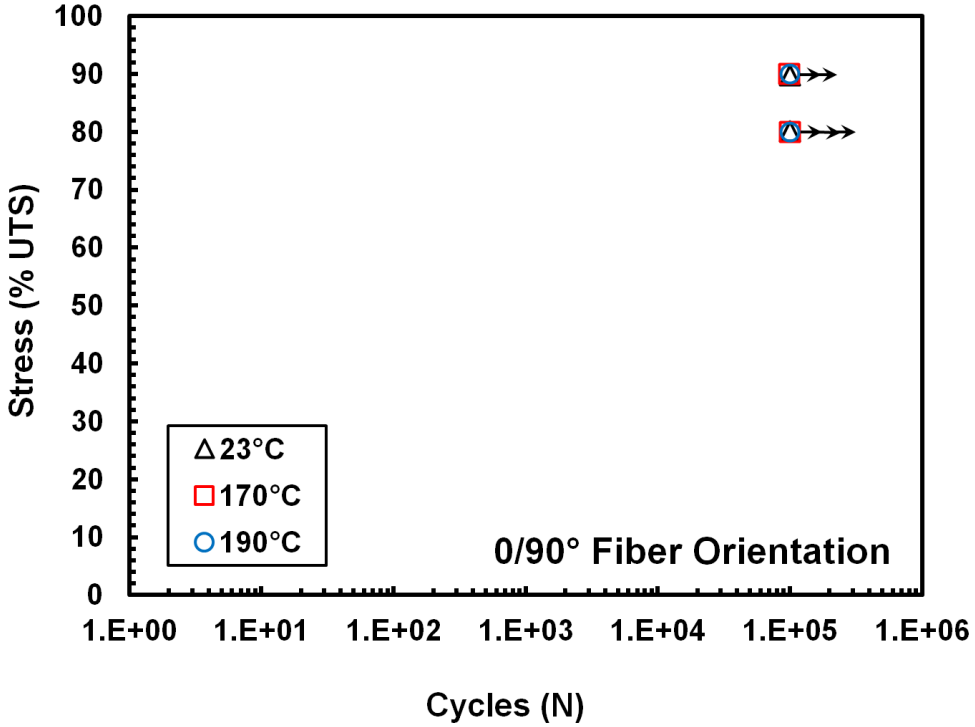

Figure 57: Maximum Stress vs. Cycles to Failure for the 0/90 Specimens at 23, 170, and 190°C. Arrow Indicates Specimen Achieved Fatigue Run-Out. Maximum Stress is Shown as % UTS.

Test temperature had a limited effect on the fatigue performance of the ±45 specimens. The S-N curve obtained at 170°C is slightly below the S-N curve produced at room temperature (Figure 58). Furthermore, the S-N curves produced at 23 and 170°C (Figure 58) have the same slope.

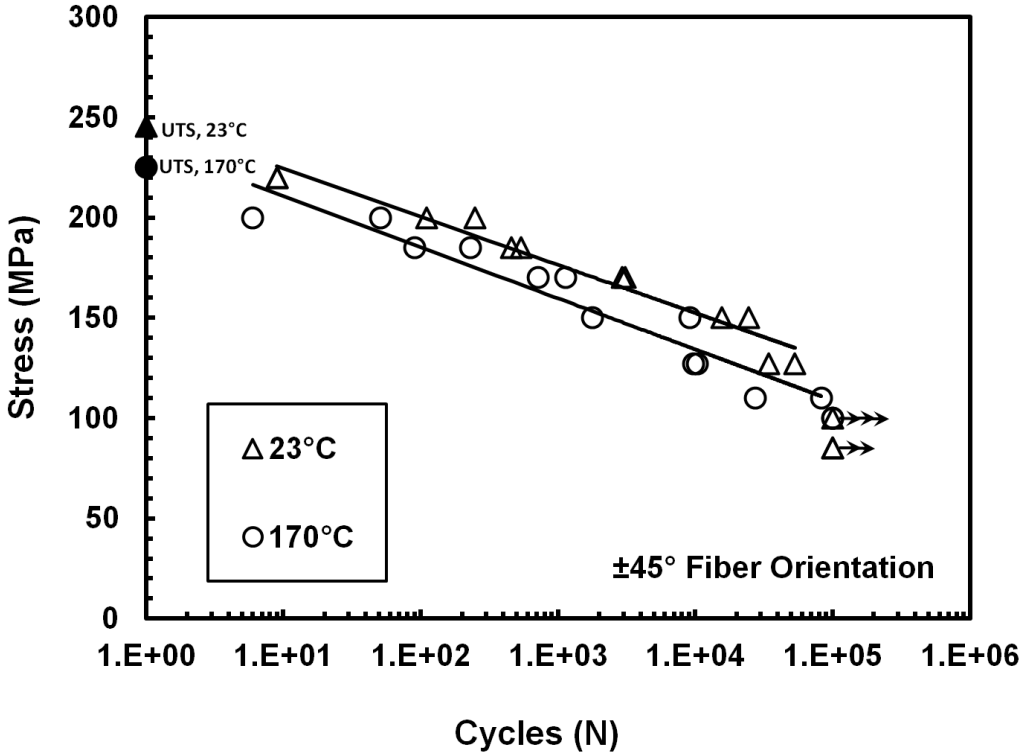

Figure 58: Maximum Stress vs. Cycles to Failure for the ±45 Specimens at 23 and 170°C. Arrow Indicates Specimen Achieved Fatigue Run-Out.

Figure 59 presents the S-N curves obtained at 23 and 170°C with the maximum stress shown as % UTS. The two S-N curves in Figure 59 are very close. At 23°C, the fatigue run-out was achieved at 100 MPa. However, it is likely that a fatigue run-out could have been reached at a higher maximum stress of 115-120 MPa. Results in Figure 59 also

demonstrate that increase in test temperature from 23 to 170°C had little influence on tension-tension fatigue performance of the composite with the ±45 fiber orientation.

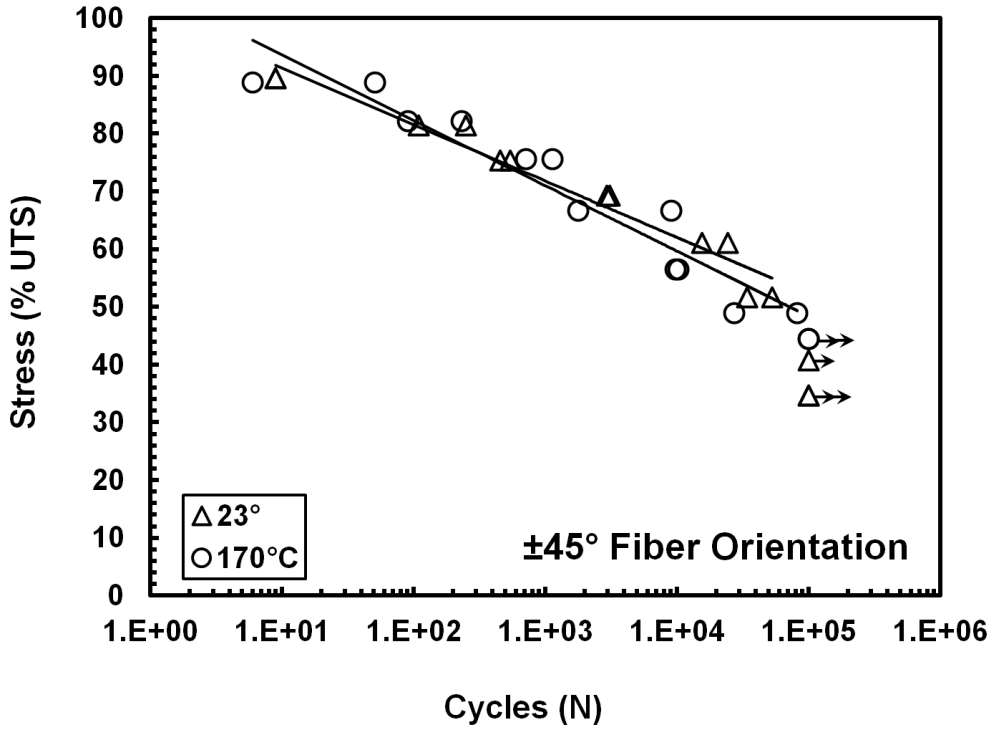

Figure 59: Maximum Stress vs. Cycles to Failure for the ±45 Specimens at 23 and 170°C. Arrow Indicates Specimen Achieved Fatigue Run-Out. Maximum Stress is Shown as % UTS.

5.5 Tension-Compression Fatigue

Tension-compression fatigue tests were performed in force control with a sinusoidal waveform at a frequency of 1 Hz at 23°C with a minimum to maximum stress ratio of R= -1. The fatigue run-out was defined as 10^5 cycles. The results of the tension-compression fatigue tests at 23°C are summarized in Table 15.

Table 15: Tension-Compression Fatigue Results of 0/90 Specimens at 23°C

Specimen #	σ_{max} (MPa)	σ_{max} (% UTS)	Cycles to Failure
C55-5	640	81.82	24
C55-19	600	76.70	48
C53-7	550	70.31	55
C54-18	500	63.92	480
C54-3	450	57.53	4089
C55-21	450	57.53	7720
C55-3	425	54.33	37649
C53-14	400	51.13	100000
C54-19	350	44.74	100000

The tension-compression fatigue results obtained are also presented as the maximum stress vs. cycles to failure (S-N) curve in Figure 60. Notably, the S-N curve produced in the tension-compression fatigue tests of the 0/90 specimens is qualitatively similar to those produced in the tension-tension fatigue tests of the ±45 specimens. The increased impact of the matrix on tension-compression fatigue response is clearly evident. This observation is not surprising, as the compression behavior of the 0/90 cross-ply is strongly influenced by the matrix.

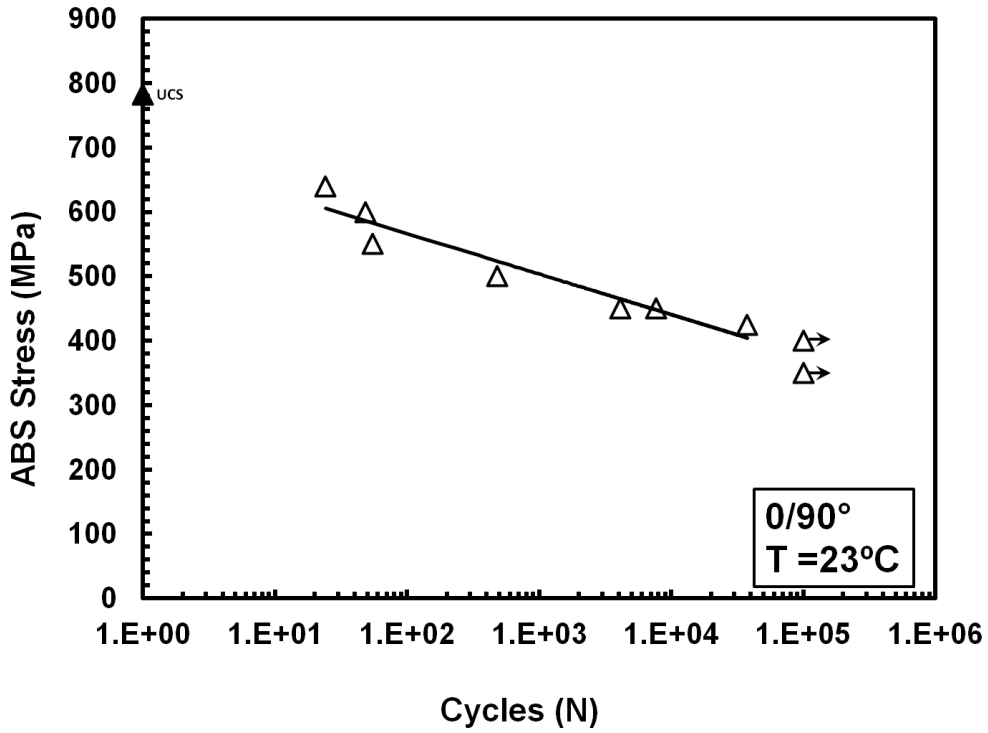

Figure 60: Tension-Compression Fatigue S-N Curve for the 0/90 at 23°C. Arrow Indicates Specimen Achieved Fatigue Run-Out.

Figure 61 shows maximum and minimum strains vs. tension-compression fatigue cycles for tests conducted at 23°C. Maximum and minimum strains change little until just before failure when the strains tend to decrease rapidly.

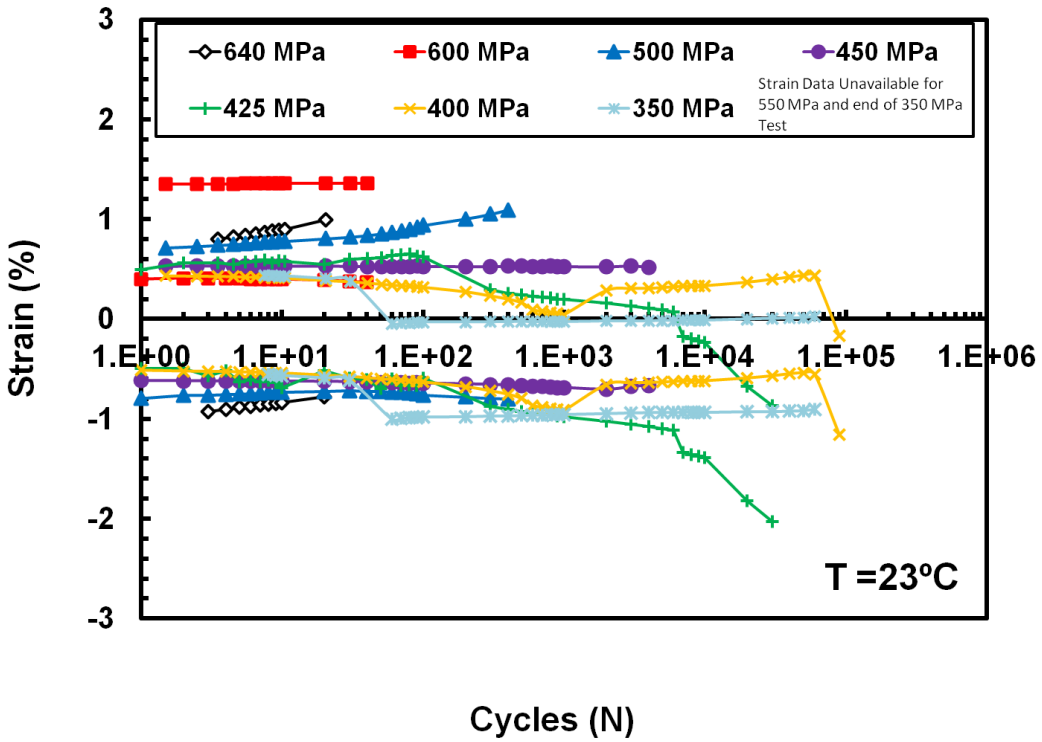

Figure 61: Minimum and Maximum Strains vs. Tension-Compression Fatigue Cycles for 0/90 Specimens at 23°C

Figure 62 shows that the normalized modulus remained nearly constant in most tension-compression tests. Only two specimens demonstrated a decrease in normalized modulus with cycles. Recall that the same trend was observed in tension-tension fatigue tests of the 0/90 fiber orientation.

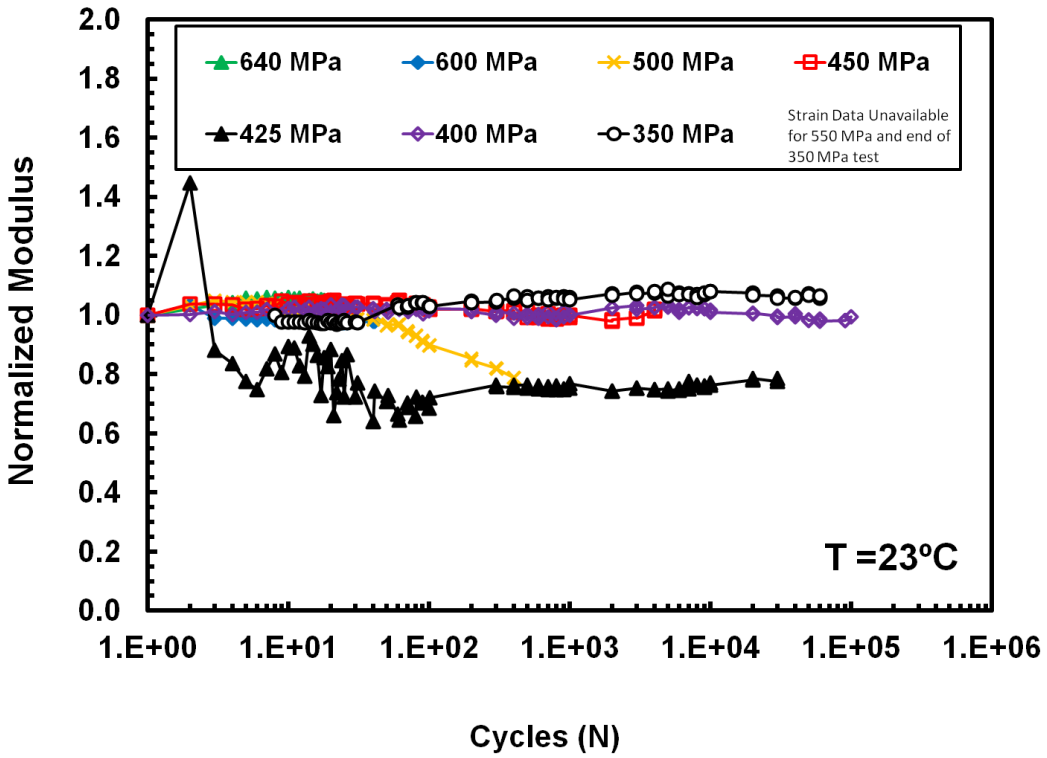

Figure 62: Normalized Modulus vs. Tension-Compression Fatigue Cycles for 0/90 Specimens at 23°C

It is instructive to compare the results obtained in tension-compression and in tension-tension fatigue tests (Figure 63). The S-N curve obtained in tension-compression fatigue for the 0/90 fiber orientation falls between the S-N curves obtained in tension-tension fatigue for the 0/90 and ±45 fiber orientations. This result is readily explained. The tension-tension fatigue behavior of the 0/90 fiber orientation is governed by the fibers. Conversely, matrix plays a role in the tension-tension response of the ±45 fiber orientation and in the tension-compression response of the 0/90 specimens. Matrix appears to have greater influence in the case of the tension-tension fatigue behavior of the ±45 fiber orientation.

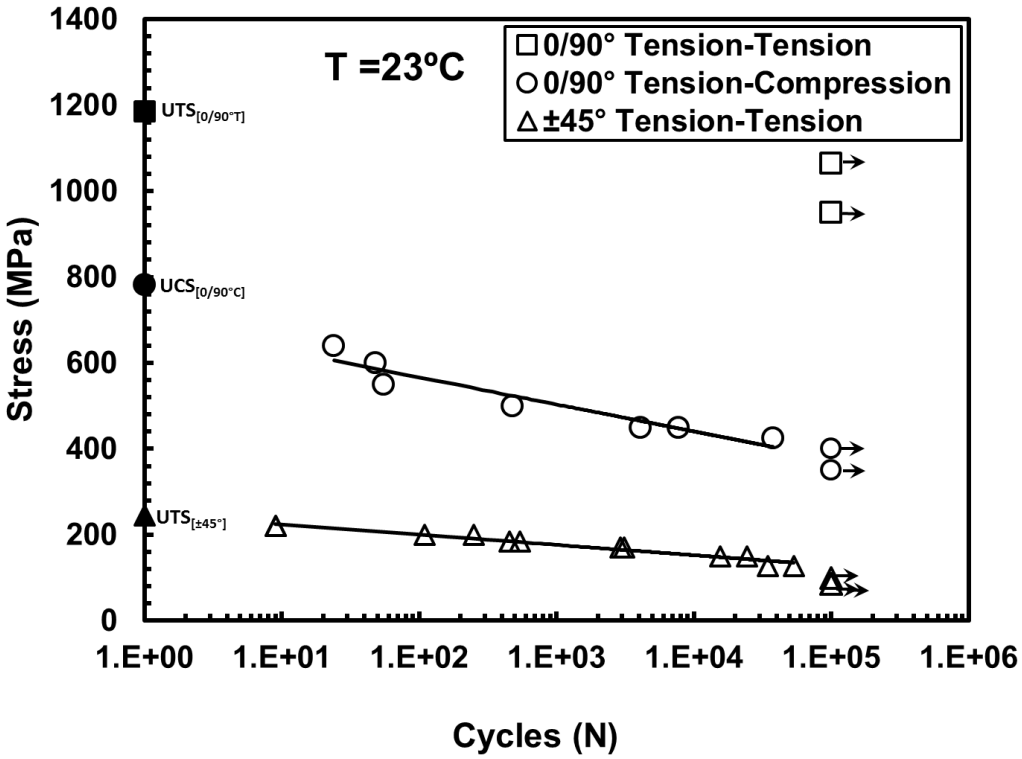

Figure 63: Tension-Tension and Tension-Compression Fatigue S-N Curves Obtained at 23°C. Arrow Indicates Specimen Achieved Fatigue Run-Out.

The S-N curves obtained under tension-tension and tension-compression fatigue are also compared in Figure 64, where the maximum stress is shown as % UTS. The order of the S-N curves is different from that in Figure 63. Now the S-N curve produced in tension-compression fatigue lies below the S-N curve obtained in tension-tension fatigue for the ±45 fiber orientation. Additional testing would have to be performed to fully evaluate the role of the matrix in these types of tests. Tension-compression tests on ±45 specimens could be attempted. It is no surprise, however, that the 0/90 specimens perform better under tension-tension than under tension-compression fatigue.

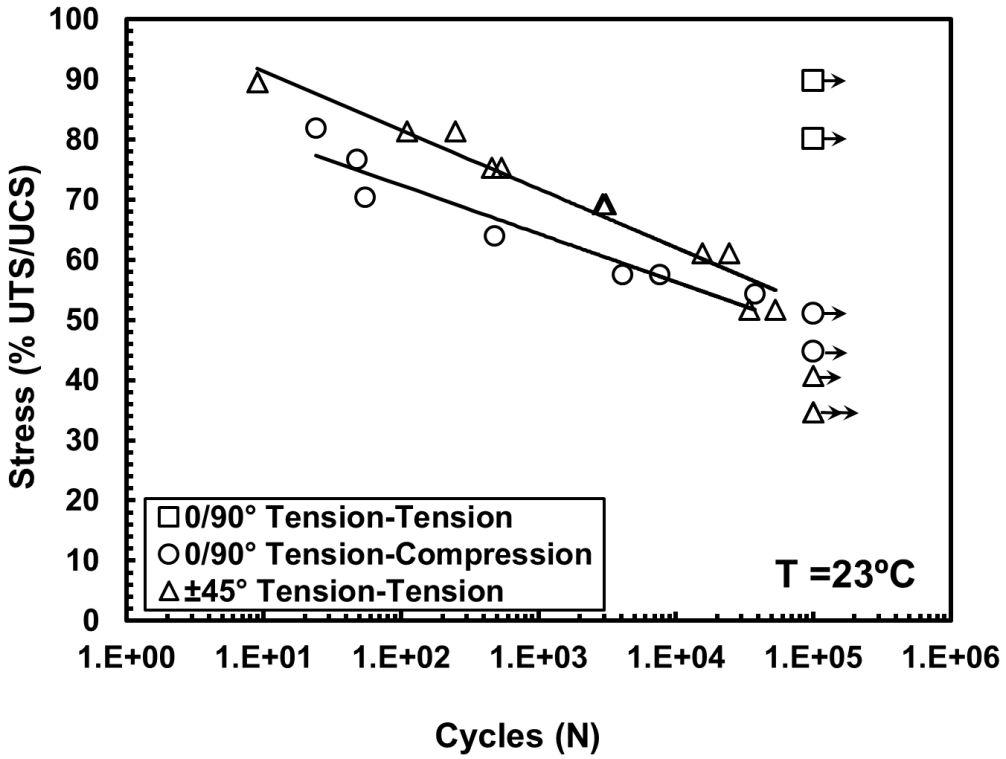

Figure 64: Tension-Tension and Tension-Compression Fatigue S-N Curves Obtained at 23°C. Arrow Indicates Specimen Achieved Fatigue Run-Out. Maximum Stress is Shown as % UTS.

5.6 Retained Tensile Properties

All specimens that achieved fatigue run-out of 10^5cyles were tested in tension to failure in order to determine the retained tensile properties. The retained strength and modulus of the specimens that achieved a run-out are summarized in Table 16 and Table 17. Tensile stress-strain curves obtained for the specimens subjected to prior fatigue are presented in Figure 65-Figure 70 together with the tensile stress-strain curve for the as-processed material.

Table 16: Retained Properties of the 0/90 Specimens Subjected to 10^5 Cycles of Prior Fatigue

Max Fatigue Stress (MPa)	Retained Strength (MPa)	Retained Modulus (GPa)	Strain at Failure (%)
Prior tension-tension fatigue at 23°C			
950	1233	75.99	1.68
1065	1279	95.86	1.37
Prior tension-tension fatigue at 170°C			
880	1201	90.31	1.34
Prior tension-tension fatigue at 190°C			
796	1128	116.26	1.00
896	1167	148.99	0.98
Prior tension-compression fatigue at 23°C			
350	1307	81.92	2.39
400	1204	54.99	1.52

Table 17: Retained Properties of the ±45 Specimens Subjected to 10^5 Cycles of Prior Fatigue

Max Fatigue Stress (MPa)	Retained Strength (MPa)	Retained Modulus (GPa)	Strain at Failure (%)
Prior tension-tension fatigue at 23°C			
85	198	21.24	7.64
85	202	19.92	4.80
100	247	18.77	13.43
Prior tension-tension fatigue at 170°C			
100	227	15.12	14.55
100	167	12.19	9.52

Notably, prior tension-tension fatigue at 23°C slightly increased the tensile strength of the 0/90 specimens by 6%. However, the stress-strain behavior of the pre-fatigued 0/90 specimens remains nearly linear to failure (Figure 65).

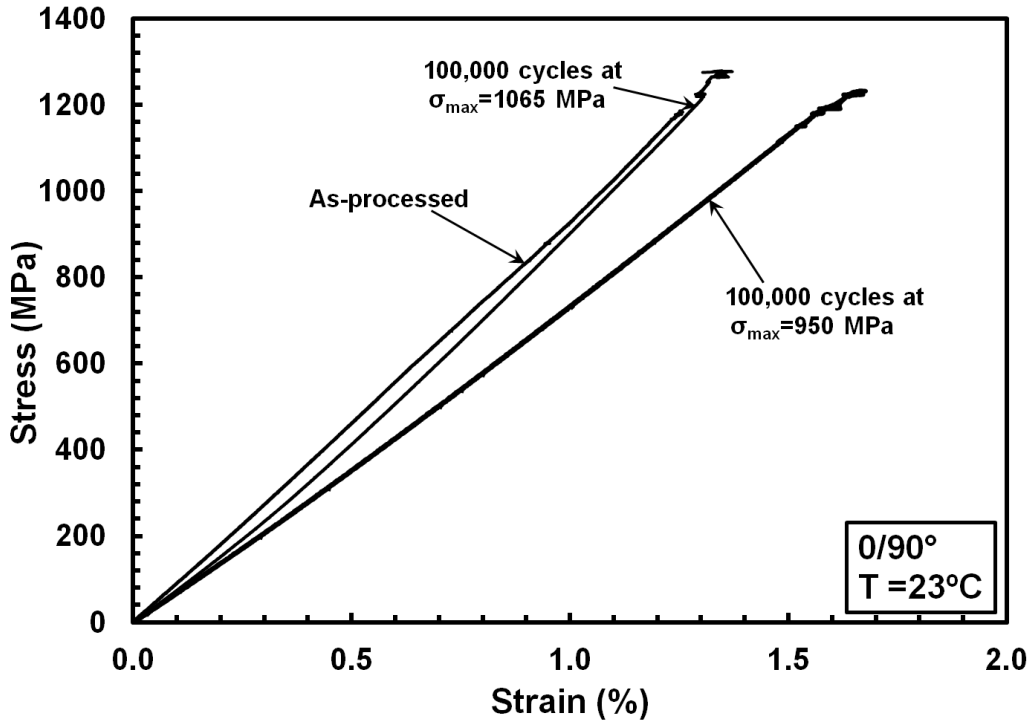

Figure 65: Effects of Prior Tension-Tension Fatigue at 23°C on Tensile Stress-Strain Behavior of the 0/90 Fiber Orientation

The ±45 specimens pre-fatigued at room temperature demonstrate at least 80% retention of the UTS (Figure 66). However, the stress-strain behavior of the pre-fatigued specimens remains qualitatively similar to that of the as-processed specimens. The loss of UTS likely occurs due to matrix degradation.

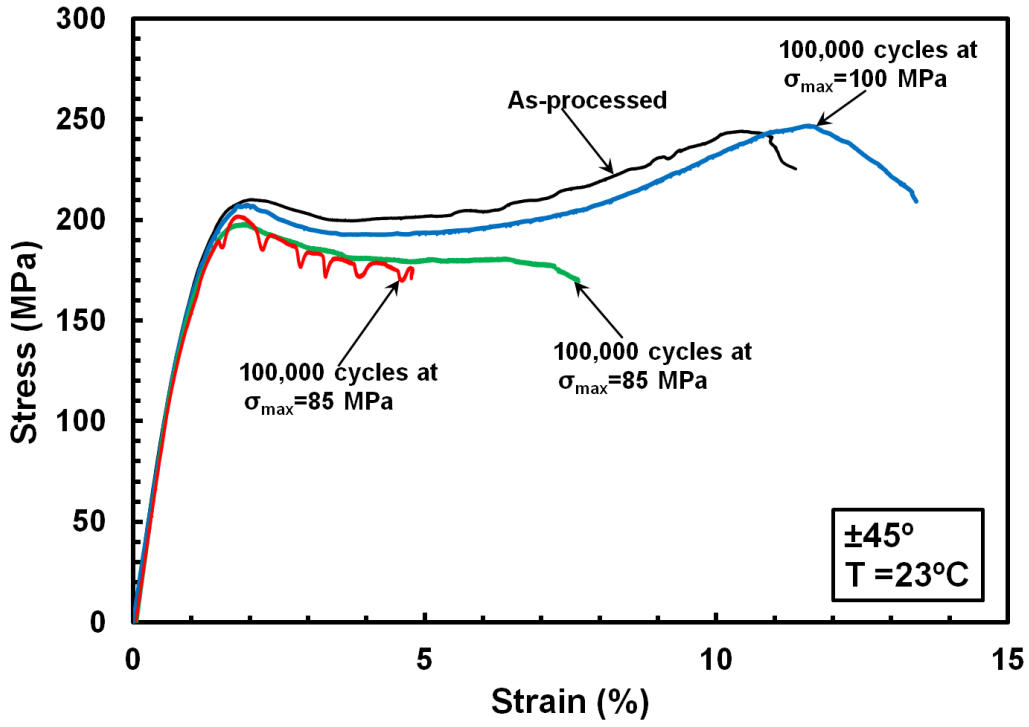

Figure 66: Effects of Prior Tension-Tension Fatigue at 23°C on Tensile Stress-Strain Behavior of the ±45 Fiber Orientation

As was the case with the 0/90 specimens pre-fatigued at 23°C, the 0/90 specimens subjected to prior fatigue at 170°C also exhibited a slight increase in tensile strength of ~9% (Figure 67).

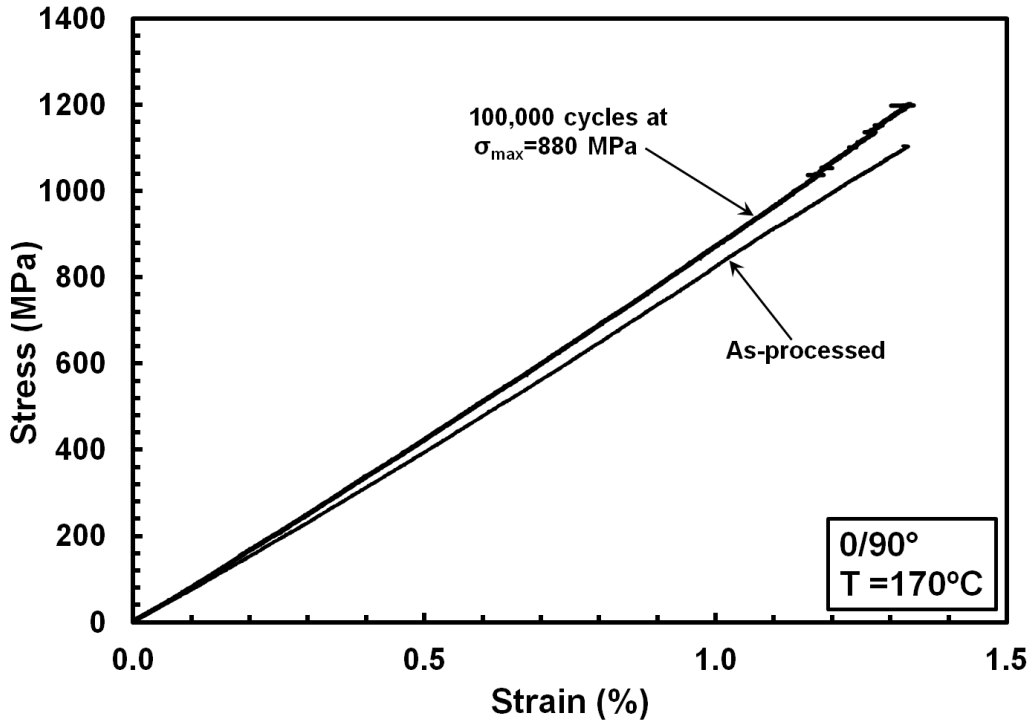

Figure 67: Effects of Prior Tension-Tension Fatigue at 170°C on Tensile Stress-Strain Behavior of the 0/90 Fiber Orientation

The ±45 specimens subjected to prior fatigue at 170°C show some scatter in the strength data as seen in Figure 68, retaining at least 75% of the UTS. However, prior tension-tension fatigue at 170°C appears to have little effect on the tensile stress-strain behavior. All tensile stress-strain curves in Figure 68 are qualitatively similar.

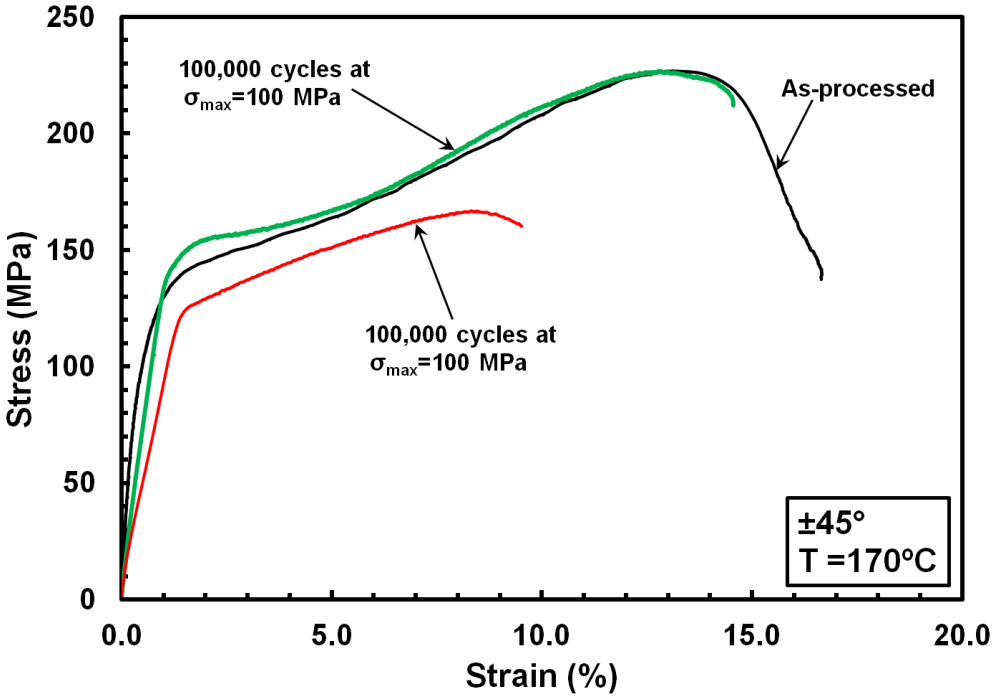

Figure 68: Effects of Prior Tension-Tension Fatigue at 170°C on Tensile Stress-Strain Behavior of the ±45 Fiber Orientation

Prior fatigue at 190°C causes an increase in tensile strength of the 0/90 specimens of ~15%. Recall that prior fatigue at 23 and 170°C had a similar effect.

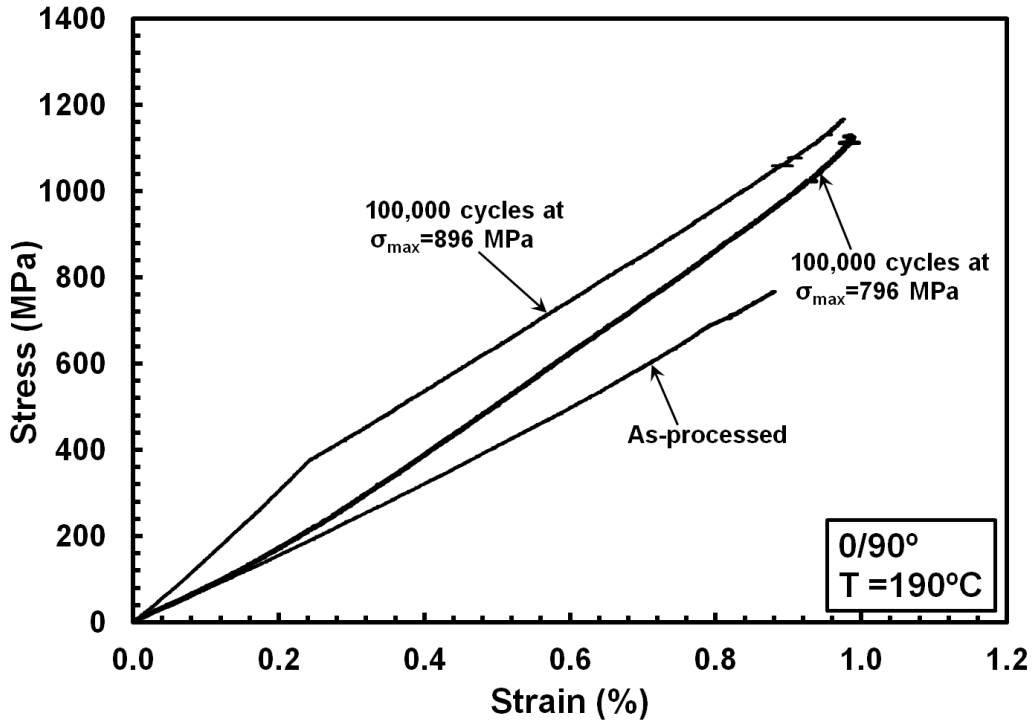

Figure 69: Effects of Prior Tension-Tension Fatigue at 190°C on Tensile Stress-Strain Behavior of the 0/90 Fiber Orientation

Notably, prior tension-compression fatigue at 23°C also caused an increase in tensile strength of the 0/90 fiber orientation of ~ 6% (Figure 70). However, considerable modulus loss of ~ 27.5% is observed in this case.

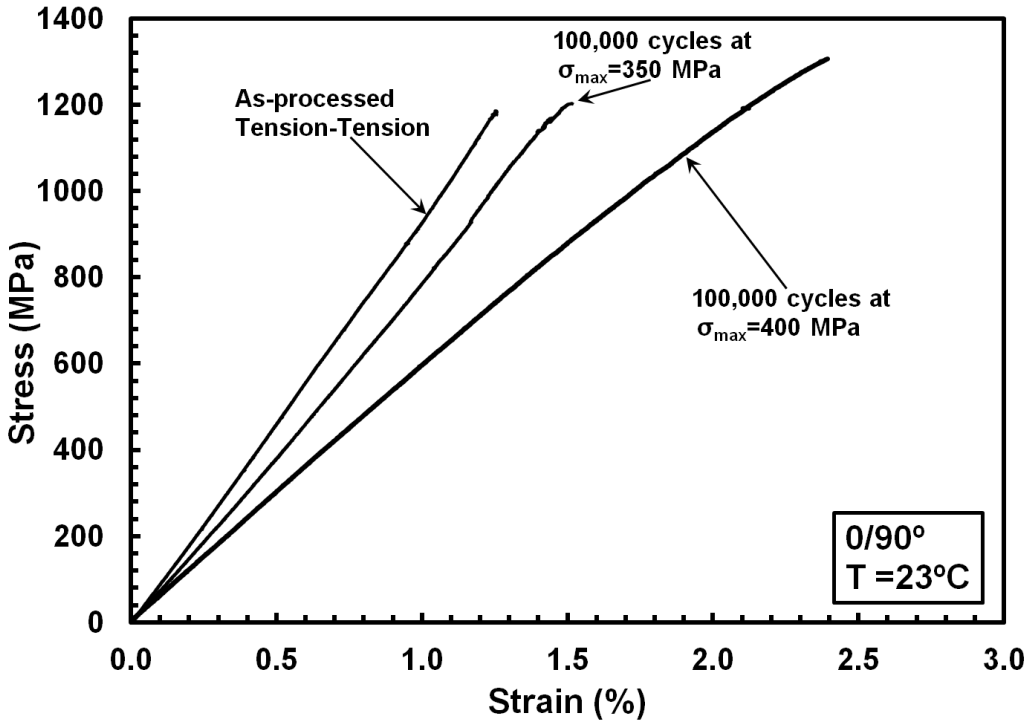

Figure 70: Effects of Prior Tension-Compression Fatigue at 23°C on Tensile Stress-Strain Behavior of the 0/90 Fiber Orientation

5.7 Optical Microscopy

Specimens subjected to each type of test in this work were analyzed under a Zeiss optical microscope in order to determine the failure mechanisms. For each fiber orientation, one as-processed specimen was also imaged.

5.7.1 Examination of 0/90 Tension-Tension Fatigue Specimens

The gage section of a typical as-processed tension-tension fatigue specimen with 0/90 fiber orientation is shown in Figure 71. The 0/90 fiber weave is clearly seen in Figure 71(a). The individual plies can be seen in the side view in Figure 71(b).

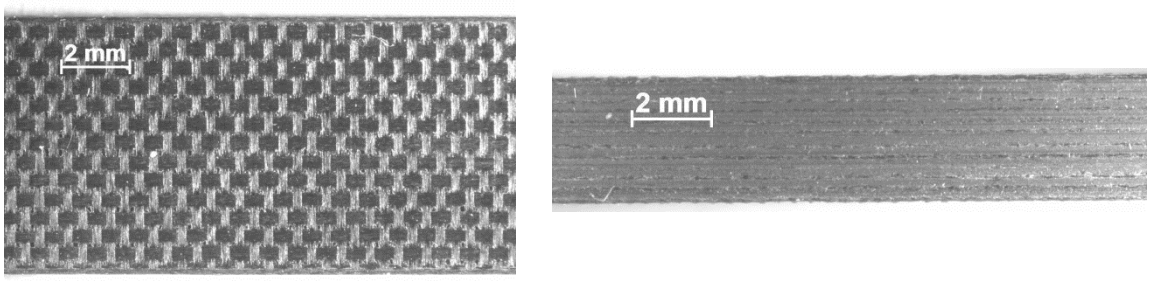

(a) (b)

Figure 71: Optical Micrographs of As-Processed 0/90 Tension-Tension Fatigue Specimen T42-3 (a) front (b) side view

Failure of the tension-tension fatigue specimens with the 0/90 fiber orientation is typified in Figure 72. Ply delamination and fiber fracture were the primary failure mechanisms of the 0/90 specimens in tension-tension fatigue at 23°C. Some fiber pullout is also observed. Most failures were localized with limited delamination.

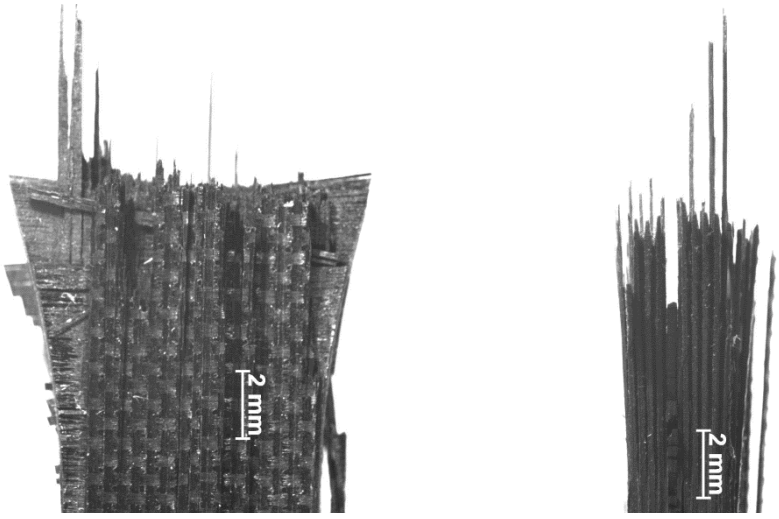

(a) (b)

Figure 72: Optical Micrographs of the 0/90 Specimen T41-18 Failed in Tension-Tension Fatigue at 23°C (a) front (b) side view

Figure 73 and Figure 74 show optical micrographs of the 0/90 specimens failed in tension-tension fatigue at 170 and 190°C, respectively. Ply delamination and fiber fracture remain the dominant failure modes.

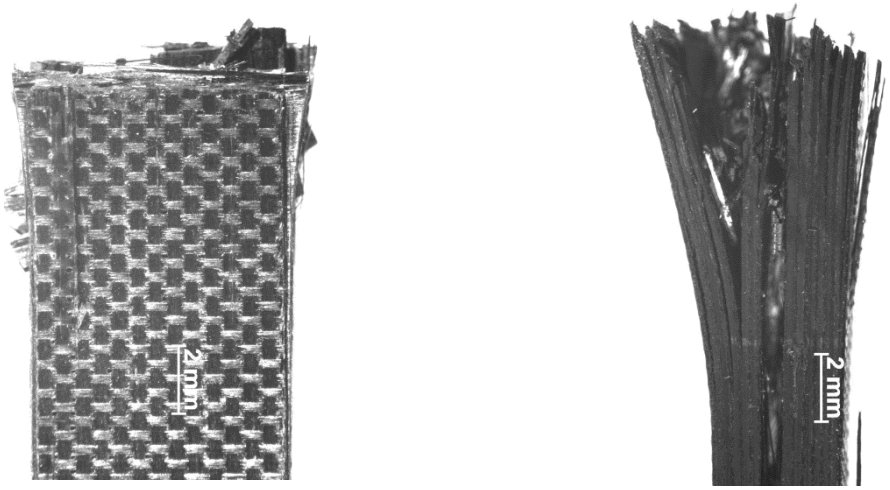

(a) (b)

Figure 73: Optical Micrographs of the 0/90 Specimen T41-1 failed in Tension-Tension at 170°C (a) front (b) side view

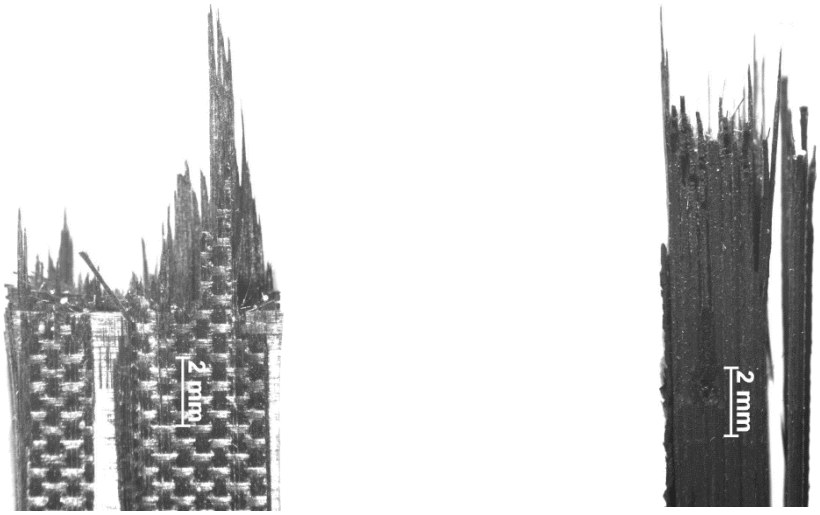

(a) (b)

Figure 74: Optical Micrographs of the 0/90 Specimen T42-24 Failed in Tension-Tension Fatigue at 190°C (a) front (b) side view

5.7.2 Examination of ±45 Tension-Tension Specimens

The gage section of a typical as-processed tension-tension fatigue specimen with ±45 fiber orientation is shown in Figure 75.

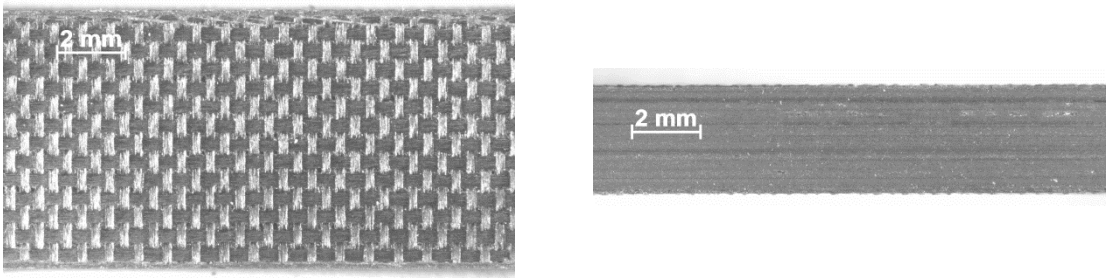

(a) (b)

Figure 75: Optical Micrographs of As-Processed ±45 Tension-Tension Fatigue Specimen T60-6 (a) front (b) side view

Optical micrographs of the ±45 specimen tested in tension-tension fatigue at 23°C are presented in Figure 76 and Figure 77. Note that the specimen shown in Figure 77 achieved fatigue run-out of 10^5 cycles then failed in a monotonic tension test. The "scissoring" effect, or the tendency of individual fibers to detach and realign themselves in the direction of loading, was observed in all tension-tension fatigue tested ±45 specimens. Note that ply delamination is the prevalent failure mechanism (Figure 76(b)). Striations can also be seen on the front surface of all ±45 specimens below the failure surface. These features form when the matrix begins to fail between tows and are often observed well before the ultimate failure of the specimen.

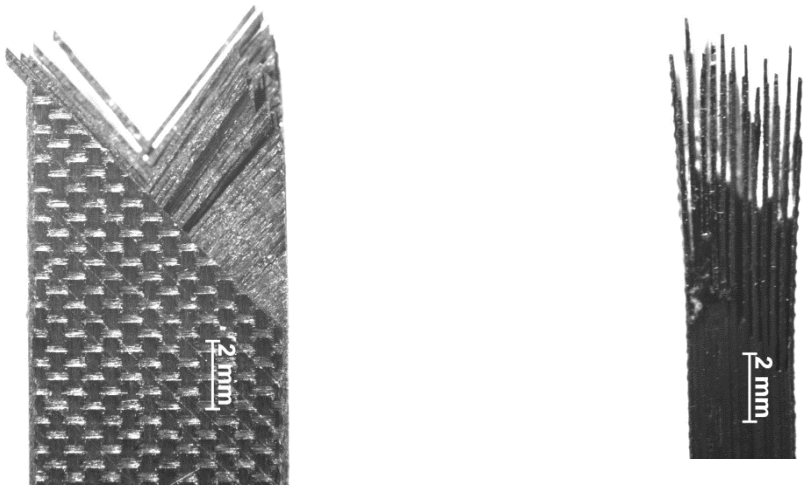

(a) (b)

Figure 76: Optical Micrographs of the ±45 Specimen T59-18 Failed in Tension-Tension Fatigue at 23°C (a) front (b) side view. σ_{max}=150 MPa, N_f=24,446.

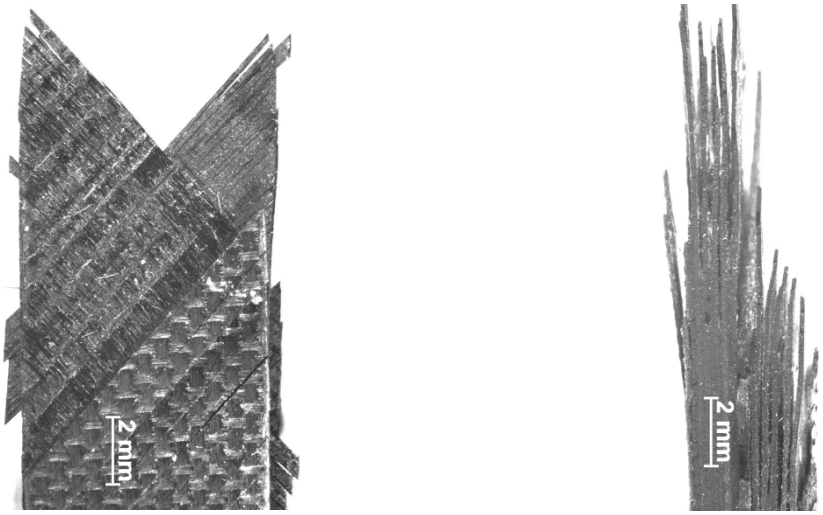

(a) (b)

Figure 77: Optical Micrographs of the ±45 Specimen T58-11 Failed in Tension-Tension Fatigue at 23°C (a) front (b) side view. σ_{max}=100 MPa, N_f>100,000.

Figure 78 and Figure 79 demonstrate that similar failure modes were also prevalent at 170°C. Once again, fiber scissoring is observed.

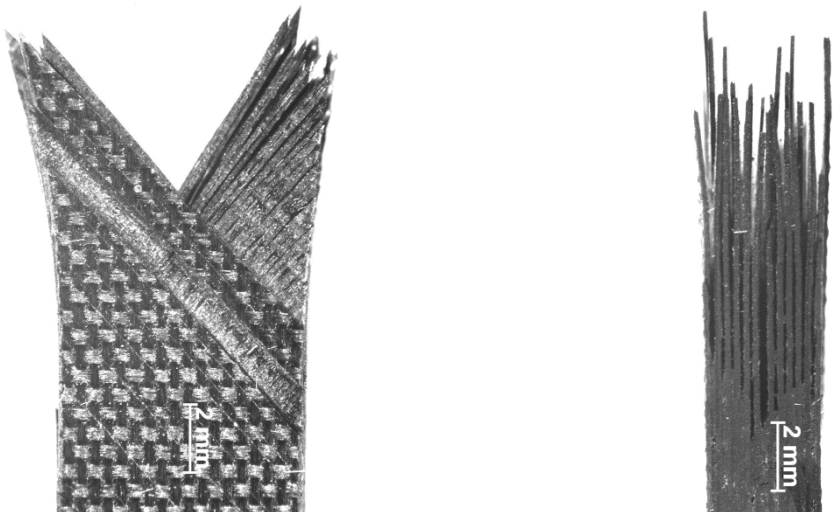

(a) (b)

Figure 78: Optical Micrographs of the ±45 Specimen T68-19 Failed in Tension-Tension Fatigue at 170°C (a) front (b) side view. σ_{max}=150 MPa, N_f>1,902.

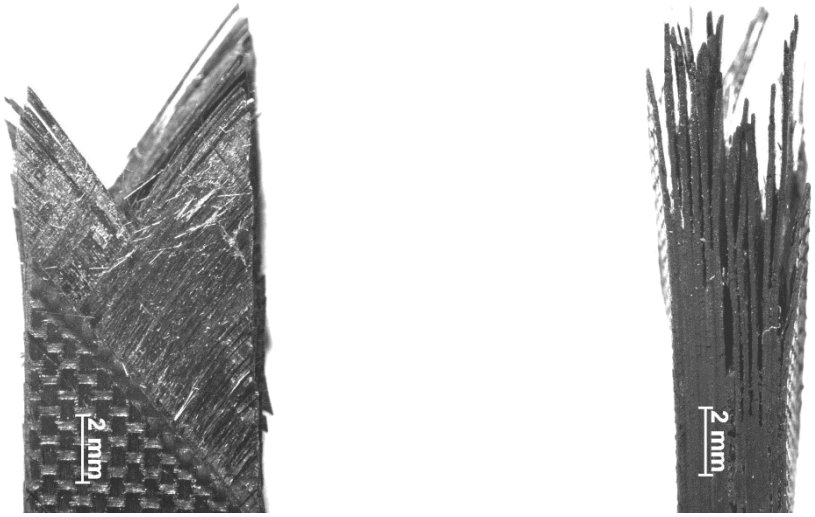

(a) (b)

Figure 79: Optical Micrographs of the ±45 Specimen T59-20 Failed in Tension-Tension Fatigue at 170° (a) front (b) side view. σ_{max}=100 MPa, N_f>100,000.

5.7.3 Examination of 0/90 Tension-Compression Fatigue Specimens

The gage section of a typical as-processed tension-compression fatigue specimen with 0/90 fiber orientation is shown in Figure 80. The 0/90 weave pattern is seen in

Figure 80(a). Note that the tension-compression fatigue specimens were thicker than the tension-tension fatigue specimens in order to minimize the possibility of buckling failure.

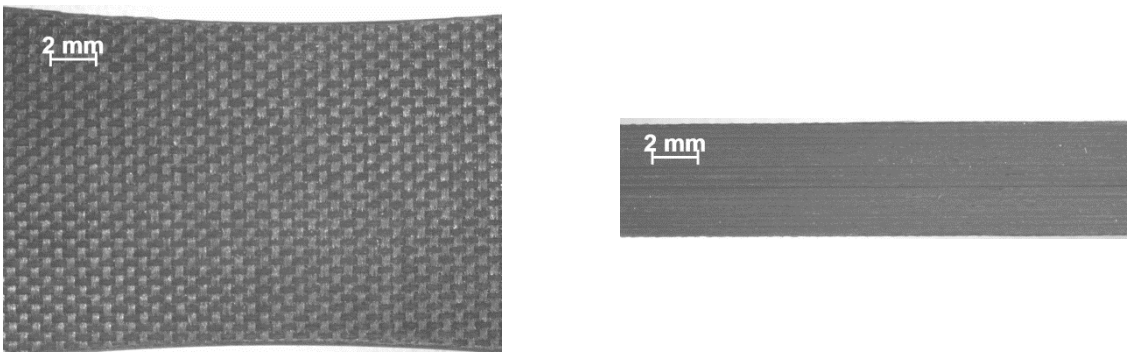

(a) (b)

Figure 80: Optical Micrographs of As-Processed 0/90 Tension-Compression Fatigue Specimen C55-23 (a) front (b) side view

Optical micrographs of the 0/90 specimens subjected to tension-compression fatigue are shown in Figure 81 and Figure 82. Note that the specimen shown in Figure 82 achieved fatigue run-out then failed in a monotonic tension-to-failure test. As expected, compressive failure occurs due to microbuckling of the fibers. As the axially loaded fibers buckle and kink, a crack in the matrix is initiated that leads to splitting of the matrix and delamination of the plies. The severity of the buckling of the fibers increased with continued cycling and eventually led to fracture of the 0° fibers [22]. Both fiber fracture, due to fiber microbuckling, and ply delamination are seen in Figure 81 (b).

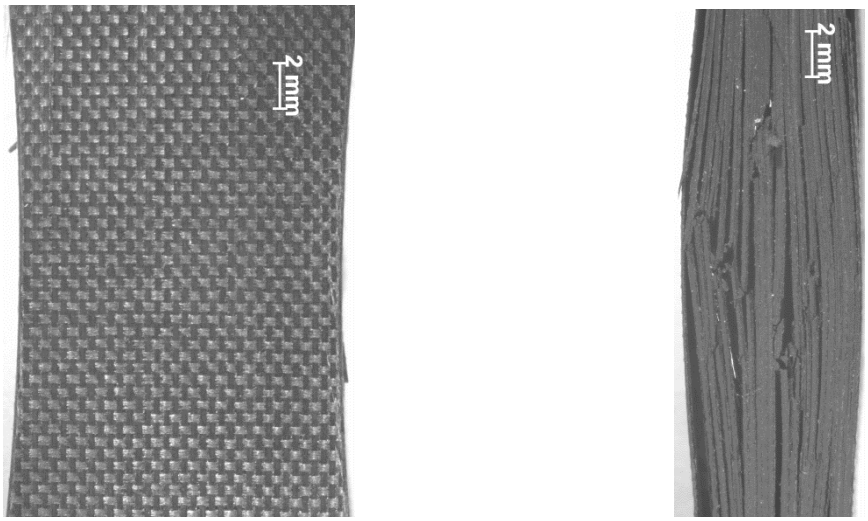

(a) (b)

Figure 81: Optical Micrographs of 0/90 Specimen C55-19 failed in Tension-Compression Fatigue at 23°C (a) front (b) side view. σ_{max}=600 MPa, N_f=48

When the pre-fatigued 0/90 specimens failed in the monotonic tension-to-failure tests, typical tensile failure was observed. Failure is localized. Fiber fracture and ply delamination are observed as shown in Figure 82.

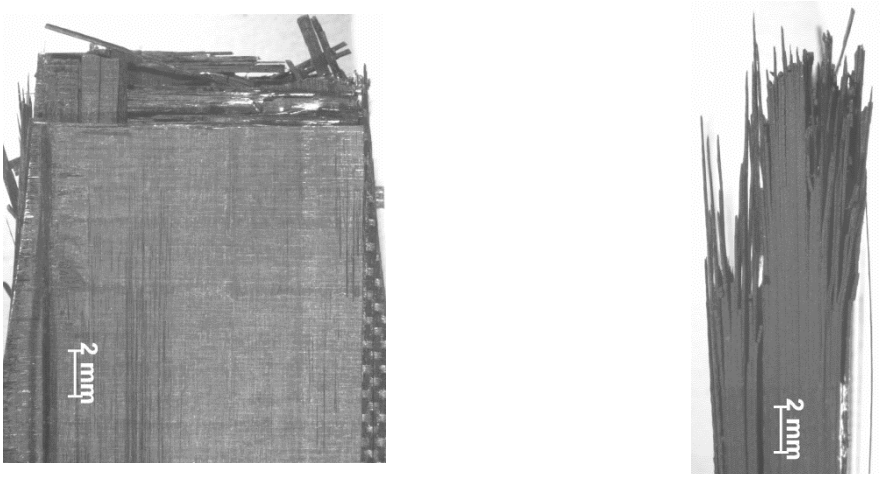

(a) (b)

Figure 82: Optical Micrographs of 0/90 Specimen C53-14 failed in Tension to Failure post Tension-Compression Fatigue at 23°C (a) front (b) side view. σ_{max}=400 MPa, N_f>100,000

VI. Conclusions and Recommendations

6.1 Conclusions

Tension-tension fatigue of the IM7/BMI 5250-4 composite at 23, 170, and 190°C was studied in this work. The tensile properties and tensile stress-strain behavior were also evaluated. As expected, the UTS values were significantly higher for the 0/90 fiber orientation than for the ±45 fiber orientation. For the 0/90 fiber orientation, the increase in temperature from 23°C to 170 or 190°C had minimal effect on the UTS, modulus, or failure strain. Notably, the stress-strain behavior of the 0/90 fiber orientation remains linear elastic to failure at all temperatures considered in this study. Conversely, temperature has a significant effect on the tensile properties of the ±45 fiber orientation. The UTS and tensile modulus decrease while the failure strain increases with increasing temperature. At 23°C, the tensile stress-strain behavior of the ±45 fiber orientation becomes strongly nonlinear as the stress exceeds 150 MPa. As the temperature increases to 170°C, departure from linearity occurs at a much lower stress.

Tension-tension fatigue performance of the composite was investigated for both 0/90 and ±45 fiber orientations at 23, 170, and 190°C. At 23°C, the composite with 0/90 fiber orientation exhibited exceptionally strong fatigue performance with the fatigue run-out stress as high as 90% UTS. Fatigue performance of the ±45 fiber orientation was considerably weaker; fatigue run-out was achieved at only 40% UTS. Increase in temperature to 170°C had little effect on the fatigue performance of the composite with either 0/90 or ±45 fiber orientation. Likewise, increase in temperature to 190°C had a negligible effect on fatigue performance of the 0/90 composite.

Tension-compression fatigue of the composite with 0/90 fiber orientation was investigated at 23°C. Compressive stress-strain behavior and compressive properties were evaluated at room and elevated temperatures. For the 0/90 fiber orientation compressive strength was significantly below the tensile strength. The difference between compressive and tensile strength was less pronounced for the ±45 fiber orientation. As in the case of tension, compressive strength and stiffness of the 0/90 fiber orientation were considerably higher than those of the ±45 fiber orientation. For both fiber orientations, compressive stress-strain curves were qualitatively similar to the tensile stress-strain curves. Increase in temperature caused a dramatic decrease in compressive strength for both fiber orientations. At 23°C, the tension-compression fatigue performance of the 0/90 fiber orientation is qualitatively similar to the tension-tension fatigue performance of the ±45 specimens. The tension-compression fatigue run-out was achieved at the maximum stress of only ~33% UTS (or ~50% UCS). The increased influence of the matrix on tension-compression fatigue response is apparent.

Throughout this research effort, a wide variation in performance between panels of the same fiber orientation was detected. Significant differences in modulus were noted for the 0/90 tension specimens, while substantial differences in UTS were observed for the ±45 tension-tension specimens. The variability in properties was attributed to fiber misalignment or other manufacturing defects.

6.3 Recommendations for Future Research

The manufacturing process should be refined in order to eliminate the observed panel-to-panel differences in mechanical properties. Fiber bunching and misalignment were noted in several test specimens, thus hampering the performance of the material.

Notably, all specimens used in this work were processed using the same cure cycle. Effects of the degree of cure on the fatigue performance should be investigated in the follow-on efforts. Additionally, effects of the fiber-matrix interphase (for example fiber sizing) on fatigue performance should also be studied.

Finally, a thorough investigation of the tension-compression fatigue performance of the composite with ±45 fiber orientation should be undertaken.

Appendix A: Fatigue Data for ±45 Specimens at 190°C

The results obtained during the fatigue testing of the ±45 fiber orientation at 190°C produced results inconsistent with previous testing. The material reached the run-out condition of 10^5 cycles at a higher maximum stress when tested at 190°C as opposed to the tests conducted at 23 and 170°C. The results of these tests are summarized in Table A-1. Figure A-1 and Figure A-2 further illustrate this data.

Table A-1: Tension-Tension Fatigue Results for ±45 Specimens at 190°C

Specimen #	σ_{max} (MPa)	σ_{max} (% UTS)	Cycles to Failure
T58-24	160	94.26	355
T68-25	160	94.26	183
T58-3	150	88.37	157
T68-16	150	88.37	1606
T69-8	142	83.65	100000
T69-18	135	79.53	100000
T59-14	127	74.82	100000
T69-6	127	74.82	100000

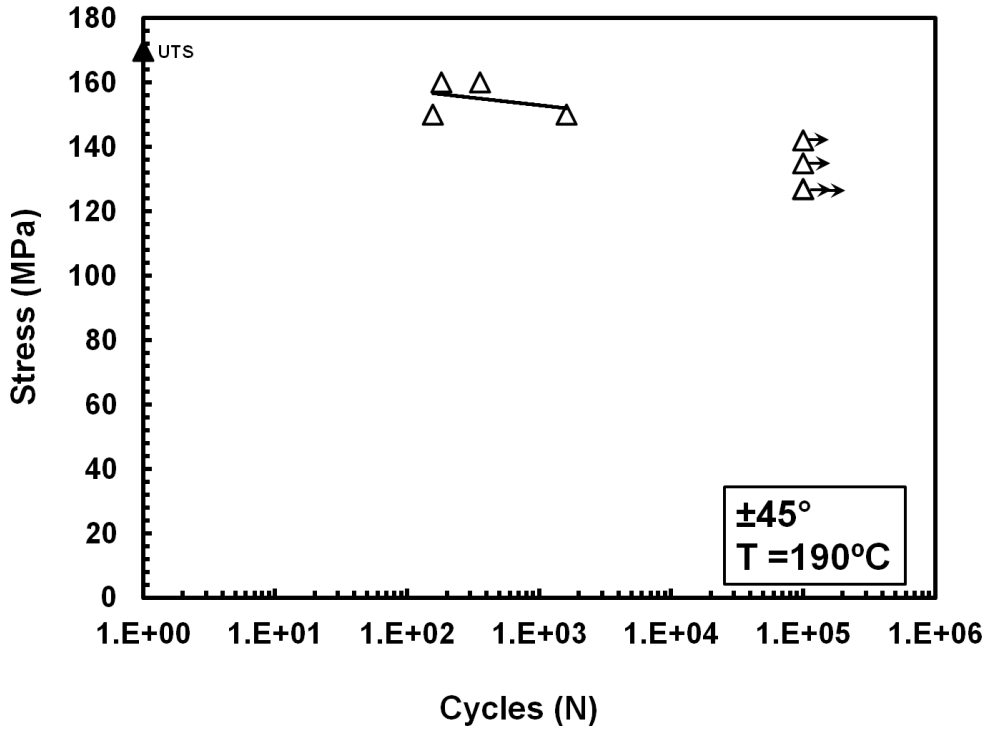

Figure A-1: Maximum Stress vs. Cycles to Failure for the ±45 Specimens at 190°C. Arrow Indicates Specimen Achieved Fatigue Run-Out.

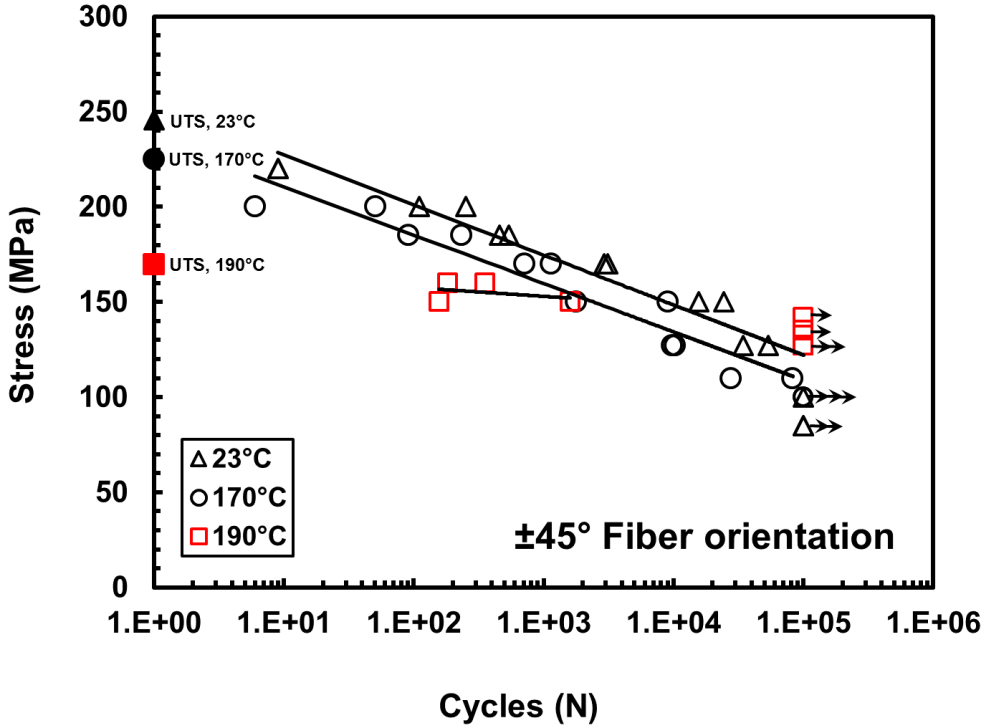

Figure A-2: Maximum Stress vs. Cycles to Failure for the ±45 Specimens at 23, 170, and 190°C. Arrow Indicates Specimen Achieved Fatigue Run-Out.

Figure A-3 through Figure A-11 demonstrate that the composite with ±45 fiber orientation tested at 190°C experienced significant strain accumulation and modulus loss during the first 1,000 cycles or less. This strain was maintained throughout subsequent cycles. Because the same test procedure from the fatigue tests conducted at 170°C was used for the tests conducted at 190°C with only a slight increase in temperature, it is unlikely that the testing procedure was flawed. Therefore, this difference was likely caused by a change that occurred in the matrix material.

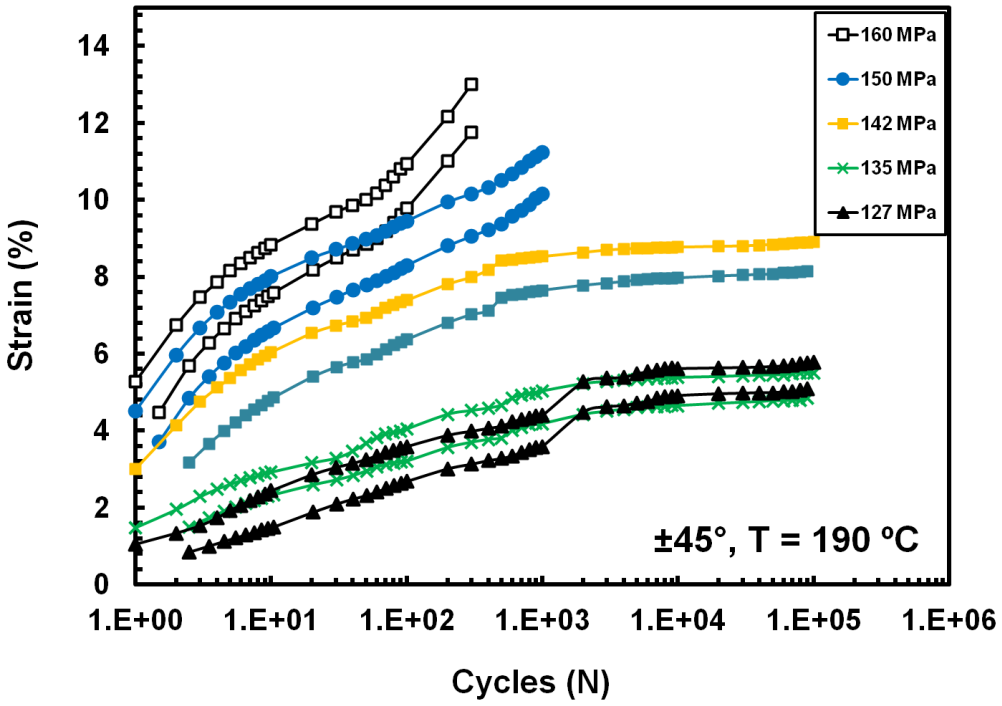

Figure A-3: Minimum and Maximum Strains vs. Fatigue Cycles for ±45 Specimens at 190°C

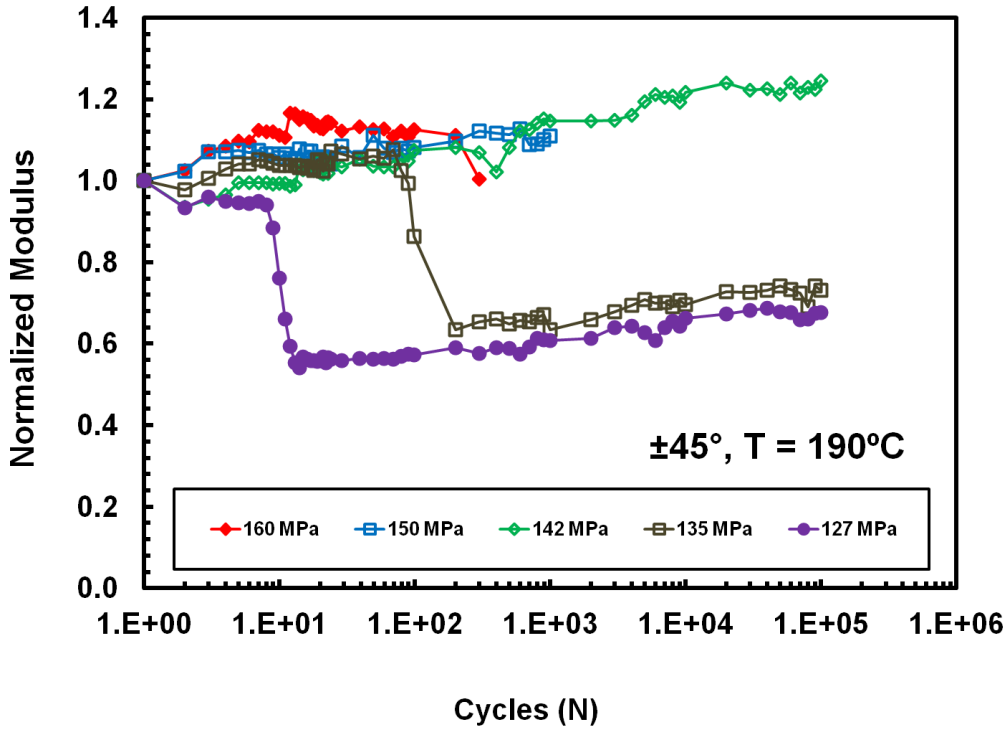

Figure A-4: Normalized Modulus vs. Fatigue Cycles for ±45 Specimens at 190°C

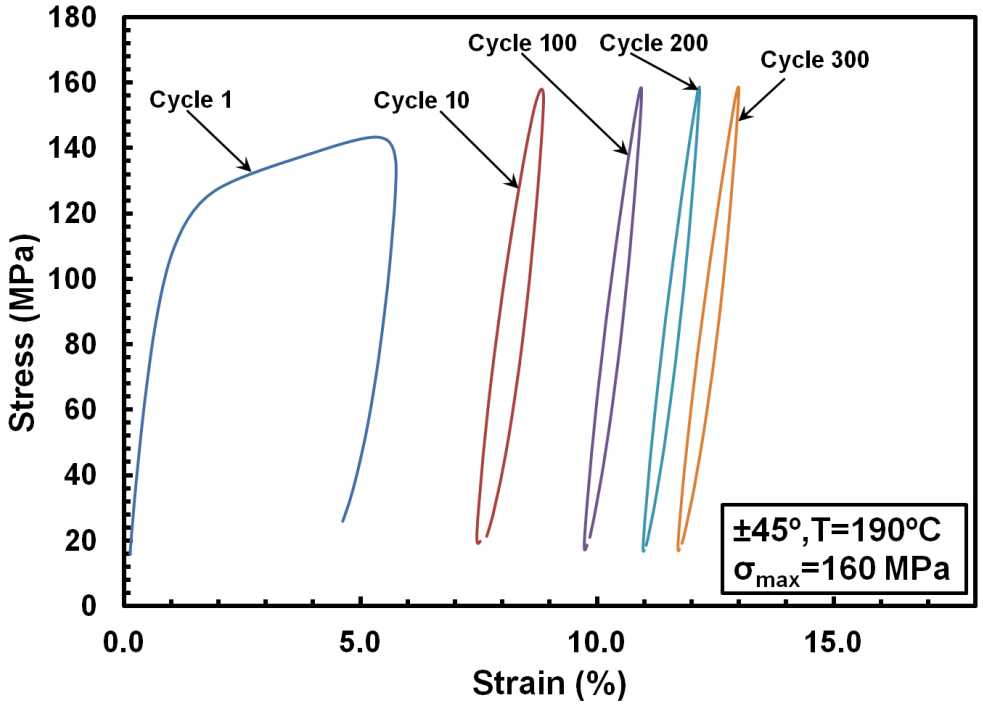

Figure A-5: Evolution of Stress-Strain Hysteresis Response with Fatigue Cycles for Specimen T58-24 with ±45 Fiber Orientation at 190°C. σ_{max}=160 MPa.

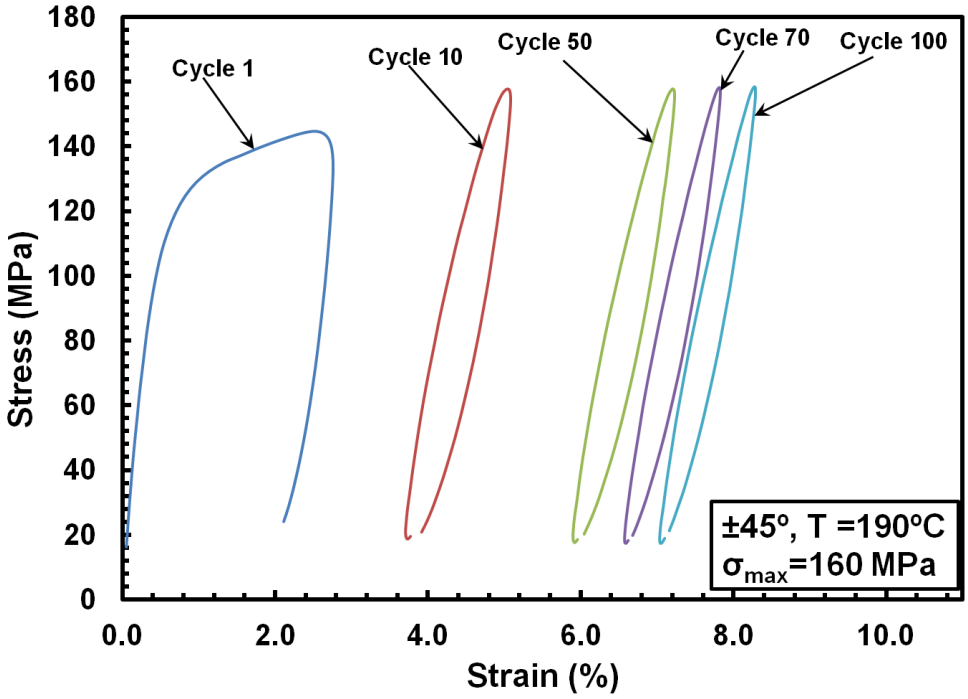

Figure A-6: Evolution of Stress-Strain Hysteresis Response with Fatigue Cycles for Specimen T68-25 with ±45 Fiber Orientation at 190°C. σ_{max}=160 MPa.

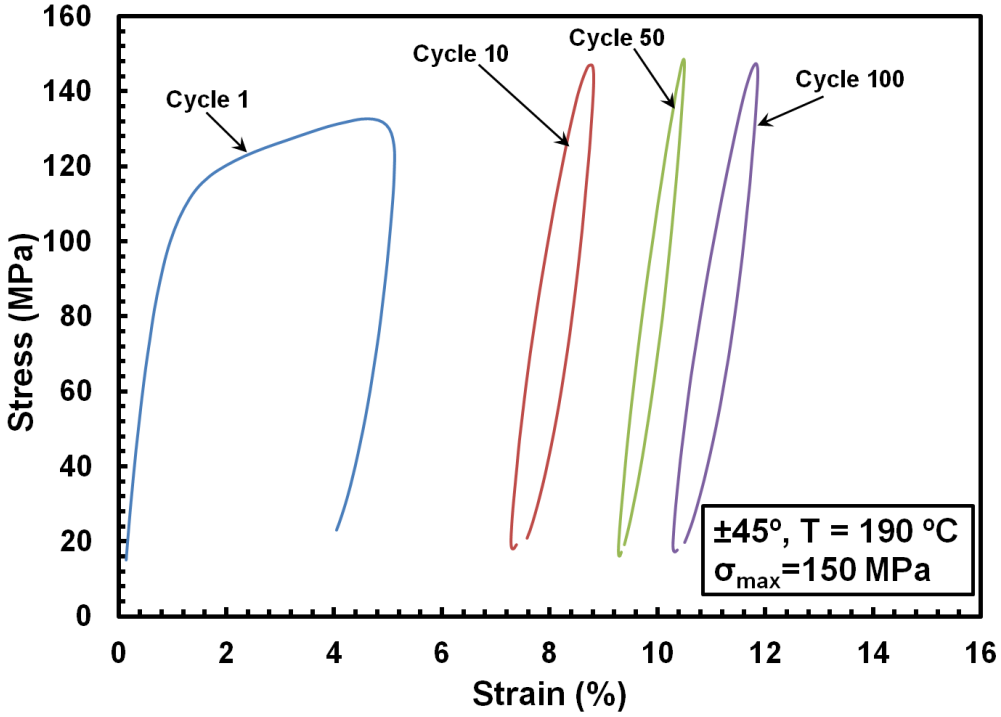

Figure A-7: Evolution of Stress-Strain Hysteresis Response with Fatigue Cycles for Specimen T58-3 with ±45 Fiber Orientation at 190°C. σ_{max}=150 MPa.

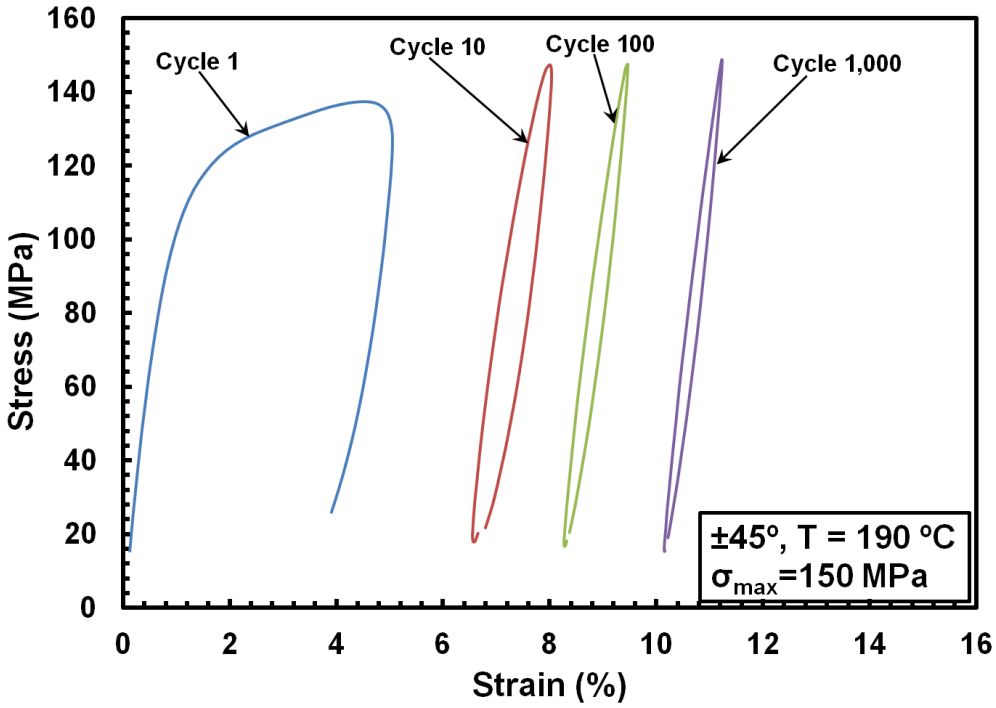

Figure A-8: Evolution of Stress-Strain Hysteresis Response with Fatigue Cycles for Specimen T68-16 with ±45 Fiber Orientation at 190°C. σ_{max}=150 MPa.

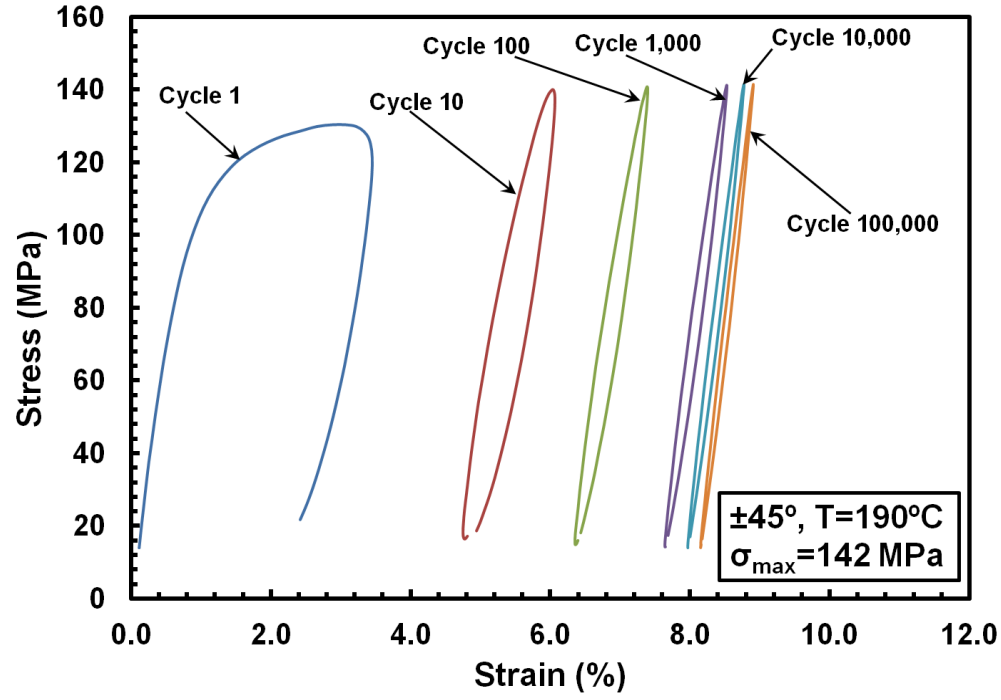

Figure A-9: Evolution of Stress-Strain Hysteresis Response with Fatigue Cycles for Specimen T69-8 with ±45 Fiber Orientation at 190°C. σ_{max}=142 MPa

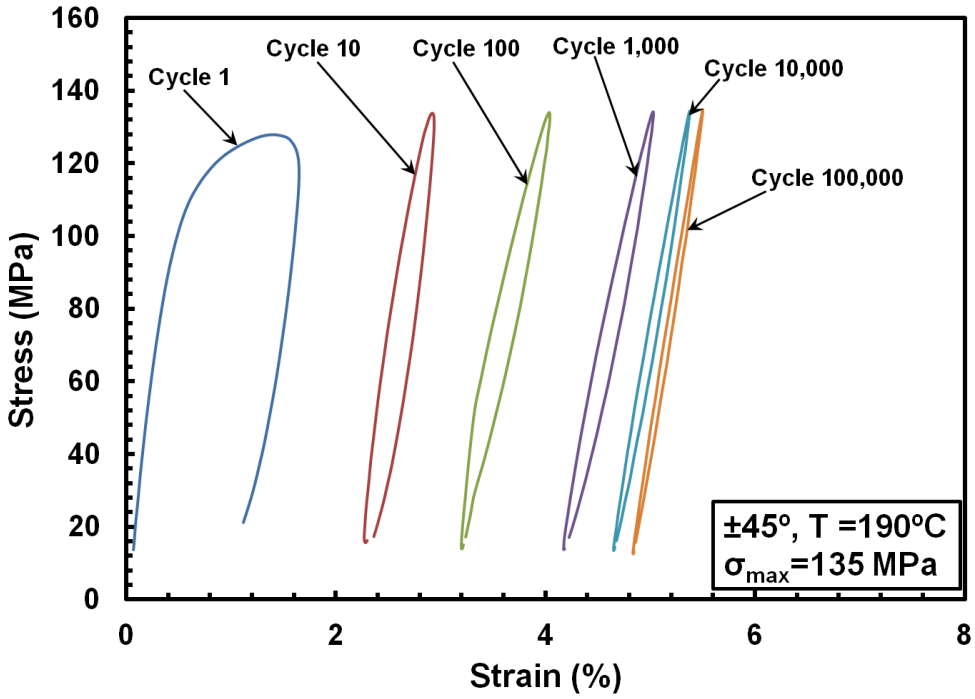

Figure A-10: Evolution of Stress-Strain Hysteresis Response with Fatigue Cycles for Specimen T69-18 with ±45 Fiber Orientation at 190°C. σ_{max}=135 MPa.

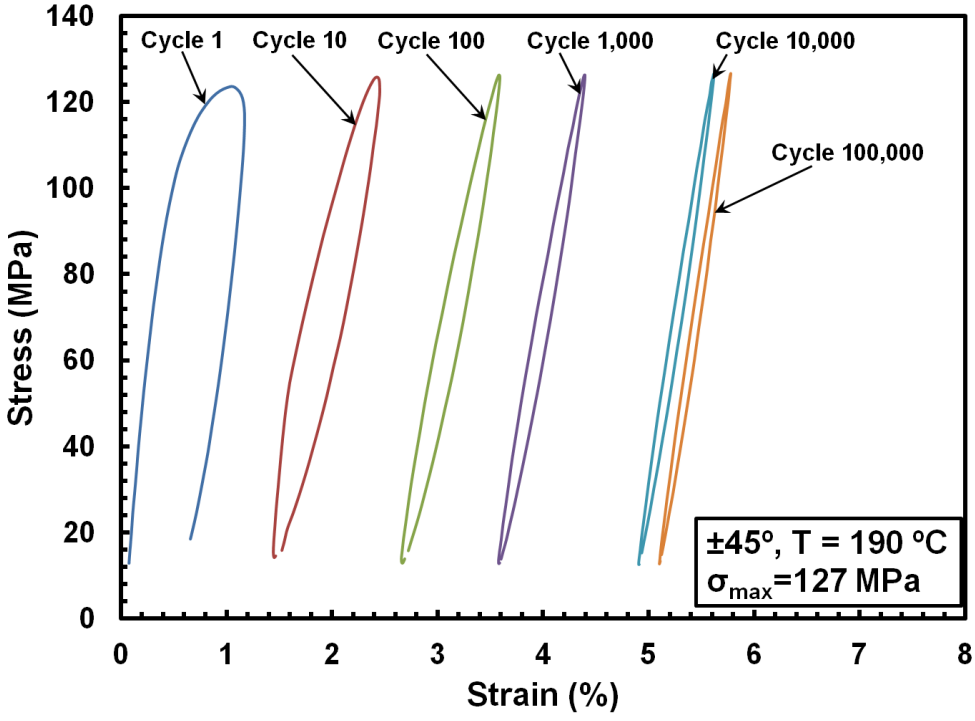

Figure A-11: Evolution of Stress-Strain Hysteresis Response with Fatigue Cycles for Specimen T59-14 with ±45 Fiber Orientation at 190°C. σ_{max}=127 MPa.

Post-fatigue at 190°C, the specimens that reached 10^5 cycles were tested in tension to failure at 190°C to determine the retained tensile properties. The results of these tests are summarized in Table A-2.

Table A-2: Retained Properties of the ±45 Specimens Subjected to 10^5 Cycles of Prior Fatigue at 190°C

Max Fatigue Stress (MPa)	Retained Strength (MPa)	Retained Modulus (GPa)	Strain at Failure (%)
127	184	17.08	3.38
127	191	17.37	5.44
135	203	18.49	5.07
142	196	17.32	3.44

Figure A-12 demonstrates that the linear region of the stress-strain curve elongates producing linear elastic behavior up to 150 MPa. A significant decrease in failure strain is observed accompanied by a slight increase in UTS.

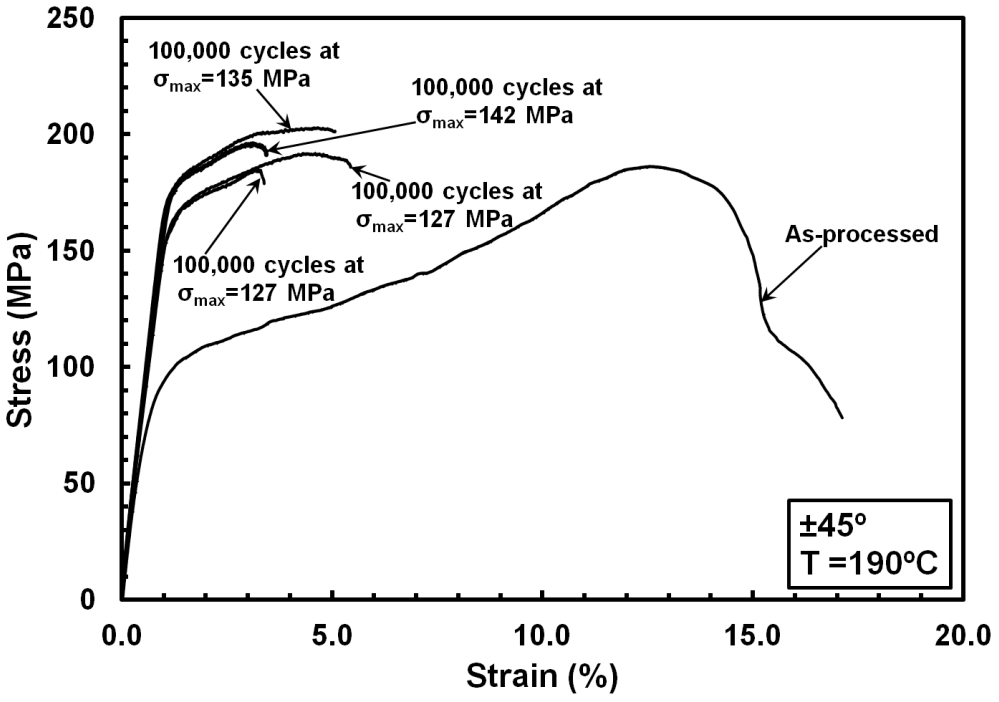

Figure A-12: Effects of Prior Tension-Tension Fatigue at 190°C on Tensile Stress-Strain Behavior of the ±45 Fiber Orientation.

As expected, the ±45 fiber orientation demonstrated fiber scissoring upon failure at 190°C.

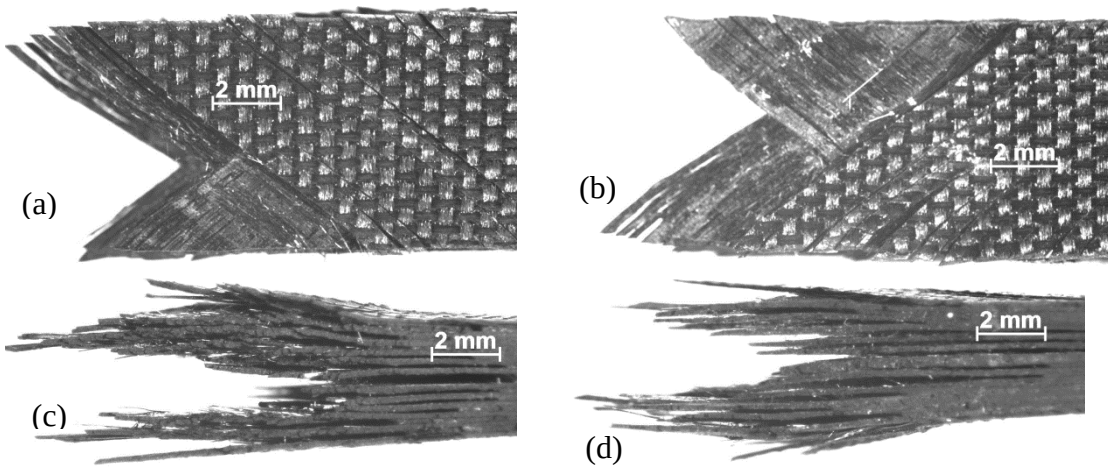

Figure A-13: Optical Micrographs of the ±45 Specimen T68-25 failed in Tension-Tension Fatigue at 190°C (a) front (b) back (c) top (d) bottom. σ_{max}=160 MPa, N_f=183.

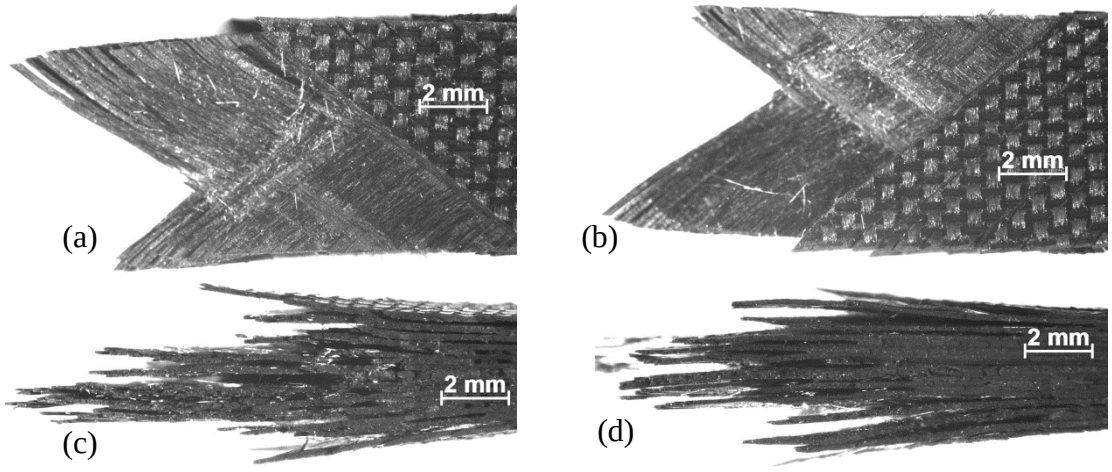

Figure A-14: Optical Micrographs of the ±45 Specimen T69-8 failed in Tension-Tension Fatigue at 190°C (a) front (b) back (c) top (d) bottom. σ_{max}=142 MPa, N_f>100,000.

Appendix B: Stress-Strain Hysteresis Loops

The hysteresis responses for all specimens with available data are presented in Figure B-1 through Figure B-28.

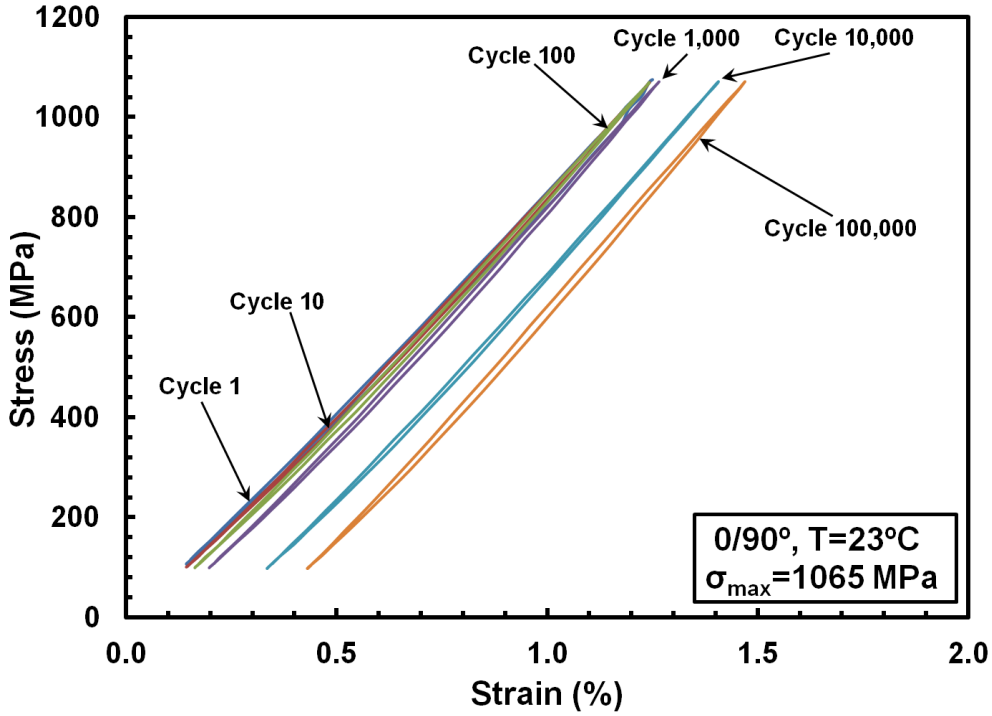

Figure B-1: Evolution of Stress-Strain Hysteresis Response with Fatigue Cycles for Specimen T43-12 with 0/90 Fiber Orientation at 23°C. σ_{max}=1065 MPa.

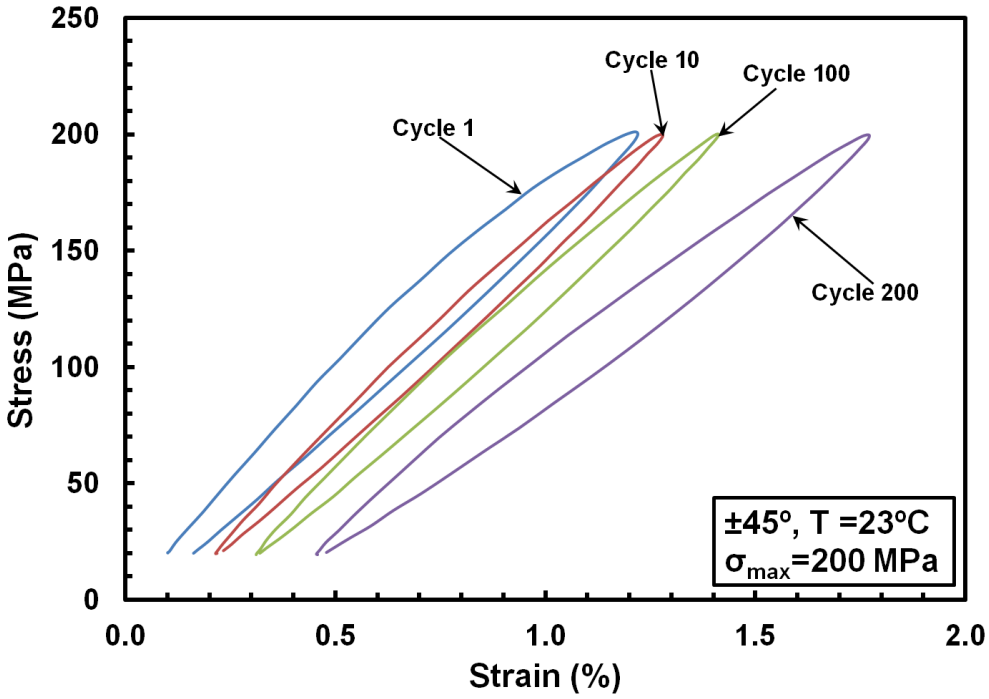

Figure B-2: Evolution of Stress-Strain Hysteresis Response with Fatigue Cycles for Specimen T68-18 with ±45 Fiber Orientation at 23°C. σ_{max}=200 MPa.

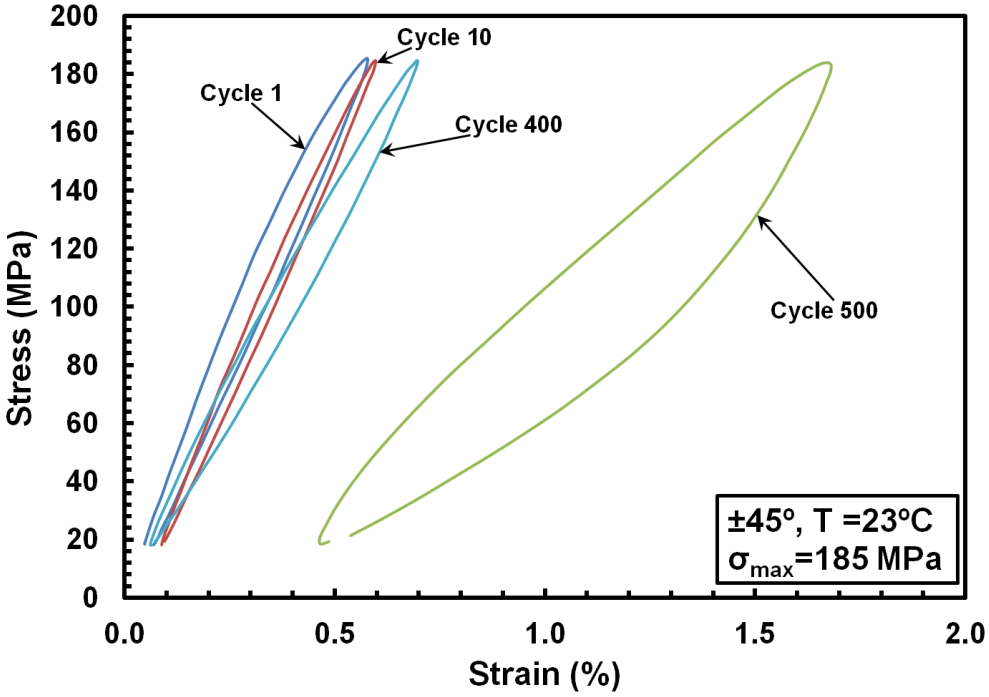

Figure B-3: Evolution of Stress-Strain Hysteresis Response with Fatigue Cycles for Specimen T68-12 with ±45 Fiber Orientation at 23°C. σ_{max}=185 MPa.

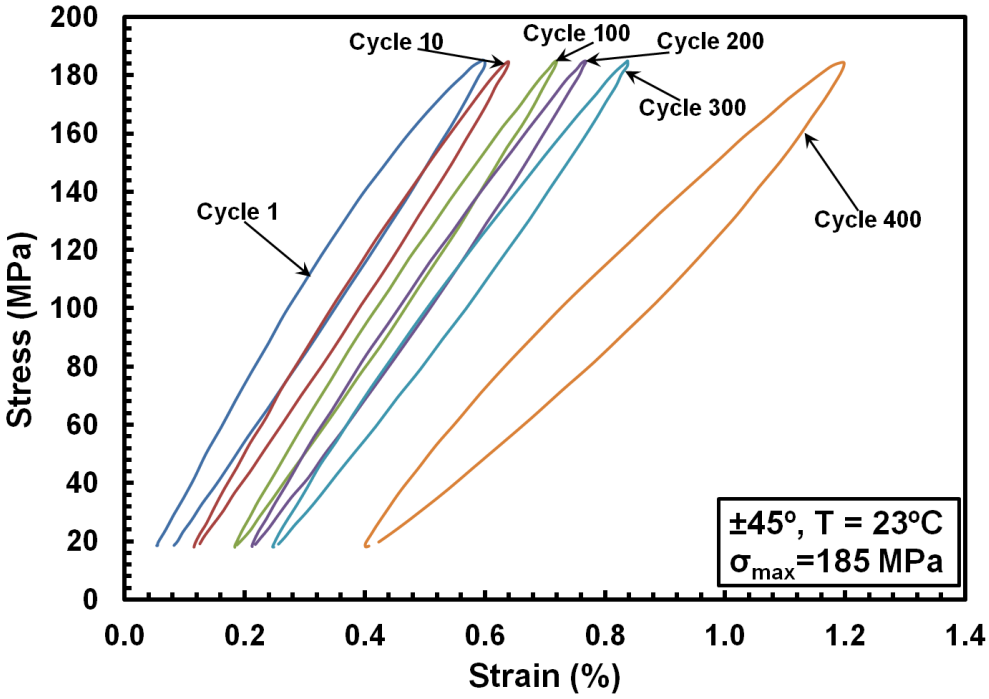

Figure B-4: Evolution of Stress-Strain Hysteresis Response with Fatigue Cycles for Specimen T69-2 with ±45 Fiber Orientation at 23°C. σ_{max}=185 MPa.

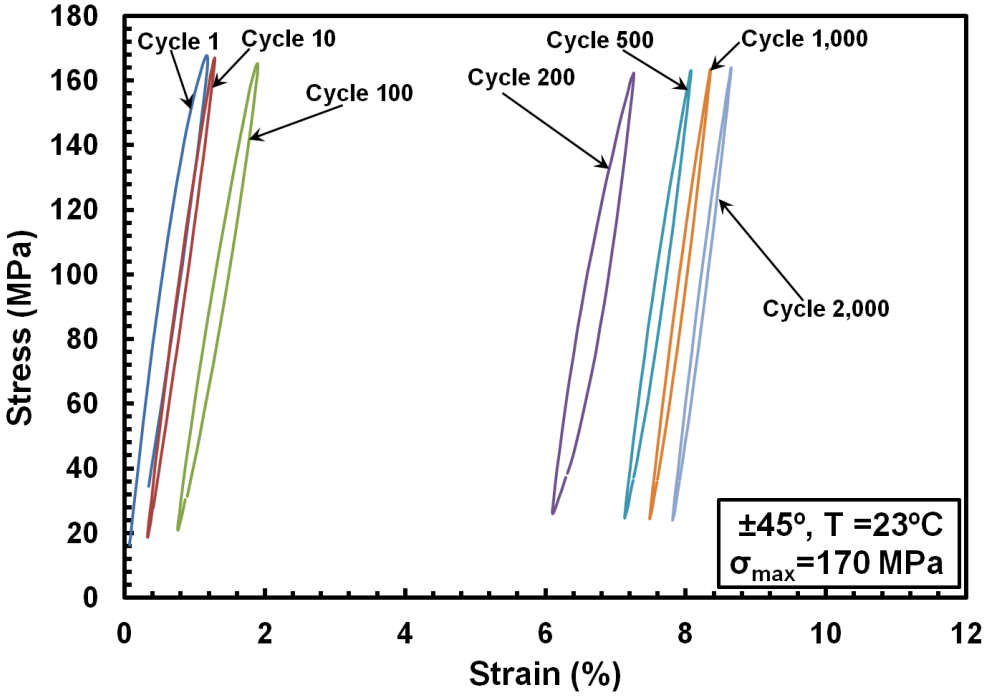

Figure B-5: Evolution of Stress-Strain Hysteresis Response with Fatigue Cycles for Specimen T59-8 with ±45 Fiber Orientation at 23°C. σ_{max}=170 MPa.

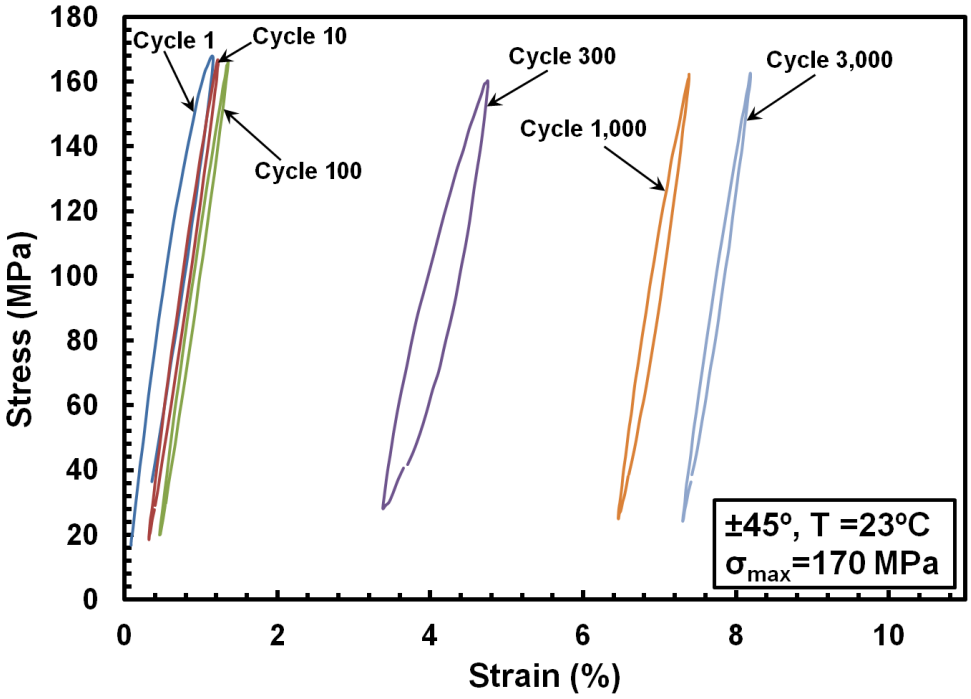

Figure B-6: Evolution of Stress-Strain Hysteresis Response with Fatigue Cycles for Specimen T68-10 with ±45 Fiber Orientation at 23°C. σ_{max}=170 MPa.

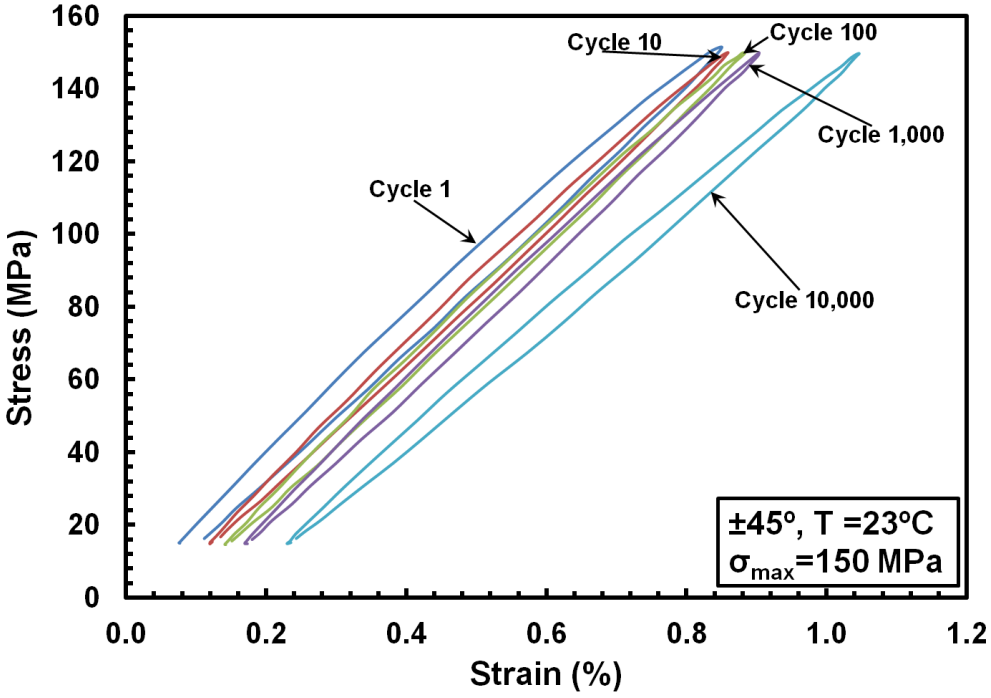

Figure B-7: Evolution of Stress-Strain Hysteresis Response with Fatigue Cycles for Specimen T68-8 with ±45 Fiber Orientation at 23°C. σ_{max}=150 MPa.

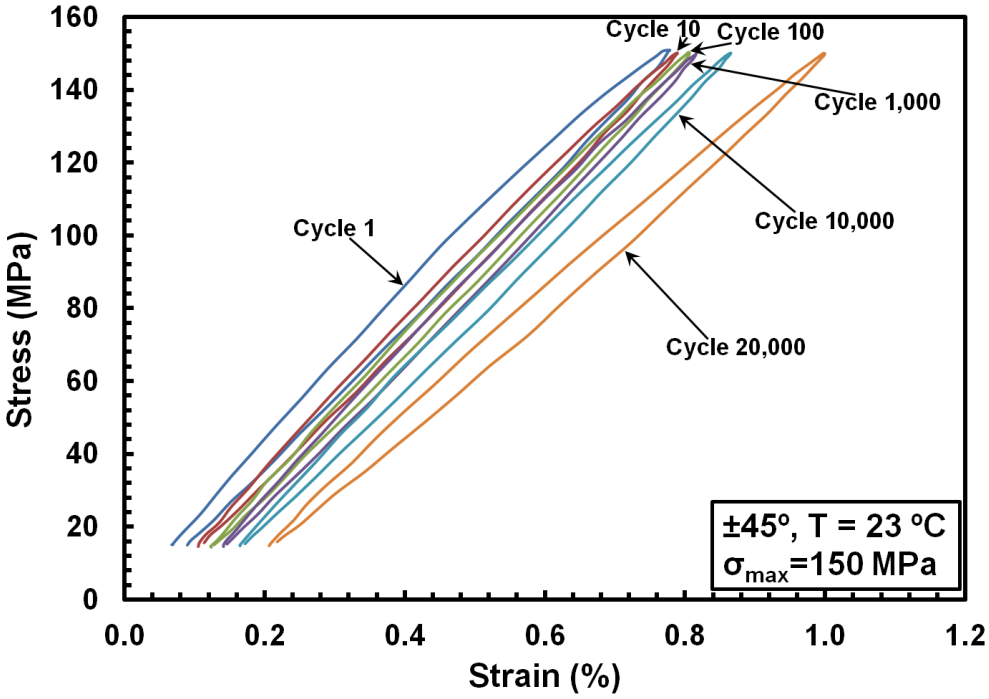

Figure B-8: Evolution of Stress-Strain Hysteresis Response with Fatigue Cycles for Specimen T59-18 with ±45 Fiber Orientation at 23°C. σ_{max}=150 MPa.

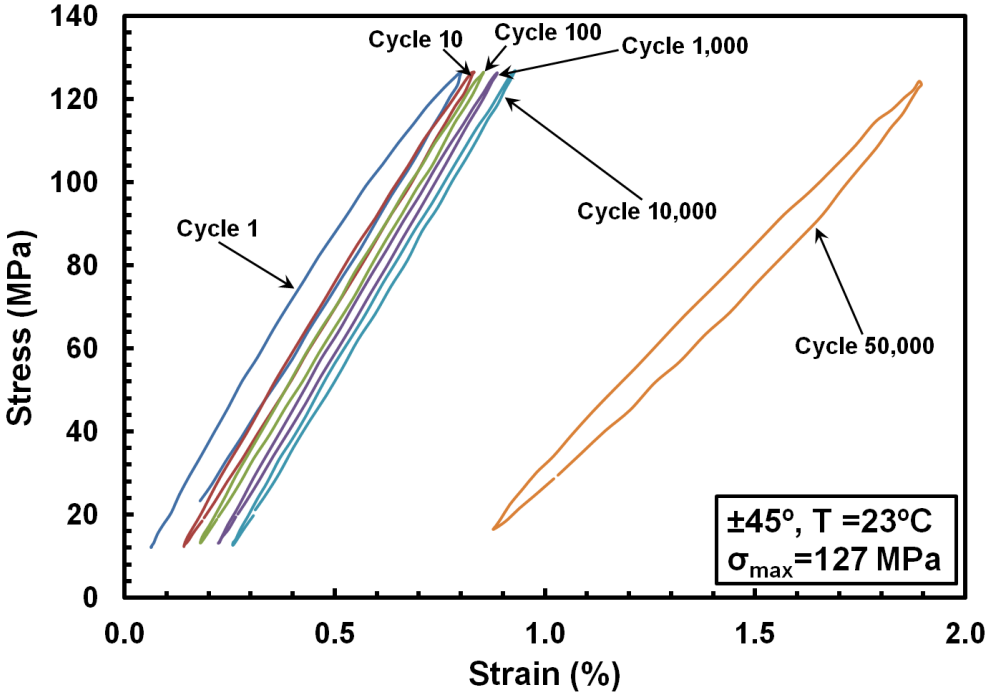

Figure B-9: Evolution of Stress-Strain Hysteresis Response with Fatigue Cycles for Specimen T58-14 with ±45 Fiber Orientation at 23°C. σ_{max}=127 MPa.

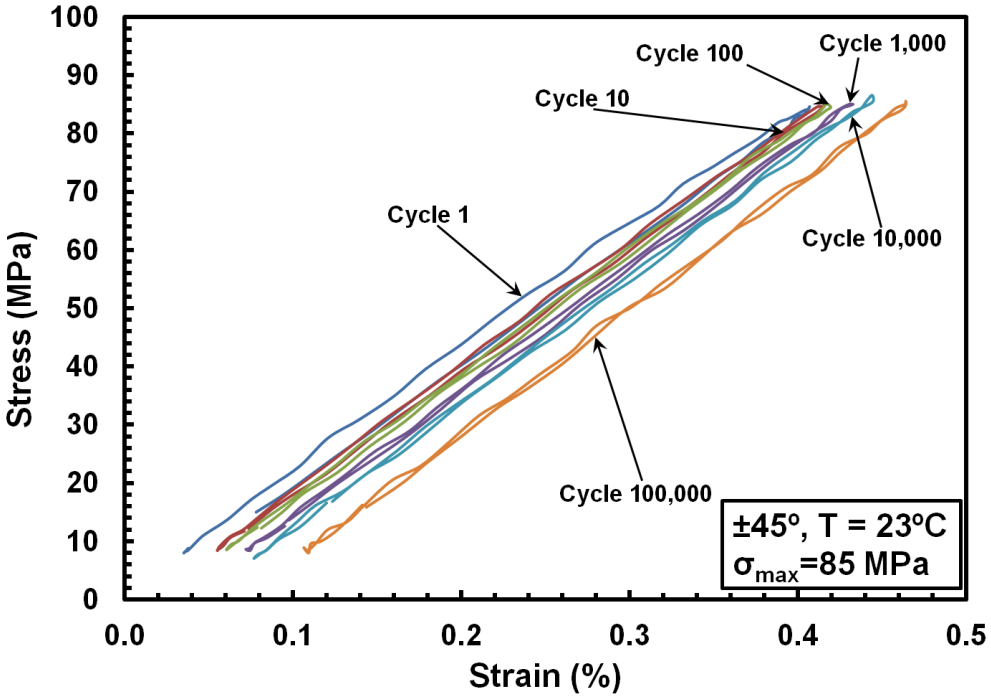

Figure B-10: Evolution of Stress-Strain Hysteresis Response with Fatigue Cycles for Specimen T60-2 with ±45 Fiber Orientation at 23°C. σ_{max}=85 MPa.

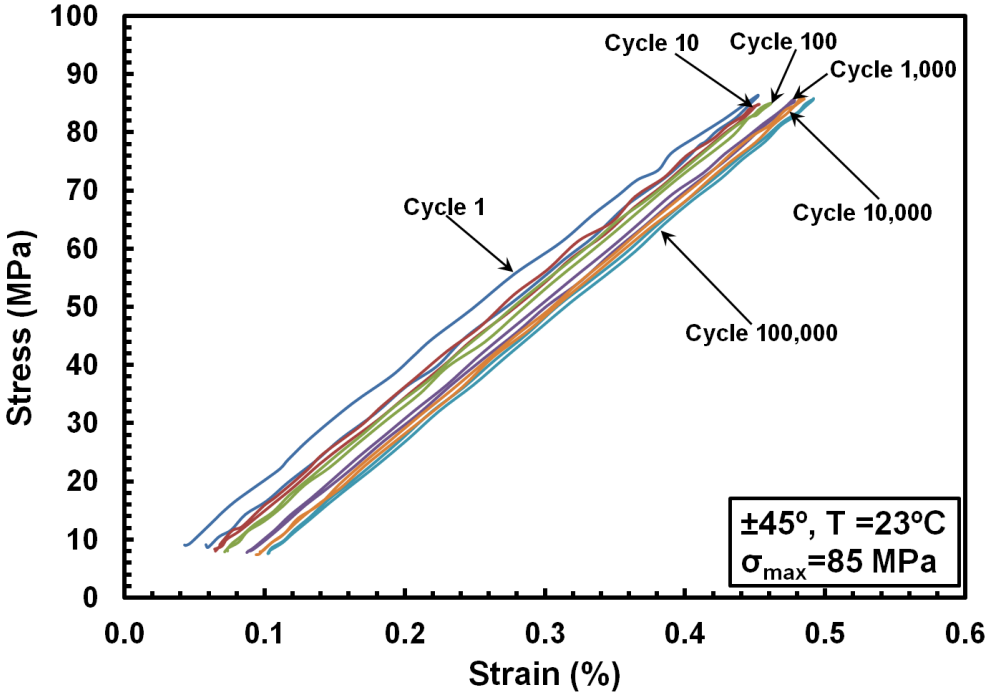

Figure B-11: Evolution of Stress-Strain Hysteresis Response with Fatigue Cycles for Specimen T60-4 with ±45 Fiber Orientation at 23°C. σ_{max}=85 MPa.

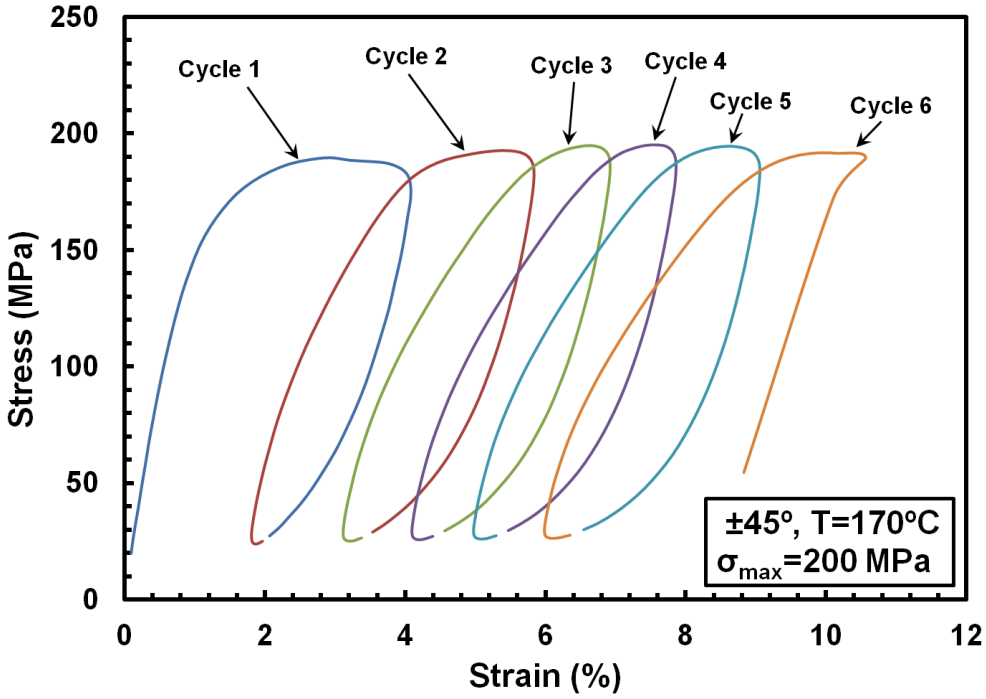

Figure B-12: Evolution of Stress-Strain Hysteresis Response with Fatigue Cycles for Specimen T60-13 with ±45 Fiber Orientation at 170°C. σ_{max}=200 MPa.

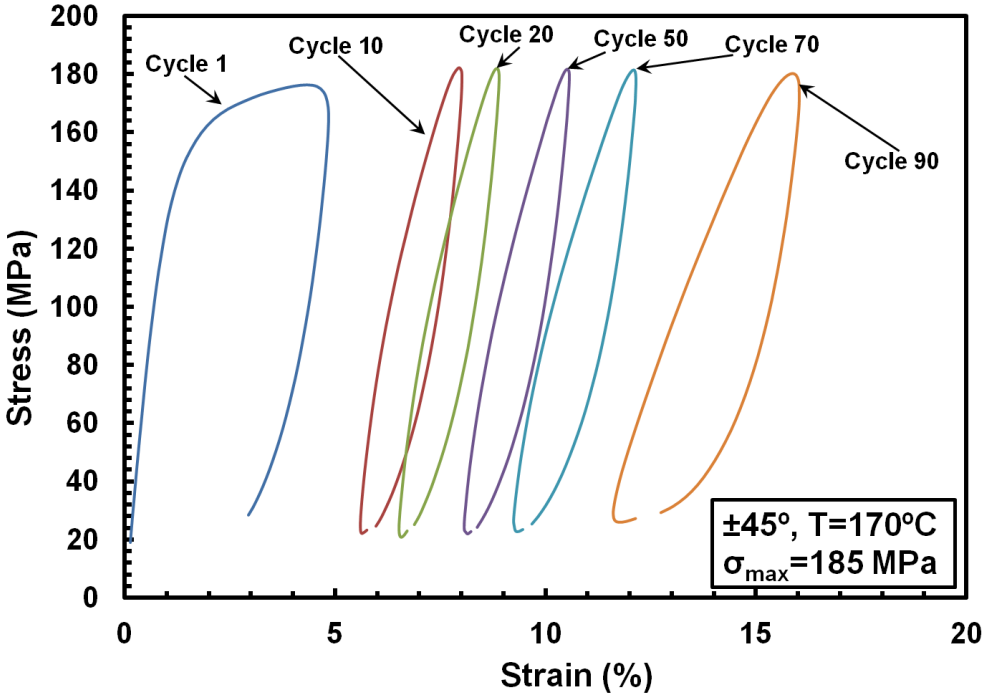

Figure B-13: Evolution of Stress-Strain Hysteresis Response with Fatigue Cycles for Specimen T68-1 with ±45 Fiber Orientation at 170°C. σ_{max}=185 MPa.

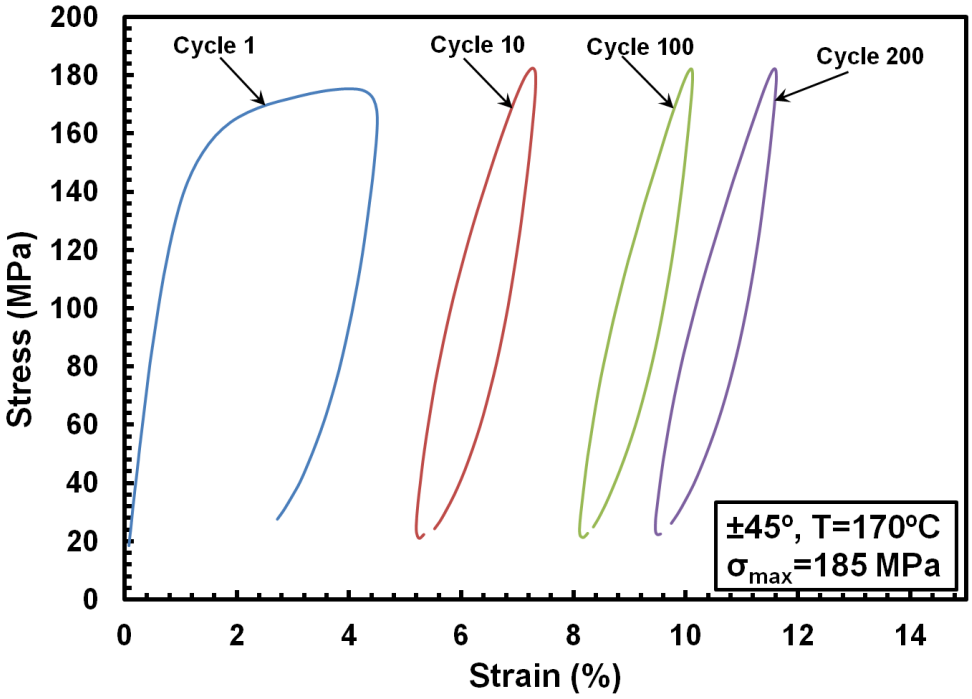

Figure B-14: Evolution of Stress-Strain Hysteresis Response with Fatigue Cycles for Specimen T59-1 with ±45 Fiber Orientation at 170°C. σ_{max}=185 MPa.

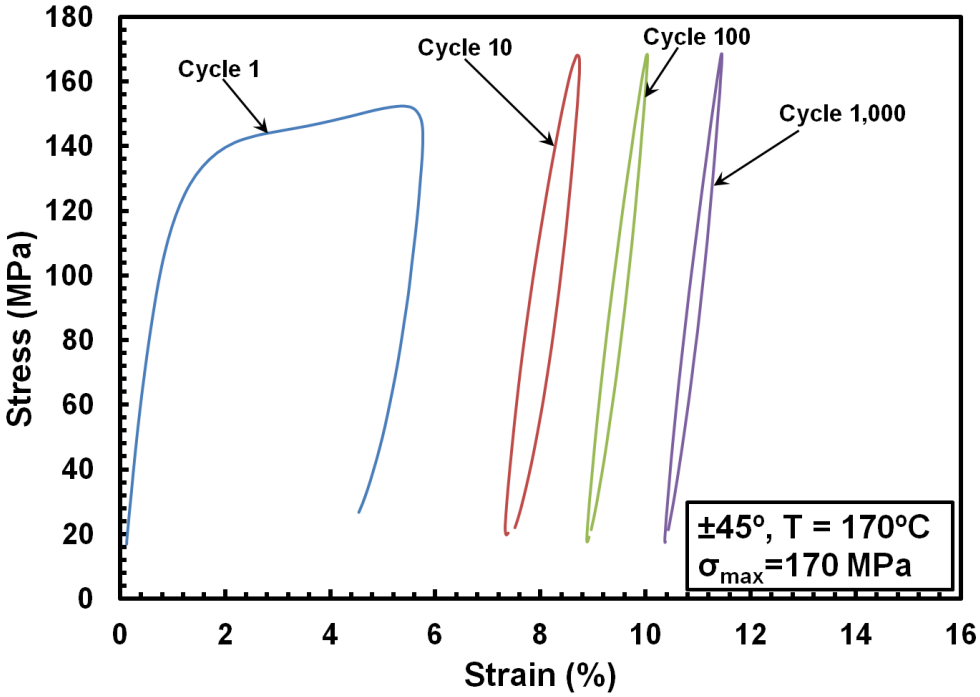

Figure B-15: Evolution of Stress-Strain Hysteresis Response with Fatigue Cycles for Specimen T58-1 with ±45 Fiber Orientation at 170°C. σ_{max}=170 MPa.

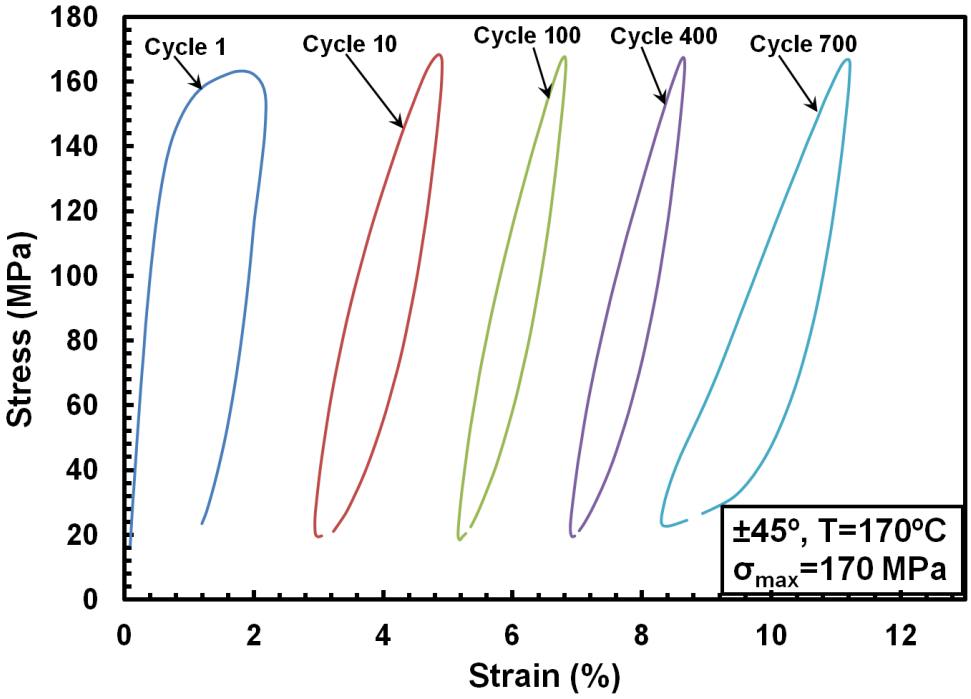

Figure B-16: Evolution of Stress-Strain Hysteresis Response with Fatigue Cycles for Specimen T58-20 with ±45 Fiber Orientation at 170°C. σ_{max}=170 MPa.

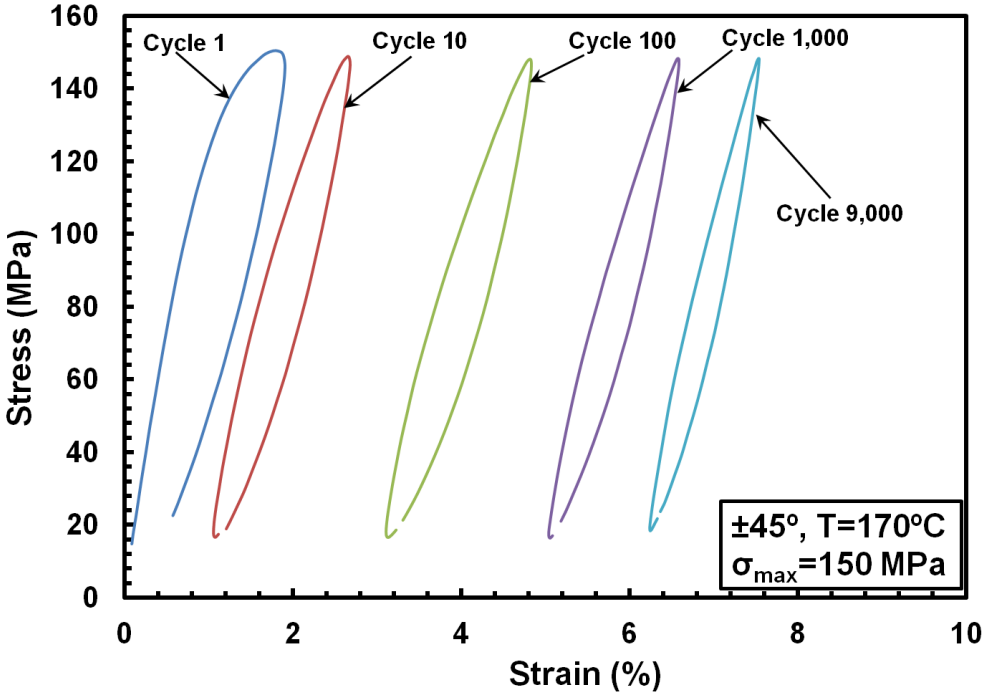

Figure B-17: Evolution of Stress-Strain Hysteresis Response with Fatigue Cycles for Specimen T68-19 with ±45 Fiber Orientation at 170°C. σ_{max}=150 MPa.

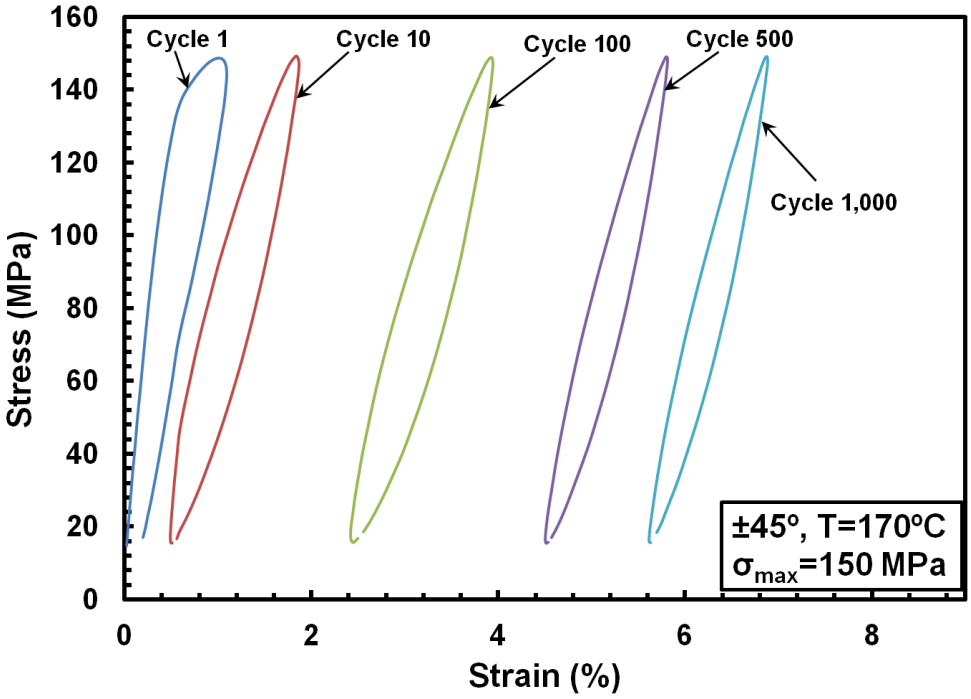

Figure B-18: Evolution of Stress-Strain Hysteresis Response with Fatigue Cycles for Specimen T69-9 with ±45 Fiber Orientation at 170°C. σ_{max}=150 MPa.

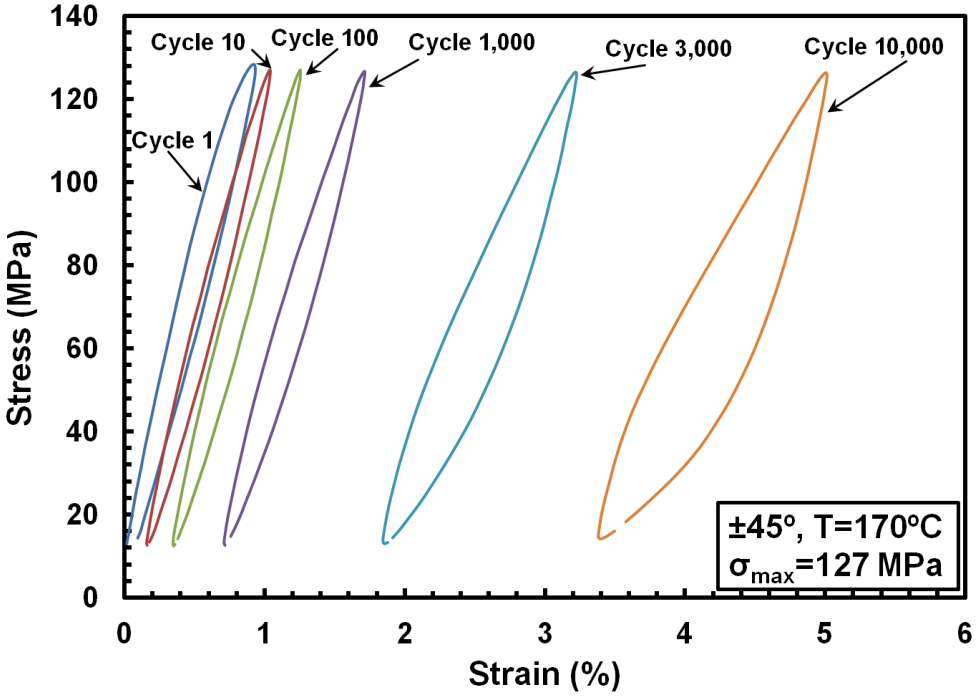

Figure B-19: Evolution of Stress-Strain Hysteresis Response with Fatigue Cycles for Specimen T69-5 with ±45 Fiber Orientation at 170°C. σ_{max}=127 MPa.

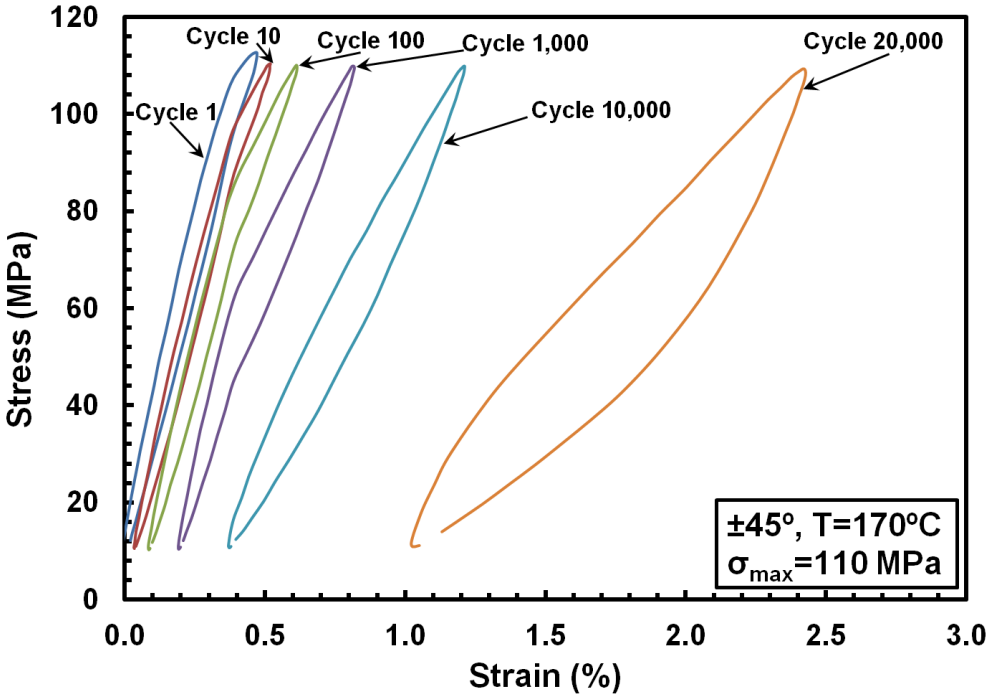

Figure B-20: Evolution of Stress-Strain Hysteresis Response with Fatigue Cycles for Specimen T58-6 with ±45 Fiber Orientation at 170°C. σ_{max}=110 MPa.

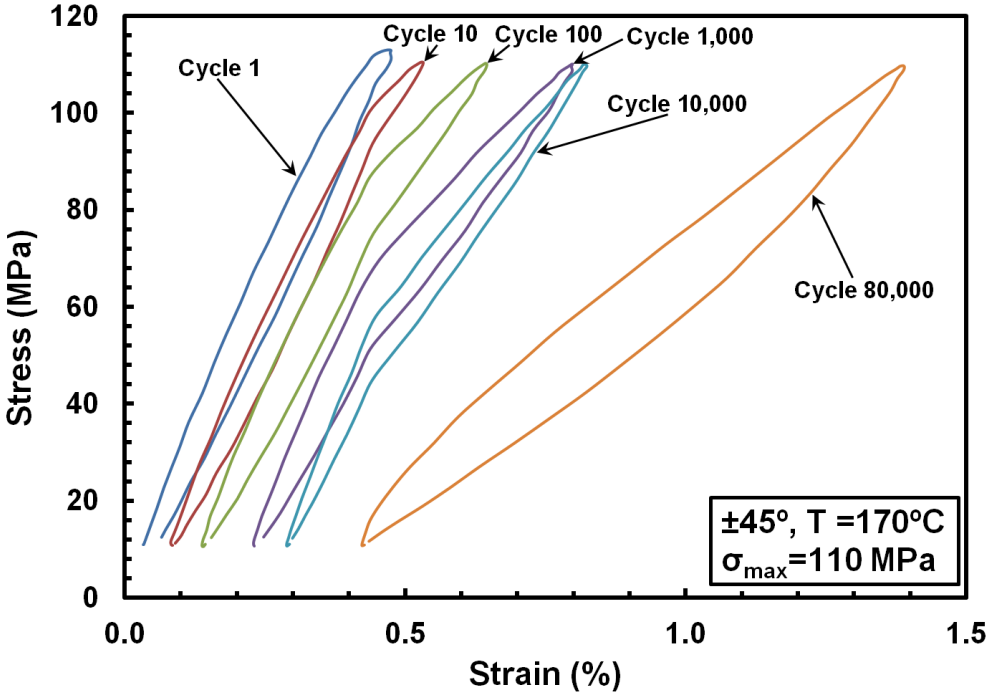

Figure B-21: Evolution of Stress-Strain Hysteresis Response with Fatigue Cycles for Specimen T60-3 with ±45 Fiber Orientation at 170°C. σ_{max}=110 MPa.

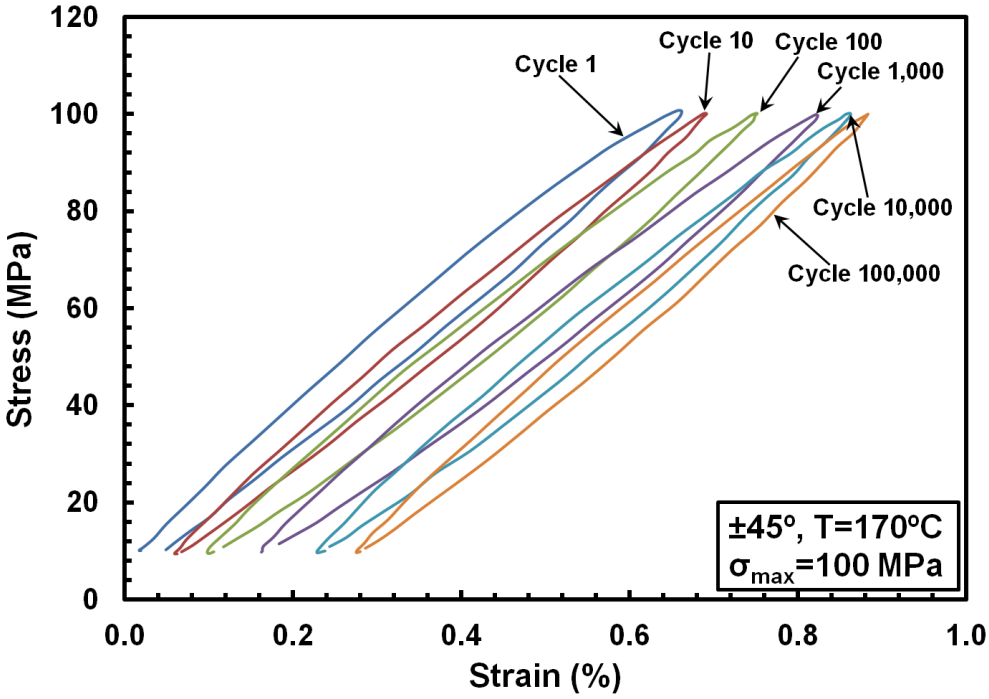

Figure B-22: Evolution of Stress-Strain Hysteresis Response with Fatigue Cycles for Specimen T59-20 with ±45 Fiber Orientation at 170°C. σ_{max}=100 MPa.

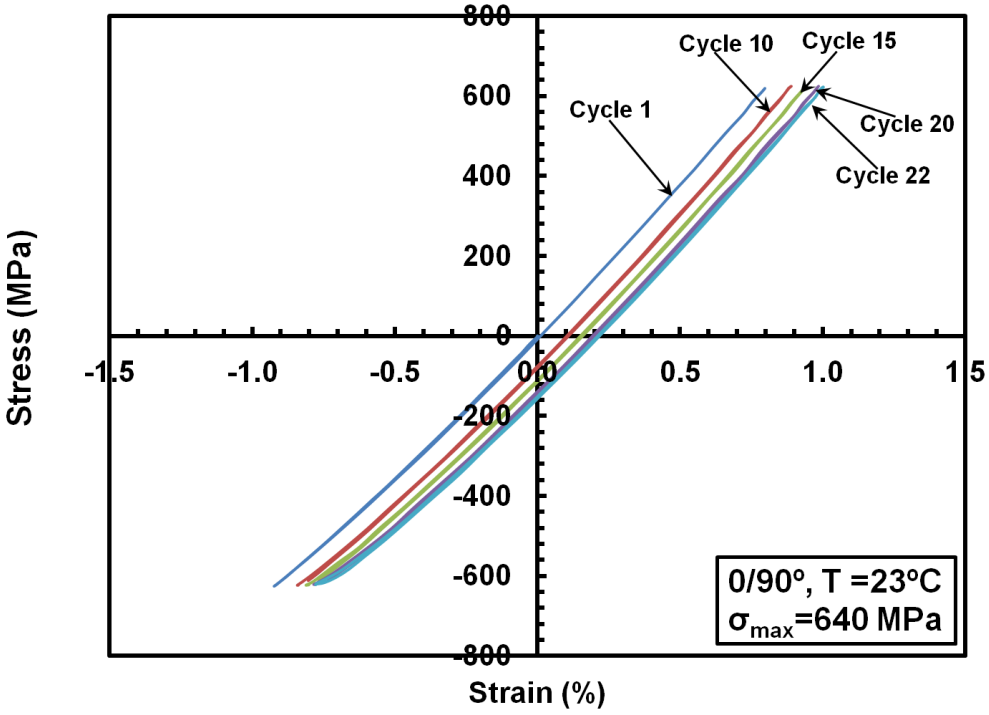

Figure B-23: Evolution of Stress-Strain Hysteresis Response with Fatigue Cycles for Specimen C55-5 with 0/90 Fiber Orientation at 23°C. σ_{max}=640 MPa.

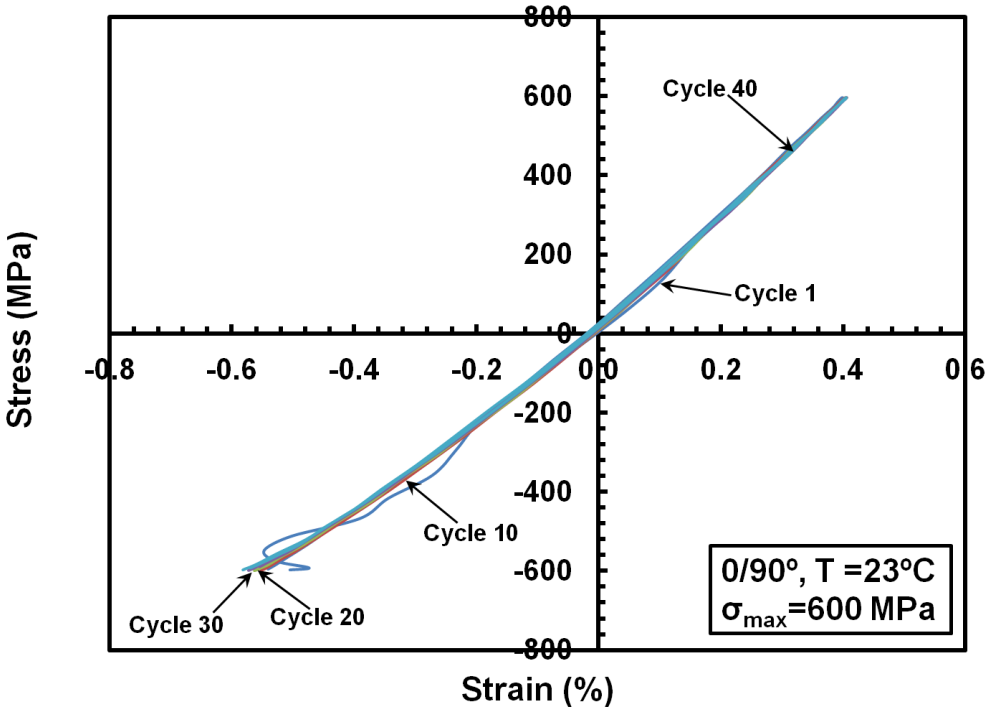

Figure B-24: Evolution of Stress-Strain Hysteresis Response with Fatigue Cycles for Specimen C55-19 with 0/90 Fiber Orientation at 23°C. σ_{max}=600 MPa.

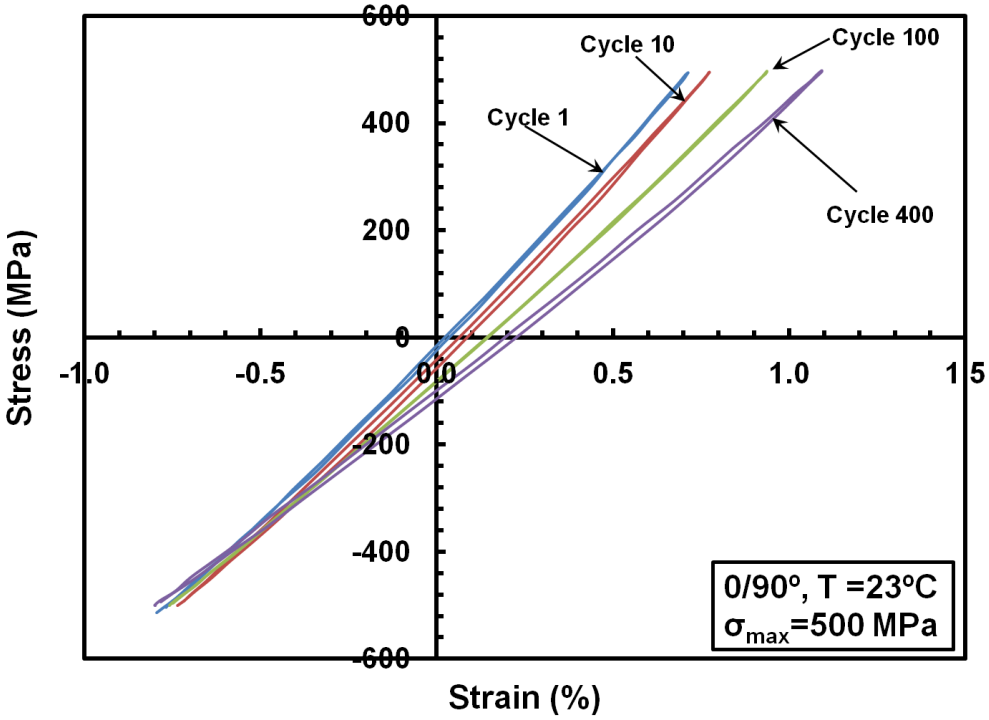

Figure B-25: Evolution of Stress-Strain Hysteresis Response with Fatigue Cycles for Specimen C54-18 with 0/90 Fiber Orientation at 23°C. σ_{max}=500 MPa.

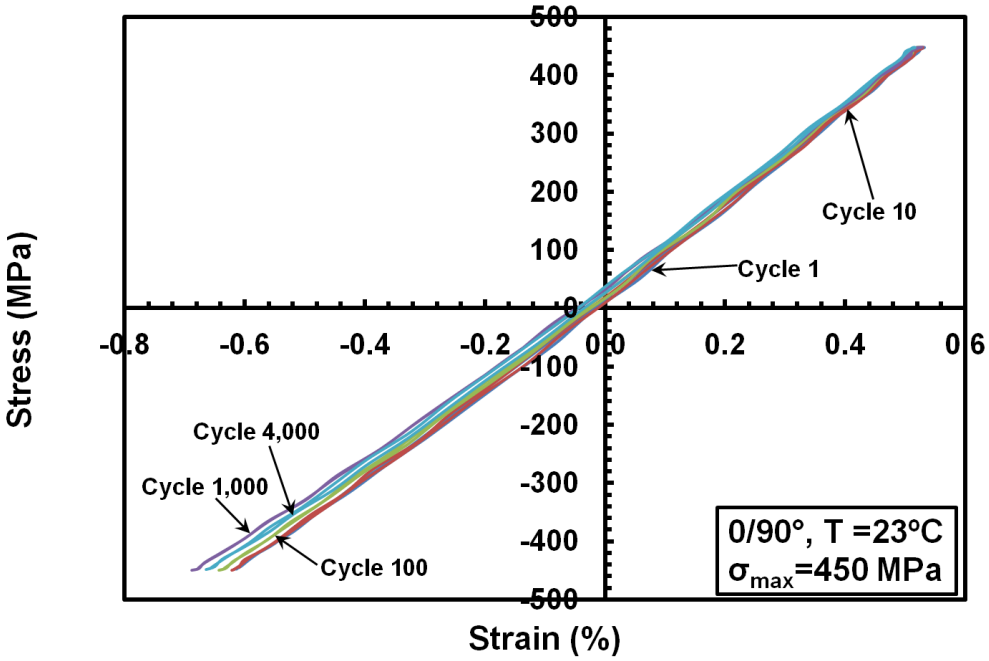

Figure B-26: Evolution of Stress-Strain Hysteresis Response with Fatigue Cycles for Specimen C54-3 with 0/90 Fiber Orientation at 23°C. σ_{max}=450 MPa.

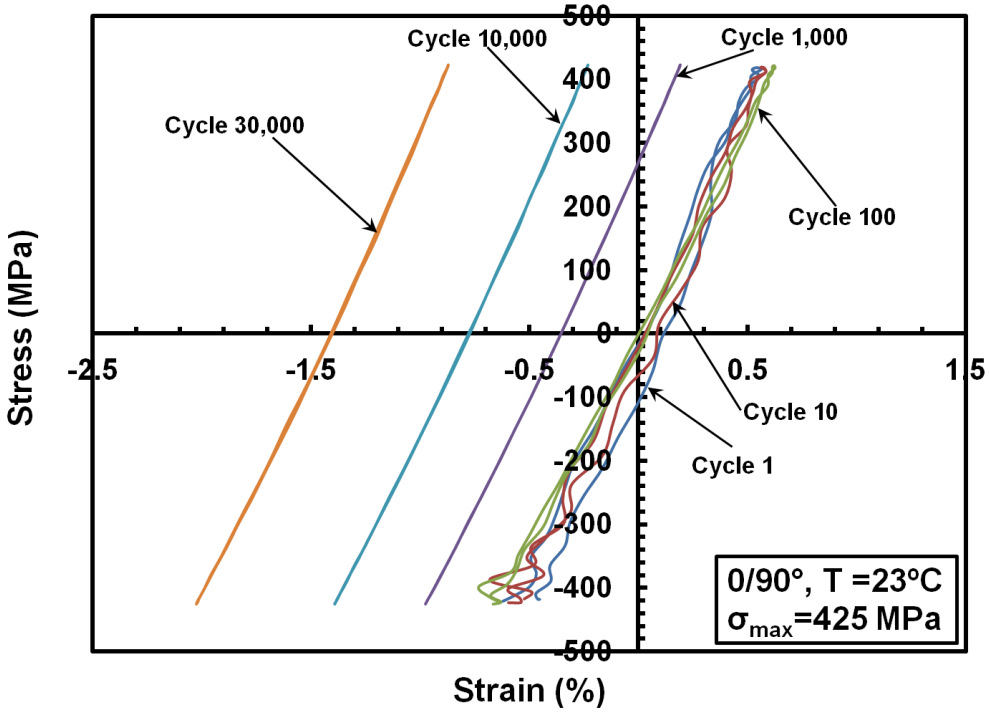

Figure B-27: Evolution of Stress-Strain Hysteresis Response with Fatigue Cycles for Specimen C55-3 with 0/90 Fiber Orientation at 23°C. σ_{max}=425 MPa.

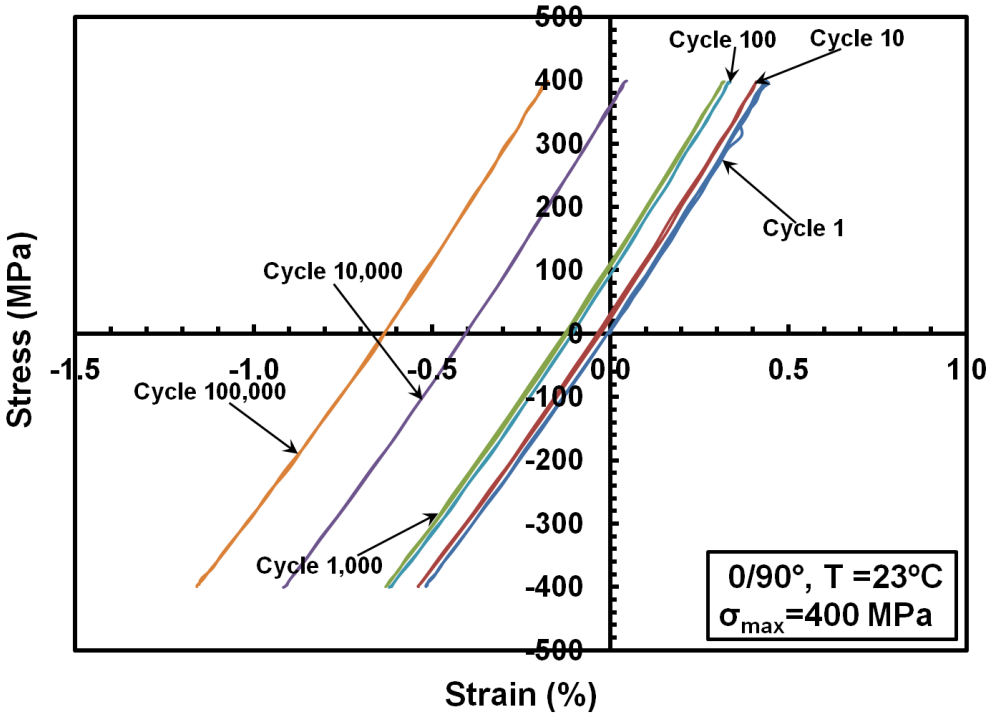

Figure B-28: Evolution of Stress-Strain Hysteresis Response with Fatigue Cycles for Specimen C53-14 with 0/90 Fiber Orientation at 23°C. σ_{max}=400 MPa.

Bibliography

[1] Oceanica, "Aerospace Composites," [Online]. Available: http://www.oceanica.ufrj.br/ocean/cursosead/materiaiscompositos/compositematerials/f_aerospace_applications.pdf. [Accessed 2015 Jan 2015].

[2] F. Smith, "The Use of composites in aerospace: Past, present, and future challenges," 2013. [Online]. Available: https://avaloncsl.files.wordpress.com/2013/01/avalon-the-use-of-composites-in-aerospace-s.pdf. [Accessed 23 Jan 2015].

[3] Firehole Composites, "Fatigue Life Prediction in Composite Materials," Firehole Composites , 24 Feb. 2010. [Online]. Available: http://www.firehole.com/documents/WP_Fatigue-Life-Prediction-in-Composite-Materials.pdf. [Accessed 2 Mar. 2015].

[4] Federal Aviation Administration, "Advanced Composite Materials," [Online]. Available: https://www.faa.gov/regulations_policies/handbooks_manuals/aircraft/amt_airframe_handbook/media/ama_Ch07.pdf. [Accessed 23 Jan 2015].

[5] I. M. Daniel and O. Ishai, Engineering Mechanics of Composite Materials, Second Edition ed., New York, NY: Oxford University Press, 2006, pp. 1-17.

[6] The Royal Society of Chemistry, "Composite Materials," [Online]. Available: http://www.rsc.org/Education/Teachers/Resources/Inspirational/resources/4.3.1.pdf. [Accessed 23 Jan 2015].

[7] J. R. Vinson and R. L. Sierakowski, The Behavior of Structures Composed of Composite Materials, Second Edition ed., Springer, dordrecht: Kluwer Academic Publishers, 2008, pp. 1-38.

[8] A. T. Nettles, "Basic Mechanics of Laminated Composite Plates," NASA, Oct 1994. [Online]. Available: http://ntrs.nasa.gov/archive/nasa/casi.ntrs.nasa.gov/19950009349.pdf. [Accessed 30 Jan 2015].

[9] Quartus Engineering, "Composites 101," Quartus Engineering, 2014. [Online]. Available: http://www.quartus.com/resources/white-papers/composites-101/.

[Accessed 2015 Jan 30].

[10] W. L. Ko, "Delamination Stresses in Semicircular Laminated Composite Bars," NASA, Jan 1988. [Online]. Available: http://www.nasa.gov/centers/dryden/pdf/88107main_H-1417.pdf. [Accessed 30 Jan 2015].

[11] J. G. Balaconis, "Some Aspects of the Mechanical Response of BMI 5250-4 Neat Resin at 191°C," Air Force Institute of Technology, Wright-Patterson AFB, Ohio, 2006.

[12] C. G. Ladrido, "Effect of Prior Aging on Fatigue Behavior of IM7/BMI 5250-4 Composite at 191°C," Air Force Institute of Technology, Wright-Patterson AFB, Ohio, 2007.

[13] R. A. Salvia, "Effects of Prior Aging at 191°C on Creep Response of IM7/BMI 5250-4," Air Force Institute of Technology, Wright-Patterson AFB, Ohio, 2007.

[14] Engineering Archives, "Endurance Limit and Ultimate Strength," Engineering Archives, 2012. [Online]. Available: http://www.engineeringarchives.com/les_machdes_endlimitandultstrength.html. [Accessed 30 Jan 2015].

[15] eFunda, "High-Cycle Fatigue," eFunda, 2015. [Online]. Available: http://www.efunda.com/formulae/solid_mechanics/fatigue/fatigue_highcycle.cfm. [Accessed 30 Jan 2015].

[16] Automated Dynamics, "Types of Fiber Reinforcement," 2015. [Online]. Available: http://www.automateddynamics.com/article/thermoplastic-composite-basics/types-of-fiber-reinforcement,. [Accessed 2015 Jan 29].

[17] Composites World, "The fiber (2015)," 12 Jan 2015. [Online]. Available: http://www.compositesworld.com/articles/the-fiber-2015. [Accessed 29 Jan 2015].

[18] Polymerics, "Bismaleimides," 2002. [Online]. Available: http://www.polymerics.de/technology/bmi_en.html. [Accessed 29 Jan 2015].

[19] H. Stenzenberger, "Bismaleimide Resins," [Online]. Available: https://polycomp.mse.iastate.edu/files/2012/01/6-Bismaleimide-Resins.pdf. [Accessed 2015 Jan 29].

[20] M. J. Owen and T. R. Smith, *Plastics and Polymers,* vol. 36, pp. 33-44, Feb. 1968.

[21] J. M. Corum et al., "Durability-Based Design Properties of Reference Crossply Carbon-Fiber Composite," Oak ridge National Laboratory, Oak Ridge, Tenn., April 2001.

[22] P. R. Jackson, M. B. Ruggles-Wrenn, S. S. Baek and K. A. Keller, "Compressive creep behavior of an oxide-oxide ceramic composite with monazite fiber coating at elevated temperatures," *Materials Science & Engineering,* Vols. 454-455(A), pp. 590-601, 2007. ISSN 0921-5093.

[23] M. P. Wilkinson, "Mechanical Properties and Fatigue Behavior of Unitized composite Airframe Structures at Elevated Temperature," Air Force Institute of Technology, Wright-Patterson AFB, Ohio, 2014.

[24] M. B. Ruggles-Wrenn and T. P. Jones, "Tension-compression fatigue of a SiC/SiC ceramic matrix composite at 1200°C in air and in steam," *International Journal of Fatigue,* vol. 47, pp. 154-160, 2013. ISSN 0142-1123.

[25] M. B. Ruggles-Wrenn, J. M. Corum and R. L. Battiste, "Short-term static and cyclic behavior of two automotive carbon-fiber composites," *Science Direct,* vol. Composites: Part A 34, pp. 731-741, 2003. ISSN 1359-835X.

REPORT DOCUMENTATION PAGE

Form Approved
OMB No. 074-0188

1. REPORT DATE *(DD-MM-YYYY)*	**2. REPORT TYPE**	**3. DATES COVERED** *(From – To)*
26-03-2015	Master's Thesis	October 2013-March 2015

TITLE AND SUBTITLE
Fatigue Behavior of IM7/BMI 5250-4 Composite at Room and Elevated Temperatures

5a. CONTRACT NUMBER
USAF CRADA No. 12-AFIT-01

5b. GRANT NUMBER

5c. PROGRAM ELEMENT NUMBER

6. AUTHOR(S)

Tipton, James, T., 2nd Lieutenant, USAF

5d. PROJECT NUMBER

5e. TASK NUMBER

5f. WORK UNIT NUMBER

7. PERFORMING ORGANIZATION NAMES(S) AND ADDRESS(S)
Air Force Institute of Technology
Graduate School of Engineering and Management (AFIT/EN)
2950 Hobson Way
WPAFB OH 45433-7765

8. PERFORMING ORGANIZATION REPORT NUMBER
AFIT-ENY-MS-15-M-241

9. SPONSORING/MONITORING AGENCY NAME(S) AND ADDRESS(ES)

Air Force Research Lab/RXCC
LtCol Chad Ryther
2977 Hobson Way, Bldg 655
WPAFB OH 45433-7734
(937)656-9153 chad.ryther@us.af.mil

Air Force Research Lab/RXCC
Dr. Richard Hall
2977 Hobson Way, Bldg 655
WPAFB OH 45433-7734
(937)255-9097 richard.hall.16@us.af.mil

10. SPONSOR/MONITOR'S ACRONYM(S)
AFRL/RXCC

11. SPONSOR/MONITOR'S REPORT NUMBER(S)

12. DISTRIBUTION/AVAILABILITY STATEMENT
Distribution Statement A: Approved for Public Release; Distribution Unlimited

13. SUPPLEMENTARY NOTES
This work is declared a work of the U.S. Government and is not subject to copyright protection in the United States.

14. ABSTRACT

The tension-tension fatigue and tension-compression fatigue behaviors of the IM7/BMI 5250-4 composite were investigated. The tension-tension fatigue of the composite with 0/90 and ±45 fiber orientations was studied at 23, 170, and 190°C. The tension-compression fatigue of the composite with 0/90 fiber orientation was examined at 23°C. The tensile and compressive properties of the composite were also evaluated at room and elevated temperatures for both 0/90 and ±45 fiber orientations. Elevated temperature had little effect on the tensile properties of the 0/90 fiber orientation, but strongly influenced the ±45 tensile properties as well as the compressive properties of both fiber orientations. The 0/90 cross-ply exhibited a much stronger tension-tension fatigue performance than the ±45 cross-ply. Elevated temperature had little influence on the tension-tension fatigue response of both fiber orientations. The 0/90 composite exhibited reduced fatigue lives under tension-compression fatigue compared to the tension-tension cycling. The increased influence of the matrix on tension-compression fatigue response is evident.

15. SUBJECT TERMS
Polymer Matrix Composites, IM7/BMI 5250-4, Tension-Tension Fatigue, Tension-Compression Fatigue, Elevated Temperature

16. SECURITY CLASSIFICATION OF:			**17. LIMITATION OF ABSTRACT**	**18. NUMBER OF PAGES**	**19a. NAME OF RESPONSIBLE PERSON**
a. REPORT	**b. ABSTRACT**	**c. THIS PAGE**			Dr. Marina Ruggles-Wrenn, (AFIT/ENY)
U	**U**	**U**	**UU**	142	**19b. TELEPHONE NUMBER** *(Include area code)* (937) 255-3636, ext 4641 (marina.ruggles-wrenn@afit.edu)

Standard Form 298 (Rev. 8-98)
Prescribed by ANSI Std. Z39-18